Final Progress Report

Stimuli-Responsive Polymers with Enhanced Efficiency in Reservoir Recovery Processes

For the work performed during the period of

March 1, 2004 through August 31, 2004

by

Charles McCormick

and

Roger Hester

Issued on September 30, 2004

DOE Award Number DE-FC26-01BC15317

The University of Southern Mississippi
Department of Polymer Science
P.O. Box 10076
Hattiesburg, MS 39406

TABLE OF CONTENTS

LIST OF FIGURES, SCHEMES, AND TABLES

Disclaimer

This report was prepared as an account of work sponsored by an agency of the United States Government. Neither the United States Government nor any agency thereof, nor any of their employees, makes any warrant, express or implied, or assumes any legal liability or responsibility for the accuracy, completeness, or usefulness of any information, apparatus, product, or process disclosed, or represents that its use would not infringe privately owned rights. Reference herein to any specific commercial product, process, or service by trade name, trademark, manufacturer, or otherwise does not necessarily constitute or imply its endorsement, recommendation, or favoring by the United States Government or any agency thereof. The views and opinions of authors expressed herein do not necessarily state or reflect those of the United States Government or any agency thereof.

Abstract

This sixth and final progress report for DOE Award Number DE-FC26-01BC15317 describes research during the period March 01, 2004 through August 31, 2004 performed at the University of Southern Mississippi on *Stimuli Responsive Polymers with Enhanced Efficiency in Reservoir Recovery* processes. Significantly, terpolymers that are responsive to changes in pH and ionic strength have been synthesized, characterized, and their solution properties have been extensively examined. Terpolymers composed of acrylamide, a carboxylated acrylamido monomer (AMBA), and a quarternary ammonium monomer (AMBATAC) with balanced compositions of the latter two, exhibit increases in aqueous solution viscosity as NaCl concentration is increased. This increase in polymer coil size can be expected upon injection of this type of polymer into oil reservoirs of moderate-to-high salinity, leading to better mobility control. The opposite effect (loss of viscosity) is observed for conventional polymer systems.

Additionally polymer mobility characteristics have been conducted for a number of hydrophilic copolymers utilizing an extensional flow apparatus and size exclusion chromatography. This study reveled that oil recovery enhancement through use of polymers in a water flood is due to the polymer's resistance to deformation as it flows through the reservoir. Individual polymers when in aqueous solution form coils. The larger the polymer's coil size, the greater the polymer's resistance to extensional flow and the more effective the polymer is in enhancing oil recovery. Large coil sizes are obtained by increasing the polymer molecular weight and having macromolecular structures that favor greater swelling of the coil by the aqueous solvent conditions (temperature, pH and electrolyte concentration) existing in the reservoir. Detailed studies of other stimuli-responsive systems may be found in DOE BC15317R01, BC15317R02, BC15317R03, BC15317R04, and BC15317R05.

EXECUTIVE SUMMARY

Our research efforts have been focused on the development of stimuli-responsive water-soluble polymers designed for use in oil field applications, particularly enhanced oil recovery (EOR). These model systems are tailored for potential application as viscosifiers and/or mobility control agents for secondary and tertiary EOR methods. Herein we describe the progress of our ongoing research of polyzwitterions, polymers derived from monomers bearing both positive and negative charges, that show the ability to sustain or increase their hydrodynamic volume (and thus, solution viscosity) in the presence of electrolytes. Such polymers appear to be well-suited for use under conditions similar to those encountered in EOR operations.

Previous semi-annual reports, DE15317R-1-05, have detailed our experimental findings on a number of new polymer systems with salt, pH, temperature, and shear-responsive behavior in aqueous media. This sixth and final progress report for DOE Award Number DE-FC26-01BC15317 describes research during the period March 01, 2004 through August 31, 2004 performed at the University of Southern Mississippi on *Stimuli Responsive Polymers with Enhanced Efficiency in Reservoir Recovery* processes. Significantly, terpolymers that are responsive to changes in pH and ionic strength have been synthesized, characterized, and their solution properties have been extensively examined. Terpolymers composed of acrylamide, a carboxylated acrylamido monomer (AMBA), and a quarternary ammonium monomer (AMBATAC) with balanced compositions of the latter two, exhibit increases in aqueous solution viscosity as NaCl concentration is increased. This increase in polymer coil size can be expected upon injection of this type of polymer into oil reservoirs of moderate-to-high salinity, leading to better mobility control. The opposite effect (loss of viscosity) is observed for conventional polymer systems.

Additionally polymer mobility characteristics have been conducted for a number of hydrophilic copolymers utilizing an extensional flow apparatus and size exclusion chromatography. Polymer enhancement of the water flood viscosity relies on the polymer coil resistance to extensional deformation. A correlation was demonstrated in this report between polymer coil hydrodynamic diameter and the fluid extension rate at which polymer coil extension begins. Ideally, the macromolecules should have a collapsed coil configuration during injection into the reservoir to reduce both pumping costs and shear degradation at the well-head, where fluid extension rates are highest. Also, because fluid extension rates decrease away from the injection well-head, polymer coils should expand after injection to reduced their yield extension rate and increase their solution extensional viscosity within the reservoir.

The solution environment in underground reservoirs is characterized by high temperature, basic pH, and the presence of monovalent and divalent ions. Thus, the desired complex polymer solution behavior may be achieved with synthetic polymers that can change their macromolecular conformation upon encountering certain environmental stimuli such as variations in solution temperature, pH, and electrolyte concentration. Proper molecular design and synthesis facilitated by theoretical prediction of the

relationships among polymer chemical structure and solvent flow properties should lead to improved sweep efficiency during polymer flooding.

This study revealed that oil recovery enhancement through use of polymers in a water flood is due to the polymer's resistance to deformation as it flows through the reservoir. Individual polymers when in aqueous solution form coils. The larger the polymer's coil size, the greater the polymer's resistance to extensional flow and the more effective the polymer is in enhancing oil recovery. Large coil sizes are obtained by increasing the polymer molecular weight and having macromolecular structures that favor greater swelling of the coil by the aqueous solvent conditions (temperature, pH and electrolyte concentration) existing in the reservoir. Detailed studies of other stimuli-responsive systems may be found in DOE BC15317R01, BC15317R02, BC15317R03, BC15317R04, and BC15317R05.

CHAPTER 1

Polymer Synthesis, Characterization, and Solution Behavior of Stimuli-Responsive Terpolymers

Background

To date, our synthetic research efforts have been focused on the development of stimuli-responsive water-soluble polymers designed for use in enhanced oil recovery (EOR) applications. These model systems are structurally tailored for potential application as viscosifiers and/or mobility control agents for secondary and tertiary EOR methods. The goal of previous synthetic work has been to design novel polymers that exhibit large dilute solution viscosities in the presence of the adverse conditions normally encountered in oil reservoirs (such as high salt concentrations, the presence of multivalent ions, and elevated temperatures). The polymers are also designed to have "triggerable" properties that can be elicited by external stimuli, such as changes in pH and/or salt concentration.

Various zwitterionic polymers have been investigated in our laboratories due to their potential for increasing viscosity thus controlling mobility in enhanced oil recovery.[1] Unlike polyelectrolytes (PEs), which bear *either* anionic or cationic charges, polyzwitterions (PZs) bear *both* anionic and cationic functionalities. PZs may be categorized as polyampholytes (anionic and cationic charges on *separate* repeat units) or polybetaines (anionic and cationic charges on the *same* repeat unit). In aqueous solution, PEs generally collapse with increasing ionic strength due to the screening of intramolecular repulsions between like charges along the polymer backbone.[1] This phenomenon, known as the polyelectrolyte effect, tends to impair the performance of PEs in applications where the polymers encounter saline media. In contrast to PEs, PZ solutions exhibit an antipolyelectrolyte effect in which the polymer adopts a more expanded conformation with increasing ionic strength.[2] This effect is attributed to the screening of intramolecular attractions between the pendant anionic and cationic moieties along the polymer backbone by the small molecule electrolytes. The increase in hydrodynamic size is also accompanied by an increase in solution viscosity, making PZs ideal candidates for salt-tolerant viscosifiers.

Polyzwitterions containing the sulfonate functionality have been thoroughly studied beginning with the pioneering work of Hart and Timmerman.[3] In that work, zwitterionic monomers were prepared by the reaction of 2-and 4-vinylpyridine with 1,4-butanesultone. Polysulfobetaines are typically insoluble in deionized water and require a relatively high content of hydrophilic comonomer or the addition of a critical concentration of electrolyte to achieve solubility and viscosity enhancement. Polysulfobetaines have also been synthesized from acrylic,[4-11] acrylamido,[12,13]

and vinyl imidazolium[14-16] monomers and more recently polysulfobetaine block copolymers have been reported.[17-18]

This report contains the synthesis, characterization, and solution studies low charge density ampholytic terpolymers composed of acrylamide (AM), sodium 3-acrylamido-3-methylbutanoate (NaAMB), and (3-acrylamidopropyl)trimethyl ammonium chloride (APTAC) prepared via free-radical polymerization in 0.5 M NaCl to yield terpolymers with random charge distributions. NaOOCH was employed as a chain transfer agent during the polymerization to eliminate the effects of monomer feed composition on the degree of polymerization (*DP*) and to suppress gel effects and broadening of the molecular weight distribution (MWD). Terpolymer compositions were obtained via ^{13}C NMR spectroscopy and residual counterion content was determined via elemental analysis for Na^+ and Cl^-. Molecular weights (MWs) and polydispersity indices (PDIs) were determined via size exclusion chromatography/multi-angle laser light scattering (SEC-MALLS); terpolymer MWs ranged from $1.3 - 1.6 \times 10^6$ g/mol, corresponding to *DP*s of $1.6 - 1.9 \times 10^4$ repeat units, with all terpolymers exhibiting PDIs < 2.0. Intrinsic viscosities determined from SEC-MALLS data and the Flory-Fox relationship were compared to intrinsic viscosities determined via low shear dilute solution viscometry and were found to agree rather well. Data from the SEC-MALLS analysis was used to analyze the radius of gyration-MW (R_g-M) relationships and the Mark-Houwink-Sakurada intrinsic viscosity-MW ([η]-M) relationships for the terpolymers. The R_g-M and [η]-M relationships revealed that most of the terpolymers exhibit little or no excluded volume effects under SEC conditions. Potentiometric titration of terpolymer solutions in deionized (DI) water showed that the apparent pK_a of the AMBATAC terpolymers increases with increasing NaAMB content in the terpolymers and increasing ratio of anionic:cationic monomer at a constant terpolymer charge density.

The solution properties of low charge density ampholytic terpolymers of acrylamide (AM), sodium 3-acrylamido-3-methylbutanoate (NaAMB), and (3-acrylamidopropyl) trimethylammonium chloride (APTAC) have been studied as functions of solution pH, ionic strength, and polymer concentration. All terpolymers examined in this study possess random charge distributions, homogeneous compositions, and similar molecular weights and molecular weight distributions. Terpolymers with low charge densities and/or large charge asymmetries exhibited excellent solubility in deionized (DI) water, and higher charge density terpolymers were readily dispersible in DI water; however, the higher charge density terpolymer solutions separated into polymer-rich and polymer-poor phases on standing over time. Charge-balanced terpolymers exhibited "antipolyelectrolyte" behavior at pH values ≥ ambient pH (6.5 ± 0.2); the same terpolymers behave increasingly as cationic polyelectrolytes with decreasing solution pH due to protonation of the AMB repeat units. Unbalanced terpolymers generally exhibited polyelectrolyte behavior, although the effects of intramolecular electrostatic attractions (i.e. polyampholyte effects) on the hydrodynamic volume of the unbalanced terpolymer coils were evident at certain values of solution pH and salt concentration. The dilute solution behavior of the terpolymers correlates well

with the behavior predicted by several polyampholyte solution theories. In the semidilute regime, solution viscosities were observed to increase with increasing terpolymer charge density, indicating significant enhancement of solution viscosity by intermolecular electrostatic associations. Upon addition of NaCl, semidilute solution viscosities tend to decrease due to disruption of the intermolecular electrostatic associations.

Experimental

Materials

All chemicals were purchased from Aldrich and used as received, unless otherwise noted. AM was recrystallized three times from acetone and dried *in vacuo* prior to use (m.p. = 83 °C). 3-Acrylamido-3-methylbutanoic acid (AMBA) was synthesized according to the procedure of McCormick and Blackmon[20] and recrystallized twice from methyl ethyl ketone prior to use (m.p. = 89-91 °C). 2,2'-Azobis[2-(2-imidazolin-2-yl)propane] dihydrochloride (VA-044) was a gift from Wako Pure Chemical Industries, Ltd. and was used as received. HCl and NaOH standard solutions (0.100 ± 0.005 M) were purchased from Fisher Scientific. Deionized (DI) water was obtained from a Barnstead NANOPure reverse osmosis/filtration unit (resistivity = 18.0 MΩ). Polyampholyte terpolymer composition of the above monomers is shown in Figure 1.1.

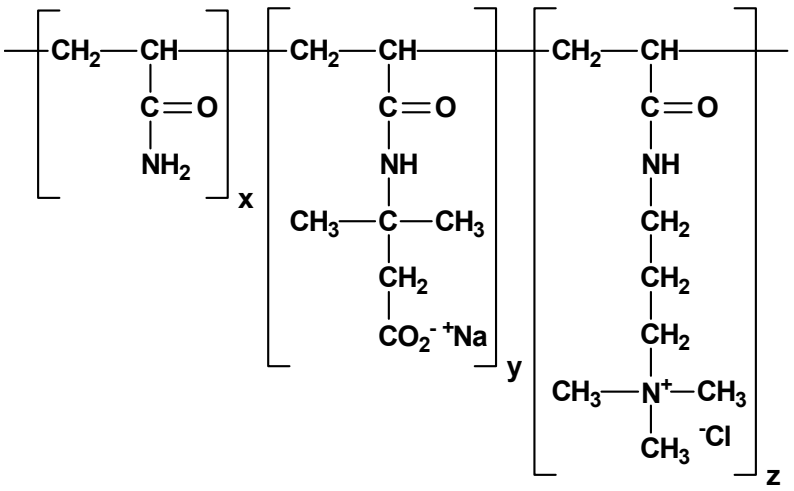

Figure 1.1. Structure of poly(acrylamide-*co*-sodium 3-acrylamido-3-methylbutanoate-*co*-(3-acrylamidopropyl)trimethylammonium chloride) (AMBATAC) ampholytic terpolymers.

Polymer Synthesis

Synthesis of AMBATAC polyampholyte terpolymers

Low charge density terpolymers of AM, NaAMB, and APTAC (referred to as AMBATAC-*Y*-*Z*, where *Y* = mol% NaAMB and *Z* = mol% APTAC in the monomer feed) were synthesized via conventional free radical polymerization in 0.5 M NaCl. Sodium formate (NaOOCH) was added as a chain transfer agent to control polymer MW, suppress gel effects, and prevent excessive broadening of the MWD. The monomer concentration was held constant at 0.46 M, and the ratio of [monomer]:[NaOOCH] was held constant at 32 to yield terpolymer samples with weight-average MWs (M_w) in the range of 1 - 2 × 10^6 g/mol. The monomer-to-initiator ratio was 1000:1, and the reaction solution pH was adjusted to 8.5 ± 0.5 by addition of NaOH to ensure neutralization of the AMBA monomer to NaAMB. A typical polymerization procedure for AMBATAC-5-5 is described below.

To a two-liter, three-neck round bottom flask equipped with mechanical stirrer and N_2 inlet/outlet was added degassed DI water (1500 mL) and NaCl (43.84 g, 0.750 mol). The flask was immersed in a 30 °C constant temperature bath, and the contents were sparged with N_2 for 20 min. AM (43.76 g, 0.616 mol), AMBA (5.86 g, 0.034 mol), APTAC (9.40 g of 75 wt% APTAC solution in water, 0.034 mol), NaOH (1.40 g, 0.035 mol), and NaOOCH (1.45 g, 0.021 mol) were added to the flask and allowed to stir for 10 min. The pH of the monomer solution was adjusted to 8.5 ± 0.5 with 6.0 M NaOH prior to initiating polymerization. VA-044 (221 mg, 0.684 mmol, dissolved in 10 mL of degassed DI water) was then added to the flask *via* syringe. The polymerization was allowed to proceed under a N_2 atmosphere for 6.7 h. Stirring speed was adjusted to maintain a shallow vortex in the reaction medium. The reactor contents were discharged to Spectra-Por No. 4 dialysis tubing (MW cut-off = 12-14,000 g/mol) and dialyzed against DI water for one week, with the dialysis water being changed every 24-48 h. The pH of the dialysate was maintained at pH = 7.0 – 7.5 to ensure that the AMBA repeat units remained ionized. The purified terpolymer was isolated *via* lyophilization to yield a white, cotton-like solid. Conversion was determined gravimetrically.

Given the extremely hygroscopic nature of the AMBATAC terpolymers, it was desirable to obtain terpolymer samples with higher bulk density and lower surface area for ease of handling and solution preparation. Therefore, the lyophilized terpolymers were dissolved in DI water ([terpolymer] ≈ 10 wt%) and precipitated into absolute ethanol. The precipitated terpolymers were dried in vacuo at 50 °C for 48-72 hr and stored under N_2.

^{13}C NMR: AMBATAC-5-5, NaAMB COO^-, 180.3, overlapping with AM C=O, 179.7 ppm; APTAC C=O, 177.2 ppm; NaAMB C=O, 175.5 ppm; APTAC quat. ammonium CH_2, 64.4 ppm; APTAC quat. ammonium CH_3, 53.3 ppm; NaAMB quat. C, 52.8 ppm; APTAC amide CH_2, 48.6 ppm; NaAMB CH_2, 48.1 ppm; backbone CH, 42.1 ppm; backbone CH_2, 35.2 ppm; NaAMB *gem* CH_3, 26.7 ppm; APTAC CH_2, 22.7 ppm.

^{1}H NMR: APTAC quat ammonium CH_2, 3.30 ppm; APTAC amide CH_2, 3.20 ppm; APTAC quat. ammonium CH_3, 3.08 ppm, NaAMB CH_2, 2.47 ppm; backbone CH, 2.12-2.27 ppm; APTAC CH_2 1.97 ppm; backbone CH_2, 1.58-1.69 ppm; NaAMB *gem* CH_3, 1.32 ppm.

Terpolymer Characterization

NMR Spectroscopy:

Samples for NMR spectroscopic analysis were prepared as 5-10 wt% solutions in D_2O containing 0.5 M NaCl. All NMR experiments were performed at ambient temperature (25.0 °C ± 1.0 °C). ^{13}C NMR spectra for the terpolymers were obtained at 125 MHz with a Varian UNITY-INOVA NMR spectrometer using a standard 5 mm two-channel probe. For quantitative determination of terpolymer composition, a gated decoupled pulse sequence with a 6-7 s relaxation delay was used to suppress NOE effects. Typically, 10000-15000 scans were accumulated for ^{13}C spectra. All shifts were referenced automatically by the acquisition software (VNMR v6.1C) using the resonance frequency of D_2O. The error associated with individual values of termonomer incorporation determined via integration of ^{13}C NMR signals is generally ± 5% of the value. ^{1}H NMR spectra were obtained at 300 MHz on a Varian Mercury PLUS spectrometer. Typical acquisition parameters were a relaxation delay of 0.05 s, a 7.1 μs pulse corresponding to a 90° flip angle, and an acquisition time of 2 s. Data analysis was performed using MestRe-C v.2.3a spectral analysis software (Departamento de Química Orgánica, Universidad de Santiago de Compostela).

Elemental Analysis:

Elemental analysis for Na^+ and Cl^- was performed by Bonner Analytical Testing Co. of Hattiesburg, MS. Samples of the AMBATAC terpolymers were analyzed to determine the content of residual counterions remaining after purification via dialysis.

Size exclusion chromatography-multi-angle laser light scattering (SEC-MALLS):

Aqueous size exclusion chromatography (SEC) was used to determine terpolymer MW and polydispersity index (PDI). The SEC system consisted of an Agilent 1100 series isocratic pump with vacuum degasser, a Rheodyne 7725i manual injector with 100 μL injection loop, two Viscogel columns (GPW_{XL}-5000 and -6000, plus a GPW_{XL} guard column, Viscotek) connected in series, a DAWN EOS 18-angle laser light scattering detector (Wyatt Technologies), and an Optilab DSP interferometric refractometer (Wyatt Technologies). Data acquisition and analysis were performed using ASTRA chromatography software (Wyatt Technologies). SEC analysis was conducted at ambient temperature (25.0 °C ± 1.0 °C). The eluent employed for SEC analysis of the AMBATAC terpolymers was 0.1 μm-filtered 0.1 M NaCl pH 7 phosphate buffer (25mM NaH_2PO_4 + 25mM Na_2HPO_4). Refractive index (RI) increments (d*n*/dc) of the

terpolymers were determined using the refractometer in offline mode at ambient temperature. The error associated d*n*/dc values determined offline was typically ± 2-3%. The SEC-MALLS data reported are the averages of three separate injections. The error associated with individual values of M_w determined via SEC-MALLS was typically ≤ ± 2%.

Dilute solution viscometry:

Stock solutions were prepared by dissolving vacuum oven-dried terpolymer samples in SEC eluent and were allowed to age 48-72 h while agitating gently on an orbital shaker. Dilutions of the stock solutions were prepared and allowed to age overnight on an orbital shaker prior to analysis. Apparent viscosities of dilute polymer solutions were determined using a Contraves LS-30 low shear rheometer with the 2T cup and bob geometry, operating at 5.96 s^{-1} and 25 °C. Dilute solution apparent viscosities were initially measured at varying shear rates, and the solutions were observed to be Newtonian fluids (i.e. non-shear thinning); thus, the apparent viscosities determined at 5.96 s^{-1} are considered to be zero-shear apparent viscosities. Measurements of apparent viscosity were repeatable with a precision of ± 1%. Intrinsic viscosities were determined by plotting reduced viscosity versus concentration and extrapolating to zero concentration. Determinations of intrinsic viscosity were repeatable to within ± 2%.

*Potentiometric Titration***:**

pH measurements for potentiometric titrations were conducted at 25.0 ± 0.5 °C using an Orion 900A pH meter with a Ross Sure-Flow 8175 pH electrode. The meter was calibrated via a two-point calibration method. Terpolymer concentrations for titration were 0.50 g/dL; minimal volume variation during titration was achieved by adding microliter aliquots of titrant. Terpolymer solutions were adjusted to pH ~ 10 with concentrated NaOH to ensure complete neutralization of all carboxylic acid groups, then backtitrated using 0.1 M HCl standard solution.

Solution Studies

*Solution Rheology***:**

Rheological measurements on semidilute polymer solutions were conducted on a controlled stress rheometer (Rheometric Scientific SR-5000). Steady-state shear stress sweeps were performed at 25.0 ± 0.05 °C using either double-wall Couette or cone and plate geometries (cone diameter = 40 mm, cone angle = 0.04 rad). Data acquisition and analysis were performed using the Orchestrator v6.5.7 software package (Rheometric Scientific). Zero-shear apparent viscosities for pseudoplastic fluids were calculated by fitting shear stress sweep data to either Ellis or Carreau viscosity models.

Turbidimetry:

Turbidimetric measurements were performed using a Brinkmann PC-800 colorimeter with a path length of 2 cm, operating at 620 nm and 25.0 °C.

Size exclusion chromatography-multi-angle laser light scattering (SEC-MALLS):

Aqueous size exclusion chromatography (SEC) was used to examine the phase separation of AMBATAC-7.5-7.5 solutions in DI water. The SEC system consisted of an Agilent 1100 series isocratic pump with vacuum degasser, a Rheodyne 7725i manual injector with 100 μL injection loop, two Viscogel columns (GPW_{XL}-5000 and -6000, plus a GPW_{XL} guard column, Viscotek) connected in series, a DAWN EOS 18-angle laser light scattering detector (Wyatt Technologies), and an Optilab DSP interferometric refractometer (Wyatt Technologies). Data acquisition and analysis were performed using ASTRA chromatography software (Wyatt Technologies). SEC analysis was conducted at ambient temperature (25.0 °C ± 1.0 °C). The eluent employed for SEC analysis of the AMBATAC terpolymers was 0.1 μm-filtered 0.1 M NaCl pH 7 phosphate buffer (25mM NaH_2PO_4 + 25mM Na_2HPO_4). The refractive index (RI) increment (d*n*/dc) of the AMBATAC-7.5-7.5 terpolymer was determined using the refractometer in offline mode at ambient temperature (d*n*/d*c* = 0.1738). Samples of the upper and lower phases were diluted (1:10) in the SEC eluent and allowed to stir gently on an orbital shaker for 24 h prior to analysis. The SEC-MALLS data reported are the average of two separate injections. The concentration of polymer in each phase was calculated via online refractometry using the d*n*/d*c* value for AMBATAC-7.5-7.5.

Results and Discussion

Polyampholyte terpolymer synthesis

Scheme 1.1 depicts the monomers employed in the synthesis of the AMBATAC polyampholyte series. Our goal was to prepare low charge density polyampholytes with high solubility and good viscosifying properties; thus we targeted terpolymer compositions containing a minimum of 80% AM. The high levels of this extremely hydrophilic, nonionic monomer promote solubility of the AMBATAC terpolymers even in the absence of added electrolytes. NaAMB was selected as the anionic monomer primarily due to its pH-responsive nature (i.e. carboxylate functionality). However, NaAMB also possesses several other features that make it a highly desirable monomer for application in brine-tolerant viscosifiers, including increased hydrolytic stability, greater steric bulk (leading to increased polymer chain stiffness), and outstanding resistance to divalent ion binding (preventing polymer phase separation in hard brines).[20-23] APTAC, a non-pH-responsive quaternary ammonium acrylamido monomer, was employed as the cationic monomer in the AMBATAC series. APTAC is commercially-available and was selected for this work due to the complexity associated with

synthesizing (three-step synthetic procedure) and purifying (high tendency for autopolymerization) the AMPTAC monomer employed in previous studies.[24-25]

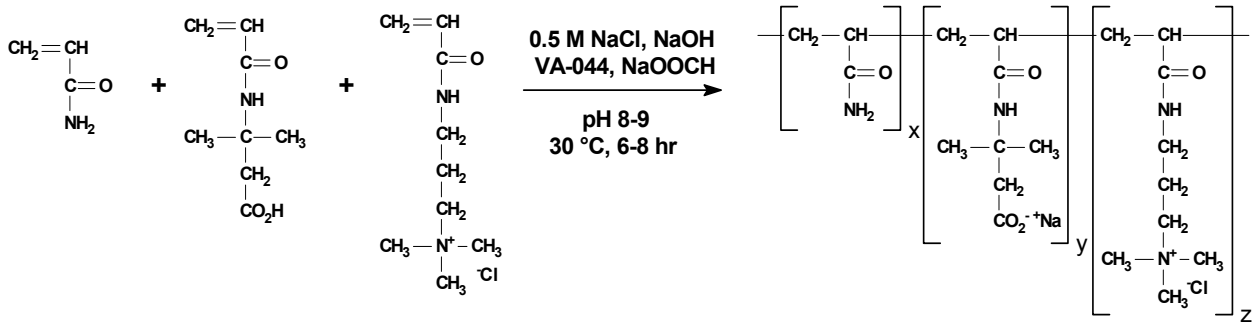

Scheme 1.1. Synthesis of poly(acrylamide-*co*-sodium 3-acrylamido-3-methylbutanoate-*co*-(3-acrylamidopropyl)trimethylammonium chloride) (AMBATAC) polyampholyte terpolymers.

The monomers and reaction conditions employed in the synthesis of the AMBATAC terpolymers were chosen to yield well-defined model terpolymers with homogeneous compositions, random charge distributions, and PDIs < 2.0. McCormick and coworkers[24, 26-28] have shown that the effects of compositional drift are negligible when all acrylamido monomers are utilized in the synthesis of PAM-based polyampholytes (i.e. due to the similar reactivities of the acrylamido polymerizable groups). Hence, AMBATAC polymerizations can be carried out to relatively high conversions (>75 %) while maintaining relatively homogeneous terpolymer compositions. To ensure random distribution of the charged groups along the terpolymer chain, the AMBATAC terpolymers were synthesized in 0.5 M NaCl. The addition of NaCl to the reaction medium screens the electrostatic interactions between ionic monomers, thus the tendency for the charged monomers to be incorporated into the terpolymer as alternating pairs is greatly reduced.[29-30] In previous studies of PAM-based polyampholytes synthesized by free radical polymerization, the degree of polymerization (*DP*) was observed to vary strongly depending on the monomer feed composition.[24-28, 31-33] To eliminate the effects of monomer feed composition on *DP*, the polymerizations in this study were conducted in the presence of sodium formate as a chain transfer agent. Sodium formate is highly effective at controlling MW and suppressing broad MWDs in the polymerization of acrylamido monomers.[34] Additionally, the polymerizations were conducted slightly above room temperature (30 °C) to minimize chain branching and hydrolysis reactions which can occur at higher temperatures.[35-36]

The first column in Table 1.1 indicates the target compositions of the AMBATAC terpolymers synthesized for this study (AMBATAC-*Y*-*Z*, where *Y* = mol % NaAMB and *Z* = mol % APTAC in the monomer feed; the balance of the monomer feed is AM). In addition to the charged balanced terpolymers containing 5–20 mol % total ionic comonomer content, two unbalanced terpolymers were also prepared, AMBATAC-3-7 and AMBATAC-7-3, each bearing 10 mol% ionic comonomer. The polymerizations were conducted for six to eight hours to obtain conversions of approximately 80 %. It is evident in Table 1.1 that longer reaction times were required to reach high conversion as the level of APTAC in the monomer feed was increased. This is attributed to the presence of the hydroquinone monomethyl ether (MEHQ) retarder present in the commercially-available APTAC monomer, which leads to longer induction periods as the level of APTAC in the feed is increased.

Table 1.1. Conversion and compositional data for AMBATAC terpolymer synthesis.

Sample	Reaction Time (hr)	Conversion[a] (%)	AM[b] (mol %)	NaAMB[b] (mol %)	APTAC[b] (mol %)
Balanced					
AMBATAC-2.5-2.5	5.8	81	94.2	3.0	2.8
AMBATAC-5-5	6.7	79	91.1	4.6	4.3
AMBATAC-7.5-7.5	8.0	84	86.2	6.8	7.0
AMBATAC-10-10	8.0	78	77.9	10.8	11.3
Unbalanced					
AMBATAC-3-7	7.8	87	90.2	3.1	6.7
AMBATAC-7-3	6.5	83	89.4	7.0	3.6

[a] conversion determined gravimetrically

[b] determined *via* inverse-gated decoupled ^{13}C NMR spectroscopy

Compositional analysis

Figure 1.2 depicts a ^{13}C NMR spectrum representative of the AMBATAC terpolymer series (AMBATAC-5-5 shown). Terpolymer compositions were determined via inverse-gated decoupled ^{13}C NMR spectroscopy, which allowed for quantitative integration of the signals in the ^{13}C spectra (Table 1.1). The terpolymer compositions determined via NMR spectroscopy are in very good agreement with the target compositions and typically deviate less than one mol % from the target values.

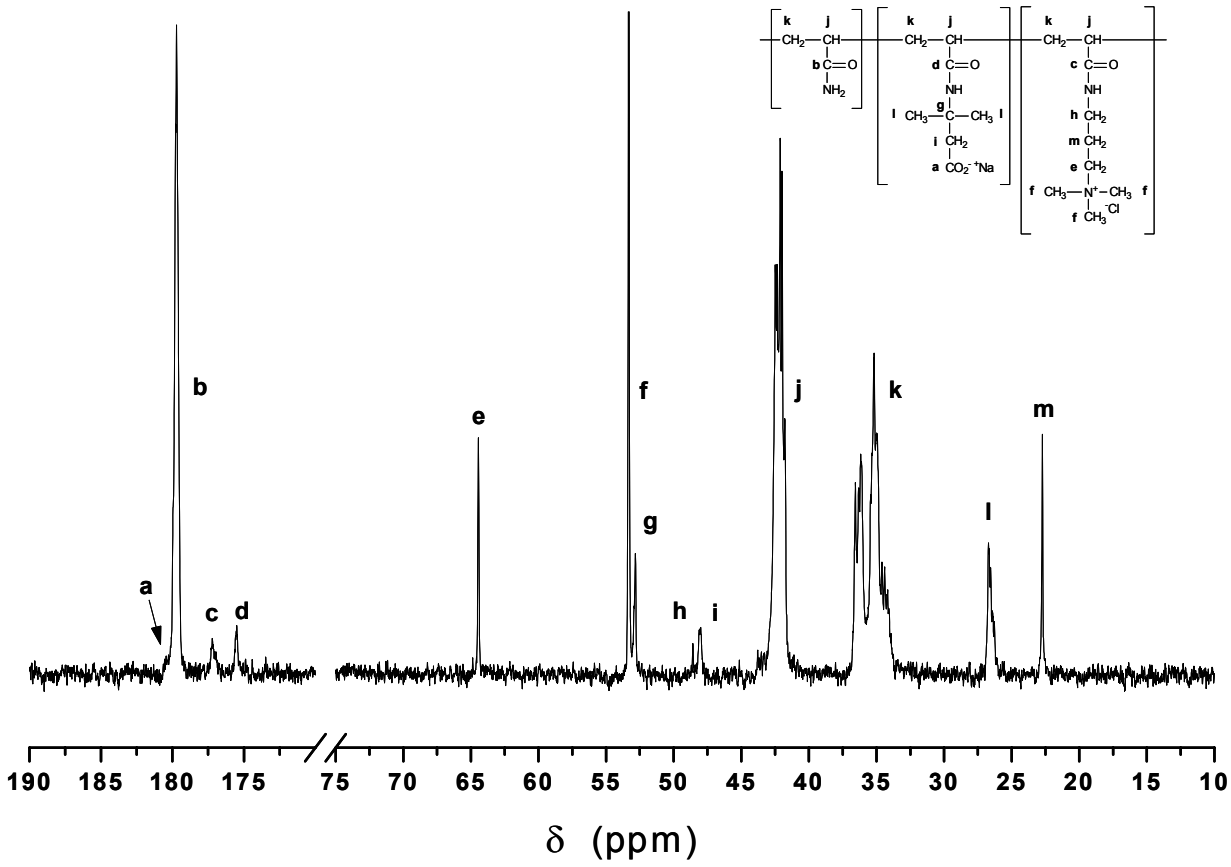

Figure 1.2. Inverse-gated decoupled ^{13}C NMR spectrum of AMBATAC-5-5.

It is has been established that the purification of polyampholytes via exhaustive dialysis against DI water leads to self-neutralization of the polyampholyte, in which the polymer-bound cations and anions pair with each other as the mobile counterions diffuse away from the polymer.[20,37-38] It should be noted that self-neutralization can occur intra- and intermolecularly. Thus, after purification via dialysis, the bulk compositions of the AMBATAC terpolymers are best represented by the structure in Figure 1.3, which consists of *m* AM repeat units, (*n* + *o*) AMB-APTA repeat unit pairs, and *p* NaAMB and/or *q* APTAC repeat units that still bear counterions. Using the compositional data in Table 1.1, the maximum number of AMB-APTA repeat unit pairs was calculated assuming 100% charge pairing of the charged repeat unit present in the least content (Table 1.2). The excess charged repeat units were assumed to retain their counterions to maintain charge neutrality of the system.

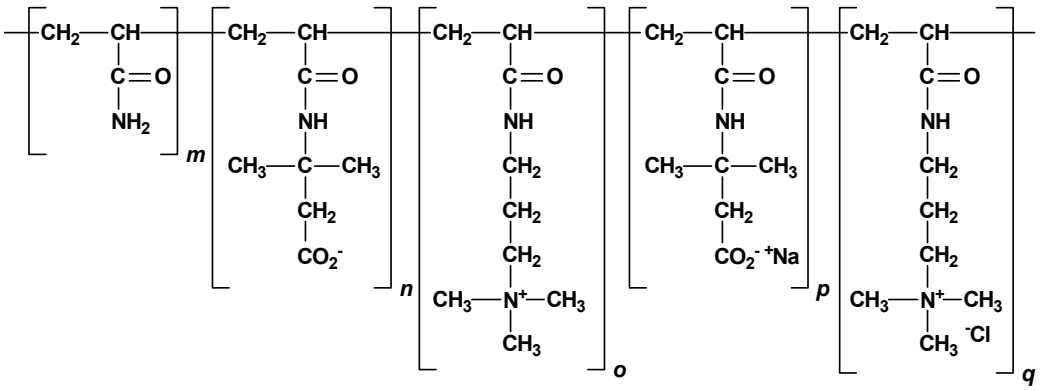

Figure 1.3. Composition of AMBATAC terpolymers following purification via dialysis.

To verify the terpolymer compositions presented in Table 1.2, samples of the terpolymers were analyzed for residual sodium (Na^+) and chloride (Cl^-) content. By assuming that each ionic repeat unit bears a counterion, the maximum theoretical Na^+ and Cl^- contents prior to dialysis and self-neutralization can be estimated from the compositional data in Table 1.1. If no self-neutralization occurred in the AMBATAC systems, then the terpolymers would be expected to contain from 0.9 – 2.5 wt % Na^+ and 1.3 – 4.0 wt % Cl^- (Table 1.3). Following dialysis and charge pairing of ionic monomers, the residual counterion contents due to the presence of excess ionic repeat units can be estimated using the compositional data in Table 1.2, assuming 100 % self-neutralization of the repeat unit present in the least content. The results of elemental analysis for Na^+ and Cl^- agree well with the expected values, indicating that the AMBATAC terpolymers are indeed highly self-neutralized and only bear counterions on ionic repeat units present in excess of the oppositely-charged repeat units. Most of the deviations from the expected values are slight and may be attributed to the error in determining terpolymer composition via ^{13}C NMR spectroscopy, although some ionic repeat units present in least content may still bear counterions due to conformational restrictions limiting chain mobility required for self-neutralization with oppositely-charged repeat units.

Table 1.2. Compositional data for dialyzed AMBATAC terpolymers.

Sample	AM (*m*) (mol %)	AMB-APTA pairs (*n* + *o*) (mol %)	NaAMB (*p*) (mol %)	APTAC (*q*) (mol %)
Balanced				
AMBATAC-2.5-2.5	94.2	2.8	0.2	0.0
AMBATAC-5-5	91.1	4.3	0.3	0.0
AMBATAC-7.5-7.5	86.2	6.8	0.0	0.2
AMBATAC-10-10	77.9	10.8	0.0	0.5
Unbalanced				
AMBATAC-3-7	90.2	3.1	0.0	3.6
AMBATAC-7-3	89.4	3.6	3.4	0.0

Table 1.3. Residual counterion content in AMBATAC terpolymers.

Sample	Na^+, predialysis[a] (wt %)	Cl^-, predialysis[a] (wt %)	Na^+, postdialysis[b] (wt %)	Cl^-, postdialysis[b] (wt %)	Na^+ found[c] (wt %)	Cl^- found[c] (wt %)
Balanced						
AMBATAC-2.5-2.5	0.9	1.3	0.1	0.0	0.1	ND[d]
AMBATAC-5-5	1.3	1.9	0.1	0.0	0.1	ND[d]
AMBATAC-7.5-7.5	1.8	2.8	0.0	0.1	<0.1	<0.1
AMBATAC-10-10	2.5	4.0	0.0	0.2	<0.1	0.2
Unbalanced						
AMBATAC-3-7	0.9	2.8	0.0	1.6	ND[d]	0.4
AMBATAC-7-3	1.9	1.5	1.0	0.0	0.9	<0.1

[a] theoretical value calculated from ^{13}C NMR compositional data, assuming each ionic repeat unit bears a counterion

[b] theoretical value calculated from ^{13}C NMR compositional data, assuming complete self-neutralization of repeat unit present in least content

[c] determined via elemental analysis

[d] ND = not detected

The very low value of Cl^- found in AMBATAC-3-7 is attributed to ion-exchange phenomena during dialysis, in which Cl^- may have been exchanged for OH^- due to the dialysate being maintained at pH 7.0 – 7.5 with NaOH. Indeed, solutions of AMBATAC-3-7 in DI water were observed to have higher ambient pH values (7.0 ± 0.2) compared to the other terpolymers in the series (6.5 ± 0.2), indicating ion-exchange for OH^- is likely to have occurred.

SEC-MALLS Analysis

MW, R_g, and PDI data for the AMBATAC terpolymer series were obtained *via* SEC coupled with multi-angle laser light scattering (MALLS) and refractive index (RI) detection. SEC was performed using 0.1 M NaCl pH 7 phosphate buffer as the eluent to ensure solubility of the charge-balanced polyampholyte terpolymers and suppression of polyelectrolyte effects in the unbalanced systems. When used in conjunction with d*n*/dc values determined offline (Table 1.4), MALLS detection enables determination of the absolute MWs without the use of polymer standards and universal calibration techniques. The results of a typical SEC-MALLS analysis are shown in Figure 1.4 for AMBATAC-10-10, where the RI response and MW of each chromatogram slice are plotted as a function of elution volume. The RI signal indicates a unimodal MWD with a low MW tail; this MWD is characteristic of high conversion PAM products synthesized in the presence of NaOOCH as a chain transfer agent.[34] The negatively-sloped linear decrease in MW as a function of elution volume indicates very good separation of the various MW fractions in the polydisperse sample by size exclusion. The scatter of MW data points observed at higher elution volumes (as the RI signal returns to baseline, indicating zero

polymer concentration at these elution volumes) indicates that polymer is not being retained on the

SEC columns due to polymer-column affinity and/or overloading of the columns. Mass recovery of injected polymer samples was typically ≥ 90 wt % as determined by RI detection.

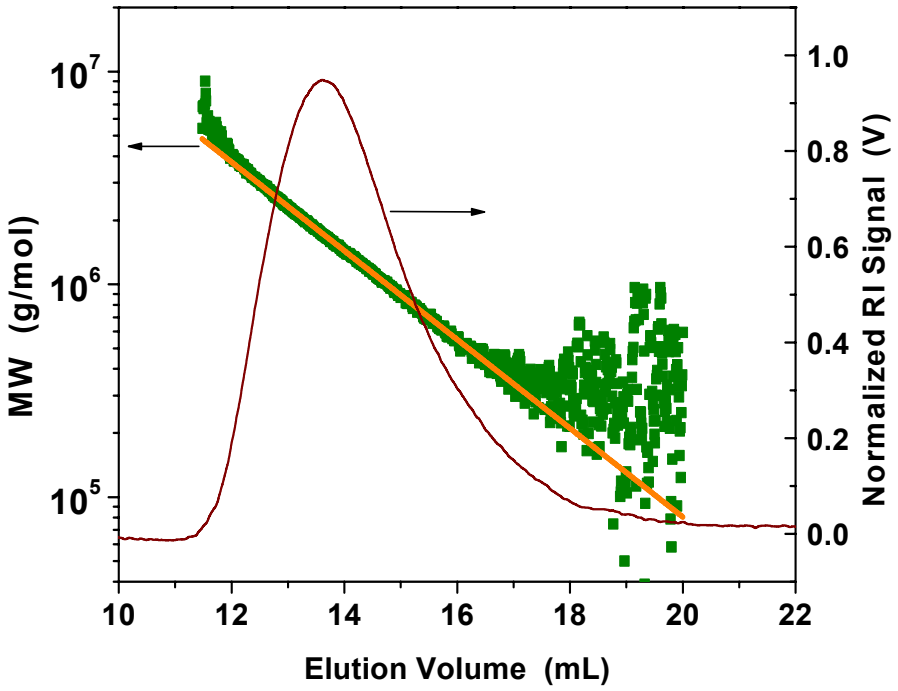

Figure 1.4. SEC-MALLS-RI data for AMBATAC-10-10 in 0.1 M NaCl pH 7 phosphate buffer.

Table 1.4. SEC-MALLS analytical data for AMBATAC polyampholytes.

Sample	d*n*/dc[a] (mL/g)	M_w[b] (10^6 g/mol)	PDI[b]	R_g[b,c] (nm)	$DP \times 10^{-4}$ [d]
Balanced					
AMBATAC-2.5-2.5	0.1729	1.38	1.63	60.9	1.79
AMBATAC-5-5	0.1737	1.51	1.51	65.7	1.90
AMBATAC-7.5-7.5	0.1738	1.56	1.72	64.6	1.84
AMBATAC-10-10	0.1861	1.52	1.65	66.5	1.63
Unbalanced					
AMBATAC-3-7	0.1754	1.34	1.83	58.8	1.63
AMBATAC-7-3	0.1765	1.53	1.80	64.5	1.91

[a] determined in 0.1 M NaCl pH7 phosphate buffer at 25 °C ± 0.5 °C

[b] determined *via* aqueous SEC-MALLS in 0.1 M NaCl pH 7 phosphate buffer

[c] R_g = weight-average radius of gyration

[d] *DP* = weight-average degree of polymerization, calculated from M_w and ^{13}C NMR compositional data

Table 1.4 lists the values of M_w, PDI, and R_g for the AMBATAC terpolymer series. The M_w values of the terpolymers range from $1.3 – 1.6 \times 10^6$ g/mol, corresponding to *DP*s of $1.6 – 1.9 \times 10^4$ repeat units. Figure 1.5 shows the MWDs of the AMBATAC terpolymers. All AMBATAC terpolymers exhibit unimodal MWDs of similar shape, with values of PDI ranging from 1.5 – 1.8. These data indicate that the use of NaOOCH in the synthesis of the AMBATAC series is effective at eliminating the effects of monomer feed composition on *DP* and maintaining PDIs < 2.0. Weight-average values of R_g for the AMBATAC terpolymers in the SEC eluent range from 61 – 67 nm (Table 1.4), further indicating that the AMBATAC terpolymers are all of similar size.

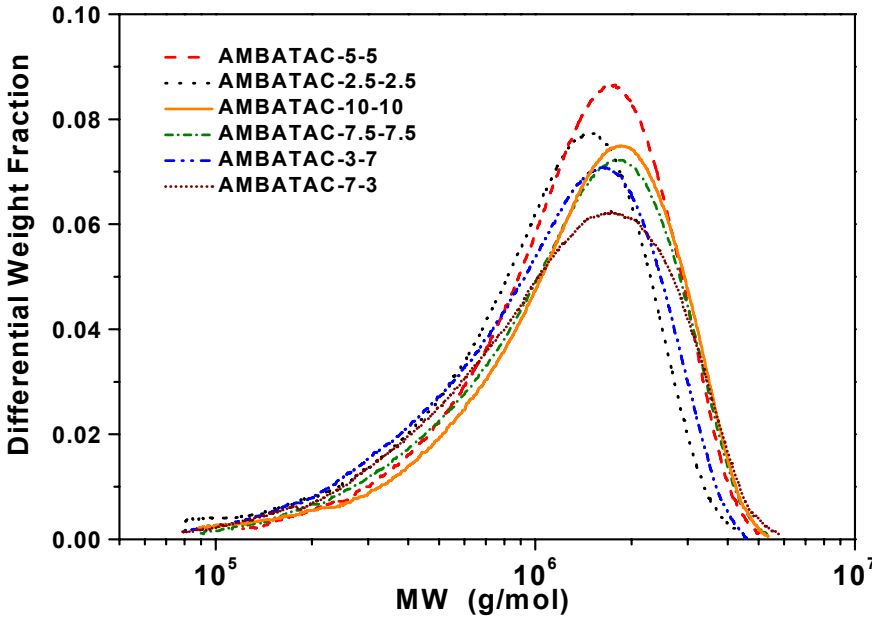

Figure 1.5. Molecular weight distributions of the AMBATAC terpolymer series.

Relationship of Radius of Gyration to Molecular Weight

Since SEC-MALLS analysis provides an R_g value for each slice of the chromatogram, the technique enables examination of the relationship between R_g and MW given by Equation 1

$$R_g = K_{Rg} \cdot M^{\rho} \quad \textbf{(1)}$$

where M is the polymer MW, and K_{Rg} and ρ are the intercept and slope of a log-log plot of R_g vs. M, respectively. The slope ρ reveals how the mass of the polymer fills space and is indicative of the macromolecular conformation in solution.[39] The theoretical slopes for hard spheres, random coils at theta conditions, random coils in good solvents, and rigid rods are 0.33, 0.50, 0.55 – 0.60, and 1.0, respectively. Figure 1.6 shows a log-log plot of R_g vs. M for AMBATAC-7-3 with ρ = 0.51, indicating that the terpolymer adopts a random conformation with slight expansion due to excluded volume effects under the given SEC conditions. Examination of the ρ values in Table 1.5 reveal that the AMBATAC terpolymers exist in conformations that range from slightly expanded random coils to slightly collapsed coils in 0.1 M NaCl pH 7 phosphate buffer. The ρ values of the charge-balanced AMBATAC terpolymers decrease with increasing ionic comonomer content, with AMBATAC-7.5-7.5 and AMBATAC-10-10 exhibiting ρ values less than 0.50. This implies that there is a net negative excluded volume effect in the higher charge density terpolymers (due to unscreened electrostatic attractions and/or greater hydrophobicity of the uncharged portion of the polymer backbone) and that these

terpolymers have slightly globular conformations under the conditions employed for SEC-MALLS analysis. It should also be noted that for the charge-balanced AMBATAC terpolymers, the preexponential term, K_{Rg}, increases with increasing ionic comonomer content and is lower for the unbalanced AMBATAC terpolymers. The former observation provides further evidence that the charge-balanced polyampholytes adopt more restricted conformations under the given SEC conditions with increasing level of ionic comonomer, while the latter observation indicates that the unbalanced terpolymers possess greater conformational freedom compared to the balanced terpolymers.

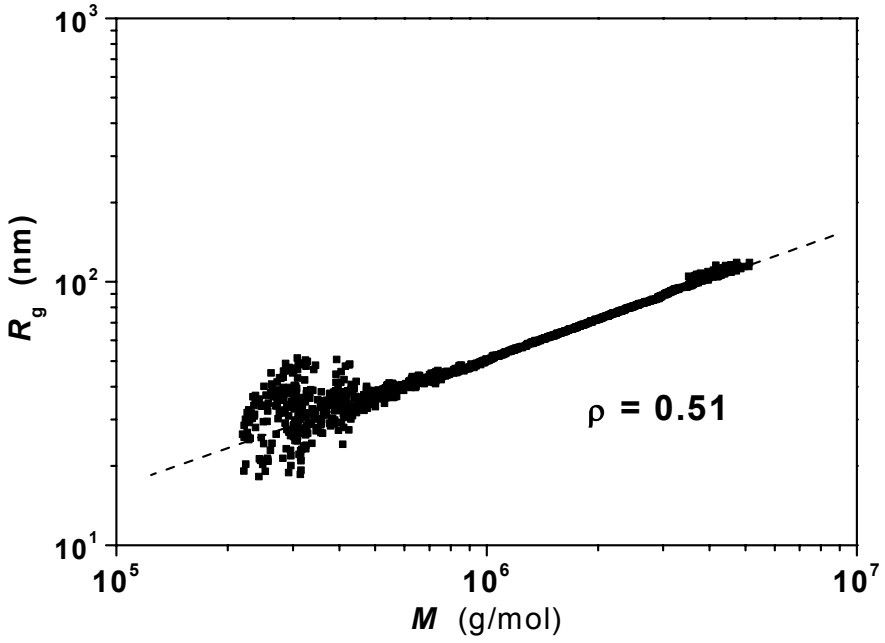

Figure 1.6. Log-log plot of R_g vs. M for AMBATAC-7-3 in 0.1 M NaCl pH 7 phosphate buffer.

Table 1.5. Coefficients of R_g-M relationship determined via SEC-MALLS.

Sample	K_{Rg}[a] (10^2 nm^{-1} (g/mol)$^{-\rho}$)	ρ[a]
Balanced		
AMBATAC-2.5-2.5	5.05	0.50
AMBATAC-5-5	6.08	0.50
AMBATAC-7.5-7.5	6.71	0.48
AMBATAC-10-10	11.5	0.46
Unbalanced		
AMBATAC-3-7	4.39	0.51
AMBATAC-7-3	4.69	0.51

[a] determined *via* aqueous SEC-MALLS in 0.1 M NaCl pH 7 phosphate buffer

Relationship of Intrinsic Viscosity to Molecular Weight

The intrinsic viscosity ([η]) of an unperturbed polymer coil in solution (i.e. at or near theta conditions, where excluded volume effects are minimal) is related to the MW and R_g of the coil by the Flory-Fox relationship (Equation 2),

$$[\eta] = 6^{\frac{3}{2}} \Phi_o \frac{\left(R_g\right)^3}{M} \quad \textbf{(2)}$$

where M is the MW of the polymer and Φ_o is the Flory viscosity constant.[40-41] Since the R_g-M relationships for the AMBATAC terpolymers reveal that the terpolymers are not exhibiting significant excluded volume effects under the given SEC conditions, the Flory-Fox relationship was used to determine the terpolymer intrinsic viscosities from the R_g and MW at each point on the SEC chromatogram. (Values of the Flory constant have been reported ranging from $1.81 - 2.87 \times 10^{23}$ mol^{-1}; for this work, the Hearst-Tagami asymptotic value of Φ_o for non-free-draining, linear flexible chains of high DP was employed, $\Phi_o = 2.19 \times 10^{23}$ mol^{-1}.[40]) The intrinsic viscosities of the unfractionated terpolymer samples (as determined via SEC-MALLS), $[\eta]_{SEC}$, were calculated using Equation 2, where $[\eta]_i$ is the intrinsic viscosity of chromatogram slice i in dL/g and c_i is the polymer concentration (determined via RI detection) of chromatogram slice i in g/dL.

$$[\eta]_{SEC} = \frac{\sum_i \left([\eta]_i \cdot c_i\right)}{\sum_i c_i} \quad \textbf{(3)}$$

The values of $[\eta]_{SEC}$ determined for the AMBATAC terpolymer series range from 4.89 – 5.67 dL/g (Table 1.6). To verify that the intrinsic viscosities calculated using the SEC-MALLS data and Flory-Fox relationship were correct, the intrinsic viscosities of the AMBATAC terpolymers in the SEC eluent were measured via low shear dilute solution viscometry at 25 °C (Table 1.6). The values of $[\eta]_{SEC}$ and $[\eta]$ determined by viscometry are in agreement, although the intrinsic viscosities for the charge-balanced AMBATAC terpolymers determined by viscometry tend to be slightly lower (7-10%) than the values determined from the SEC-MALLS data. These differences may be attributed to errors in viscometry sample concentrations due to associated water present (despite exhaustive drying) in the weighed terpolymers, leading to lower values of $[\eta]$. It should be noted that SEC-MALLS with RI detection is not susceptible to errors due to associated water, as the RI detector only detects the mass of polymer present in a given sample. Overall, the intrinsic viscosity data obtained by different methods agree, which further validates the use of the Flory-Fox relationship to calculate $[\eta]$ from SEC-MALLS data.

Table 1.6. Viscometric and SEC-MALLS data for the $[\eta]$-*M* relationship of the AMBATAC terpolymer series.

Sample	$[\eta]_{SEC}$[a] (dL/g)	$[\eta]$[b] (dL/g)	k_H[b]	K_{MHS}[c] (10^3 dL/g (g/mol)$^{-a}$)	a[c]	a (calculated)[d]
Balanced						
AMBATAC-2.5-2.5	4.89	4.53	0.41	2.83	0.53	0.50
AMBATAC-5-5	5.57	5.14	0.43	4.43	0.50	0.50
AMBATAC-7.5-7.5	5.40	4.96	0.40	7.12	0.46	0.44
AMBATAC-10-10	5.67	5.09	0.47	9.67	0.44	0.38
Unbalanced						
AMBATAC-3-7	4.96	4.78	0.30	3.36	0.55	0.53
AMBATAC-7-3	5.30	5.34	0.32	2.53	0.54	0.53

[a] determined using Flory-Fox relationship and SEC-MALLS data

[b] determined in 0.1 M NaCl phosphate buffer (pH 7) at 25 °C and 5.96 s^{-1}

[c] determined *via* aqueous SEC-MALLS in 0.1 M NaCl pH 7 phosphate buffer

[d] calculated using ρ value from R_g-M relationship

Table 1.6 also contains values of the Huggins constant, k_H, for the AMBATAC terpolymers in the SEC eluent, as determined via dilute solution viscometry. The k_H data provide additional information on polymer-solvent interaction and macromolecular conformation and correlate well with the ρ data in Table 1.5. The values of k_H range from 0.40 – 0.47 for the charge-balanced terpolymers; such k_H values are characteristic of polymers which are at or slightly below theta conditions.[42] However, the unbalanced terpolymers have k_H values in the range 0.30 – 0.32, indicating more favorable polymer-solvent interactions and more expanded random coil conformations in these systems.

The Mark-Houwink-Sakurada relationship (Equation 4) relates the intrinsic viscosity of a polymer coil in solution to the MW of the polymer; the coefficients K_{MHS} and a are determined from a log-log plot of [η] vs. M.[42] Like the R_g-M relationship, the MHS relationship provides information about the properties of macromolecules in solution which are correlated to macromolecular structure and polymer-solvent interactions.

$$[\eta] = K_{\mathrm{MHS}} \cdot M^{a} \qquad \textbf{(4)}$$

Using the MW and [η] data from SEC-MALLS analysis, MHS parameters (i.e. K_{MHS} and a) for the AMBATAC terpolymers in 0.1 M NaCl pH 7 phosphate buffer at 25 °C were determined (Table 1.6). Values of [η] for each slice of the chromatogram ($[\eta]_i$) were plotted as a function of the MW of each slice (M_i) to yield MHS plots; Figure 1.7 shows the log-log plot of [η] versus M from which the MHS parameters for AMBATAC-5-5 were calculated. Examination of the MHS parameters listed in Table 1.6 reveals that the a values for the charge-balanced terpolymers increase with increasing ionic comonomer content, while the values of K_{MHS} for the charge-balanced terpolymers decrease with increasing ionic comonomer content. This trend indicates that the charge-balanced terpolymer coils adopt more collapsed conformations and interact less favorably with the SEC eluent as the terpolymer charge density increases. The a values for the unbalanced terpolymers are greater than those of the balanced systems, and the values of K_{MHS} are lower than that of AMBATAC-5-5, the charge-balanced terpolymer of similar charge density. The a values are expected to be higher for the unbalanced systems due to their polyelectrolyte character, which would lead to more expanded conformations under the SEC conditions (i.e. due to any unscreened electrostatic repulsions). While the unbalanced terpolymers contain levels of AM similar to those found in AMBATAC-5-5, the lower values of K_{MHS} for these terpolymers suggest that increased polymer-solvent interactions and greater conformational mobility occur in the unbalanced systems.

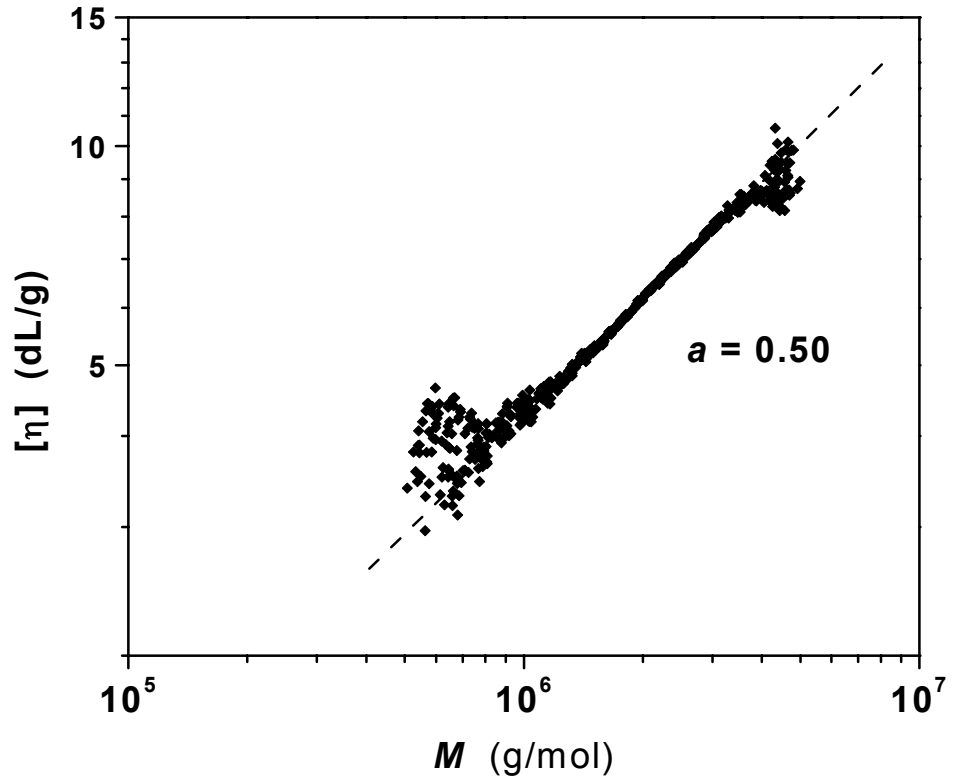

Figure 1.7. Mark-Houwink-Sakurada plot for AMBATAC-5-5 in 0.1 M NaCl pH 7 phosphate buffer at 25 °C.

The MHS *a* value is related to the ρ value of the R_g-*M* relationship by Equation 5, which derives from the Flory-Fox theory.[40] To verify the applicability of the Flory-Fox equation to these systems, values of *a* were calculated from the ρ values in Table 1.5. Overall, the calculated values of *a* (Table 1.6) were found to agree well with the experimentally determined *a* values. However, the calculated (i.e. via the Flory-Fox relationship) *a* value for AMBATAC-10-10 (a_{calc} = 0.38) was significantly lower than the experimental value (a_{expt} = 0.44). This difference may be attributed to negative excluded volume effects (collapse due to unscreened electrostatic attractions and increased backbone hydrophobicity) that occur for AMBATAC-10-10 under the SEC conditions. Such negative excluded volume effects cause deviation from ideal Flory-Fox behavior, which relies on the assumption that the polymer adopts a random coil conformation with zero net excluded volume.

$$a = (3 \cdot \rho) - 1 \qquad \textbf{(5)}$$

Potentiometric Titration

Potentiometric titration of the AMBATAC terpolymer solutions in DI water was conducted to determine the apparent pK_a values for the carboxylate groups on the AMB repeat units. Figures 1.8 and 1.9 show potentiometric curves for the charge-balanced AMBATAC terpolymers and the AMBATAC terpolymers of similar charge density with differing ratios of anionic to cationic monomer content, respectively. The curves in Figure 1.8 are shifted upward with increasing levels of NaAMB content in the terpolymers. This shift to higher pH values at similar degrees of ionization indicates that the terpolymers become less acidic as the level of NaAMB in the terpolymer is increased. This phenomenon is similar to that observed by McCormick and Elliot[23] in copolymers of AM with NaAMB. A analogous trend is observed in Figure 1.9 for the AMBATAC terpolymers of similar charge density: As the ratio of AMB:APTA units in the terpolymers increases, the titration curves shift upward, indicating decreased acidity of the terpolymers with increasing NaAMB content. The decrease in cationic character of the terpolymers with increasing NaAMB incorporation may also play a role in the shifting of the titration curves in Figure 1.9, as ionization of the AMB carboxylic acid groups will be more favorable in terpolymers with greater cationic character (due to stabilization of negative carboxylate charges by positive quaternary ammonium charges). Table 1.8 lists the apparent pK_a values for the AMBATAC terpolymer series in DI water. Knowledge of such pK_a values is important in the study of pH-responsive polyampholytes, as the degree of ionization of the AMBATAC terpolymers at a given pH dictates whether the terpolymer will exhibit polyampholyte or polyelectrolyte behavior.

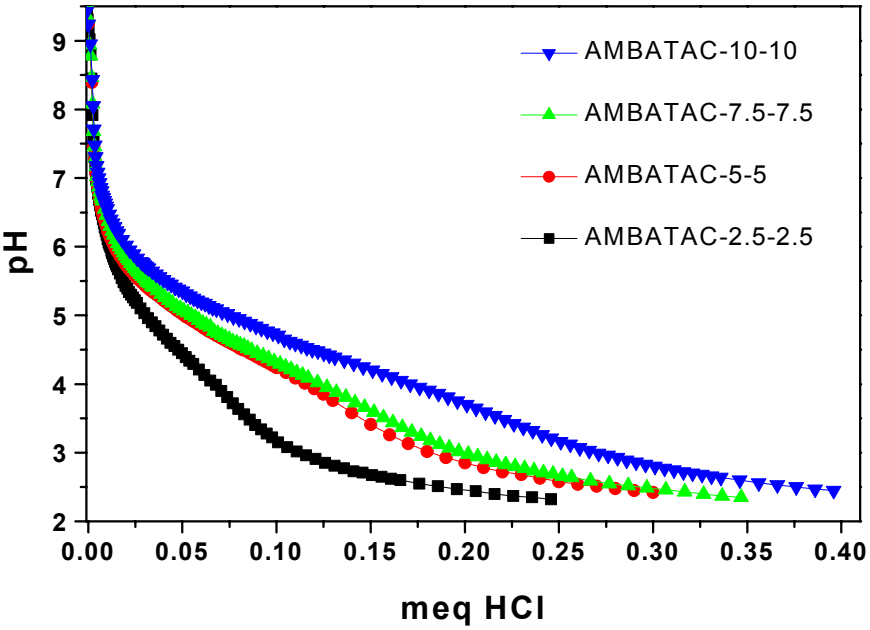

Figure 1.8. Potentiometric titration curves for the charge-balanced AMBATAC terpolymers.

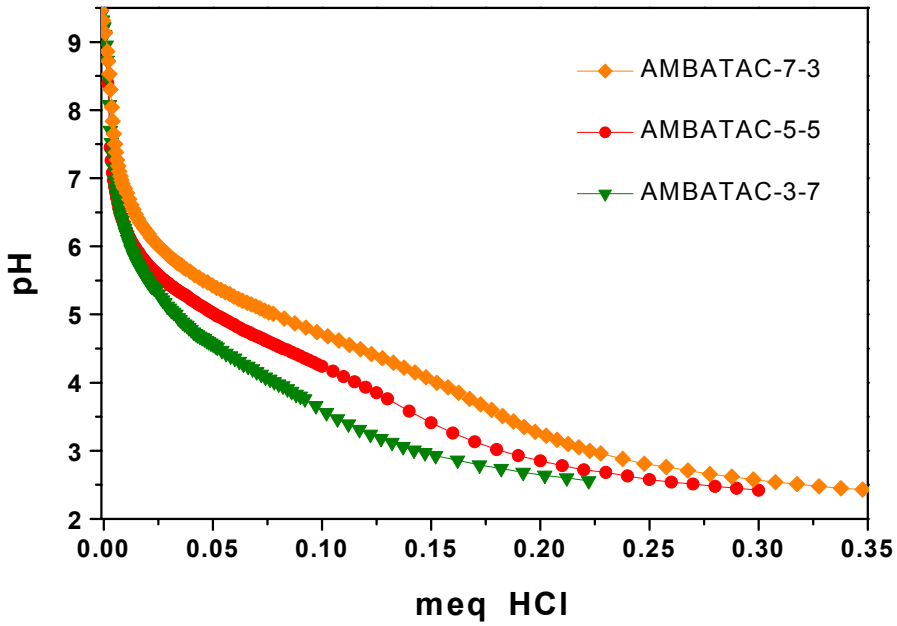

Figure 1.9. Potentiometric titration curves for the AMBATAC terpolymers of similar charge density with varying ratio of AMB:APTA units.

Table 1.7. Apparent pK_a values for the AMBATAC terpolymer series.

Sample	Apparent pK_a of AMB COOH group [a]
Balanced	
AMBATAC-2.5-2.5	5.11
AMBATAC-5-5	5.13
AMBATAC-7.5-7.5	5.51
AMBATAC-10-10	5.73
Unbalanced	
AMBATAC-3-7	5.06
AMBATAC-7-3	5.28

[a] determined in DI water at 25 °C

Terpolymer solubility

Solubility in the absence of electrolytes: The solubility of the AMBATAC polyampholytes in DI water was examined at both semidilute (c = 2.0 g/dL) and dilute (c = 0.1 g/dL) concentrations. The ambient pH of terpolymer solutions in DI water was

typically 6.5 ± 0.2, corresponding to degrees of AMB unit ionization of ≥ 90 % (based on the apparent pK_a values listed in Table 1.7).

The unbalanced AMBATAC terpolymers (-3-7 and -7-3) exhibited the greatest solubility in DI water, yielding totally transparent solutions under dilute and semidilute conditions. The unbalanced terpolymers were also observed to dissolve faster than the charge-balanced systems. The charge-balanced polyampholytes AMBATAC-2.5-2.5 and -5-5 also exhibited excellent solubility in DI water, yielding transparent solutions at dilute concentrations and transparent solutions with a slight haze under semidilute conditions. Semidilute solutions of the higher charge density AMBATAC-7.5-7.5 and -10-10 terpolymers were also transparent, yet slightly hazier than the lower charge density terpolymer solutions. The increased haziness of these solutions is most likely caused by microaggregates of oppositely-charged repeat units that scatter light; however, no decrease in optical transmittance was detectable via turbidimetry. At dilute concentrations, AMBATAC-7.5-7.5 and -10-10 were readily dispersible in DI water under gentle mixing, yielding hazy, yet exceedingly translucent solutions. When left to stand for long periods of time (days to weeks), phase separation of the dilute solutions was observed, with two transparent layers forming in the solution. Phase separation occurred within 48 h for AMBATAC-7.5-7.5, while AMBATAC-10-10 remained dispersed for one to two weeks before phase separation was observed. (This phase separation phenomenon was further investigated for AMBATAC-7.5-7.5; the results are discussed in a later section.)

The solubility of the AMBATAC terpolymers in DI water is readily explained in terms of terpolymer charge density and charge asymmetry. The charge density is defined in terms of the number of anionic and cationic groups incorporated into the polymer. Charge asymmetry describes the degree of charge imbalance present in a polyampholyte.[43] For a polyampholyte of N repeat units containing a fraction, f_+, of positive repeat units and a fraction, f_-, of negative repeat units, the charge asymmetry, σN, is given by Equation 6, where $N_+ = f_+ \cdot N$ is the number of cationic repeat units and $N_- = f_- \cdot N$ is the number of anionic repeat units present in the terpolymer. Table 1.2 lists the charge densities and charge asymmetries for the AMBATAC polyampholytes. The charge asymmetries in Table 1.8 were calculated assuming 100 % neutralization of the AMB repeat units to the carboxylate form. It should be noted that the charge densities and charge asymmetries of the AMBATAC polyampholytes are pH-dependent and will change significantly on protonation of the AMB repeat units at lower solution pH values (i.e. $N_- = f_- \cdot N$ is a function of pH) . Figure 1.10 shows the charge asymmetries of the AMBATAC terpolymers as a function of pH.

$$\sigma N = \frac{(N_+ - N_-)^2}{N_+ + N_-} \qquad \textbf{(6)}$$

Table 1.8. Charge densities and charge asymmetries of the AMBATAC terpolymers.

Sample	Charge density[a] (mol %)	Charge Asymmetry σN^a
Balanced		
AMBATAC-2.5-2.5	5.8	1.23
AMBATAC-5-5	8.9	1.92
AMBATAC-7.5-7.5	13.8	0.53
AMBATAC-10-10	22.1	1.84
Unbalanced		
AMBATAC-3-7	9.8	216
AMBATAC-7-3	10.6	208

[a] assuming complete ionization of AMB repeat units

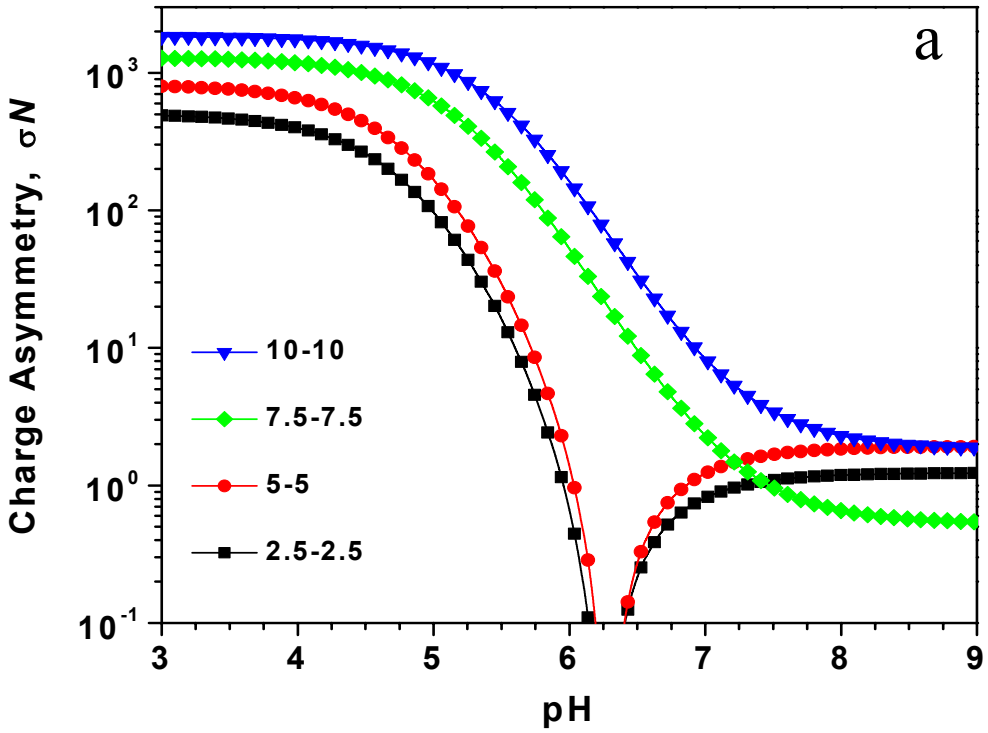

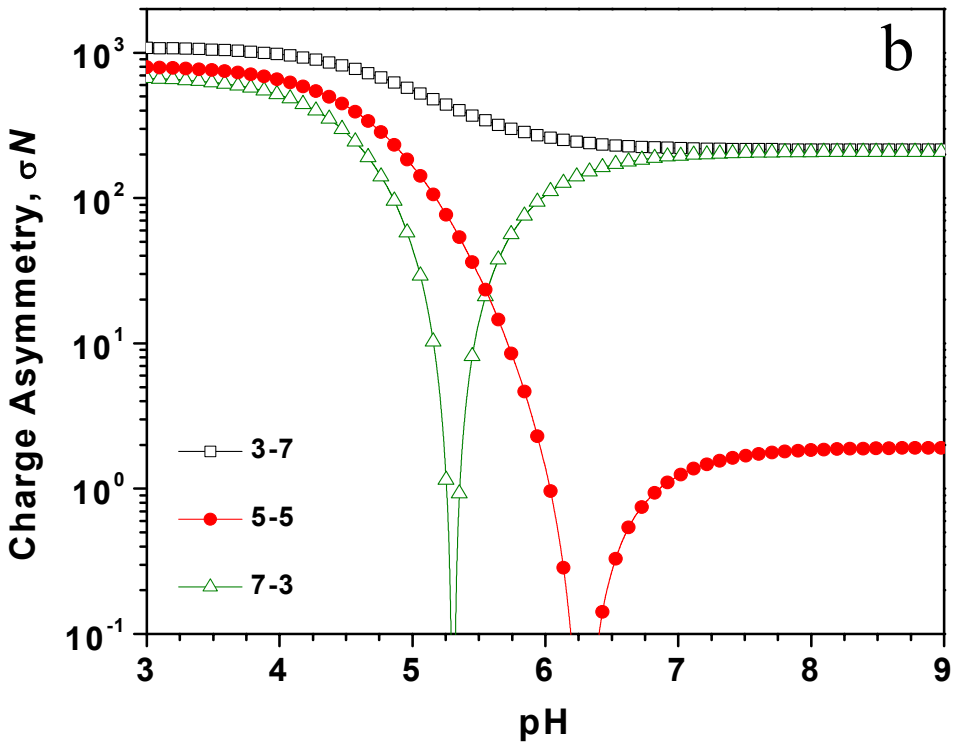

Figure 1.10. Charge asymmetry, $\sigma \cdot N$, of the AMBATAC terpolymers in DI water as a function of solution pH: a) charge-balanced terpolymers, b) unbalanced terpolymers with AMBATAC-5-5 (charge-balanced) shown for comparison.

The extremely favorable solubility of the unbalanced AMBATAC terpolymers is due to the high charge asymmetries of these systems. The repulsion between uncompensated charges in AMBATAC-3-7 and -7-3 result in intra- and intermolecular electrostatic repulsions that dominate polymer-polymer and polymer-solvent interactions, imparting polyelectrolyte-like solubility to the unbalanced systems. The high degree of solubility in DI water observed for AMBATAC-2.5-2.5 and -5-5 is attributed not only to the high level of AM content in the polymers, but also to the minor charge asymmetries; both features serve to stabilize the polyampholyte coils against phase separation.

The diminished solubilities and subsequent phase separation of AMBATAC-7.5-7.5 and -10-10 are due to the higher charge densities of these systems; the terpolymers lack sufficient AM content to counter the effects of electrostatic attraction that induce coil collapse and intermolecular aggregation. Although the charge density of AMBATAC-10-10 is greater than that of AMBATAC-7.5-7.5, the phase separation process is slower in AMBATAC-10-10 due to its greater charge asymmetry, suggesting initial electrostatic stabilization of the terpolymer coils. With time, the AMBATAC-10-10 coils may undergo conformational changes that allow electrostatic attractions to overcome the stability offered by the charge asymmetry, and phase separation occurs.

The ability of AMBATAC terpolymers to relax into more energetically-favorable conformations over time is enhanced due to the semiquenched nature of these pH-responsive polyampholytes.[44] The cationic APTA groups are characteristic of those found in quenched polyampholytes; that is, the distribution of non-pH-responsive quaternary ammonium monomers is "locked" in place during polymerization. In contrast, the anionic AMB units are representative of charged groups found in annealed polyampholytes, in which the distribution of charges (negative charges, in the case of the AMBATAC terpolymers) depends upon solution pH. At solution pH values where the degree of AMB ionization is < 100 %, the anionic charges can be redistributed via proton transfer from one carboxylate group to another until an equilibrium distrubution is attained. For AMBATAC-10-10 at ambient pH (6.7), approximately 10 % of the AMB units are still protonated, suggesting that the terpolymer undergoes an annealing process in which an equilibrium distribution of charges and more energetically favorable polymer conformation are attained. This proposed annealing process ultimately leads to the observed phase separation.

Phase separation of AMBATAC-7.5-7.5: When left to stand for 48 h, the AMBATAC-7.5-7.5 solution in DI water (c = 0.1 g/dL) was observed to phase-separate into two transparent layers. The lower phase was of significantly smaller volume (ca. 5-10 %) than the upper phase and exhibited a slight bluish haze; the upper phase was completely clear. Upon gentle mixing, the lower phase was readily dispersed in the upper phase, the resulting solution having the appearance of the initial AMBATAC-7.5-7.5 solution. Similar behavior was observed for dilute solutions of AMBATAC-10-10 in DI water; however the phase-separation process was much slower, requiring one to two weeks before distinct layers were observed in the solution.

Because differences between the two phases could not be accurately measured via turbidimetry (due to lack of sensitivity), SEC-MALLS was used to determine the terpolymer concentration in each phase. Figure 1.11 shows SEC-MALLS chromatograms of the initial AMBATAC-7.5-7.5 solution and the upper and lower phases following phase separation. Using online refractometry and the dn/dc value for AMBATAC-7.5-7.5, the terpolymer concentrations were determined to be 0.09 g/dL, 0.04 g/dL, and 0.76 g/dL in the initial solution, upper phase, and lower phase, respectively. The concentration data indicate that 95 % of the polymer in solution partitions into the lower phase. SEC-MALLS analysis also indicated a difference in the MW of the terpolymer fractions in each phase. The M_w of the terpolymer in upper phase was 0.97×10^6 g/mol, and the terpolymer M_w in the lower phase was 2.35×10^6 g/mol. Rheological analysis was also performed on the initial solution and phase separated layers. The viscosity of the initial solution was 1.02 cP, whereas the viscosities of the upper and lower phases were 0.92 cP and 9.8 cP, respectively.

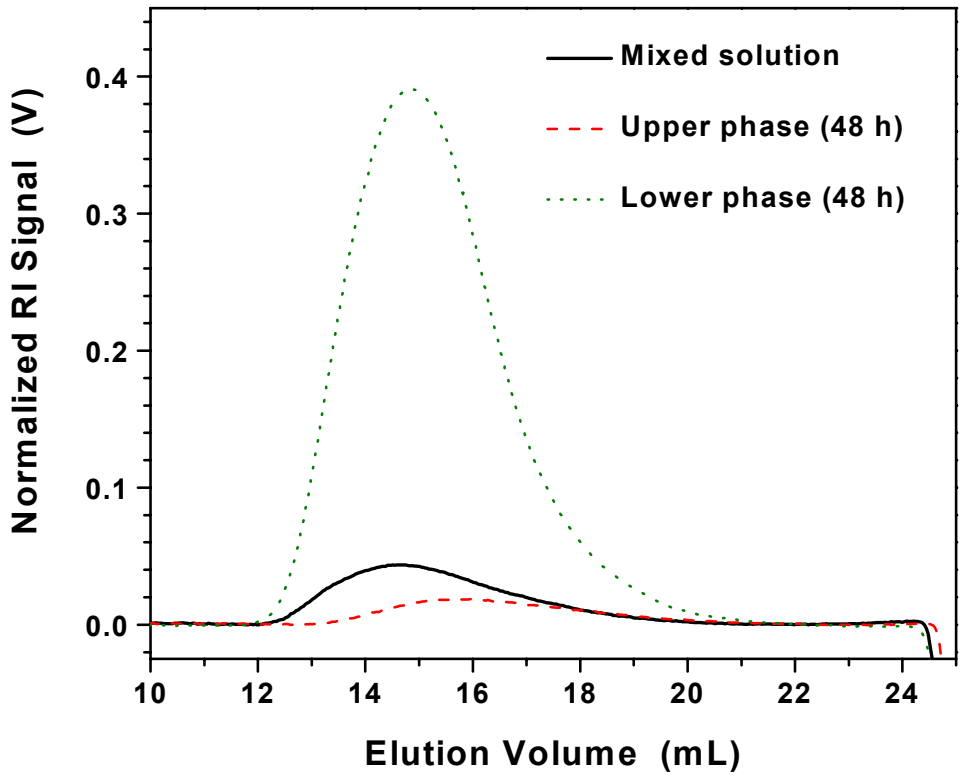

Figure 1.11. SEC chromatograms for AMBATAC-7.5-7.5 solution in DI water, before and after phase separation.

These data indicate that the dilute solution of AMBATAC-7.5-7.5 in DI water separated into a dilute, polymer-poor phase and a semidilute, polymer-rich phase, with the higher MW fractions of the polydisperse sample partitioning into the polymer-rich phase. The observed phenomenon is consistent with the theoretical predictions of Joanny and coworkers,[45-46] which state that neutral polyampholytes will separate into a high concentration phase of interpenetrating polymer chains and a dilute solution of collapsed globules, even in good solvents (in the absence of salt).

Salt-responsive solution viscosity

Figure 1.12 shows the reduced viscosity of the charge-balanced AMBATAC terpolymers as a function of [NaCl]. All the charge-balanced terpolymers exhibit increases in viscosity with increasing [NaCl], indicating classic "antipolyelectrolyte" behavior. The magnitude of coil expansion (as implied from the viscosity increases) becomes greater with increasing ionic comonomer content due to greater electrostatic interactions at higher charge densities. The solution viscosities at low [NaCl] (10^{-2} M) increase with decreasing terpolymer charge density in the order AMBATAC-10-10 < -7.5-7.5 < -5-5 < -2.5-2.5, and at [NaCl] ≥ 0.1 M the higher charge density terpolymers tend to exhibit greater viscosities. However, in high ionic strength solutions,

AMBATAC-5-5 exhibits higher viscosities than AMBATAC-7.5-7.5. Although AMBATAC-7.5-7.5 exhibits a slightly lower *DP* and slightly greater PDI than AMBATAC-5-5 (Table 1.4), these differences in MW and MWD do not seem significant enough to explain the observed trend.

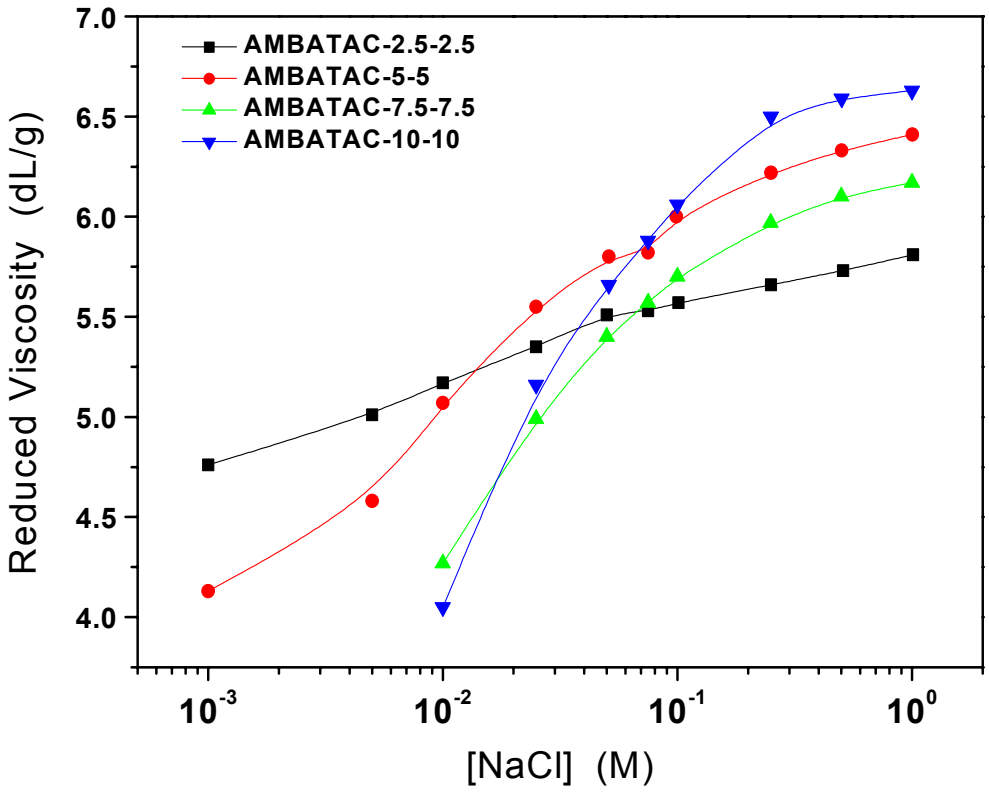

Figure 1.12. Reduced viscosity of charge-balanced AMBATAC terpolymers as a function of NaCl concentration at ambient pH (6.5 ± 0.2). Polymer concentration = 0.1 g/dL.

Because electrostatic interactions are greatly diminished at elevated ionic strengths (due to charge screening), the salt-responsive behavior at high [NaCl] (> 0.1 M) indicates that the polymer-solvent interaction of the uncharged portion of the terpolymers is affecting the solution viscosities. As the AM content of the AMBATAC terpolymers decreases, the polymer backbone is rendered more hydrophobic by the increased levels of AMB and APTA side chains, causing decreased polymer-solvent interaction upon screening of electrostatic interactions by added electrolyte. However, the steric bulk of the AMB and APTA side chains increases polymer chain stiffness, countering the effects of decreased polymer-solvent interaction. Therefore, the observed salt-response at [NaCl] > 0.1 M results from the composite effects of decreasing polymer-solvent interaction and increasing chain stiffness.

To assess the effect of ionic strength on the PAM backbone, the reduced viscosity of a PAM homopolymer with a *DP* comparable to those of the AMBATAC terpolymers (DP_{PAM} = 1.94 × 10^4 repeat units) was examined as a function of [NaCl] (Figure 1.13). The uncharged PAM exhibits increasing reduced viscosity with increasing [NaCl], indicating greater polymer-solvent interaction with increasing ionic strength. Munk and coworkers[47] have also shown that PAM exhibits increased polymer-solvent interaction in aqueous solution with increasing [NaCl]. Thus, the "antipolyelectrolyte" effect in the lower charge density AMBATAC-2.5-2.5 and -5-5 terpolymers is actually enhanced due to the high AM content of these terpolymers.

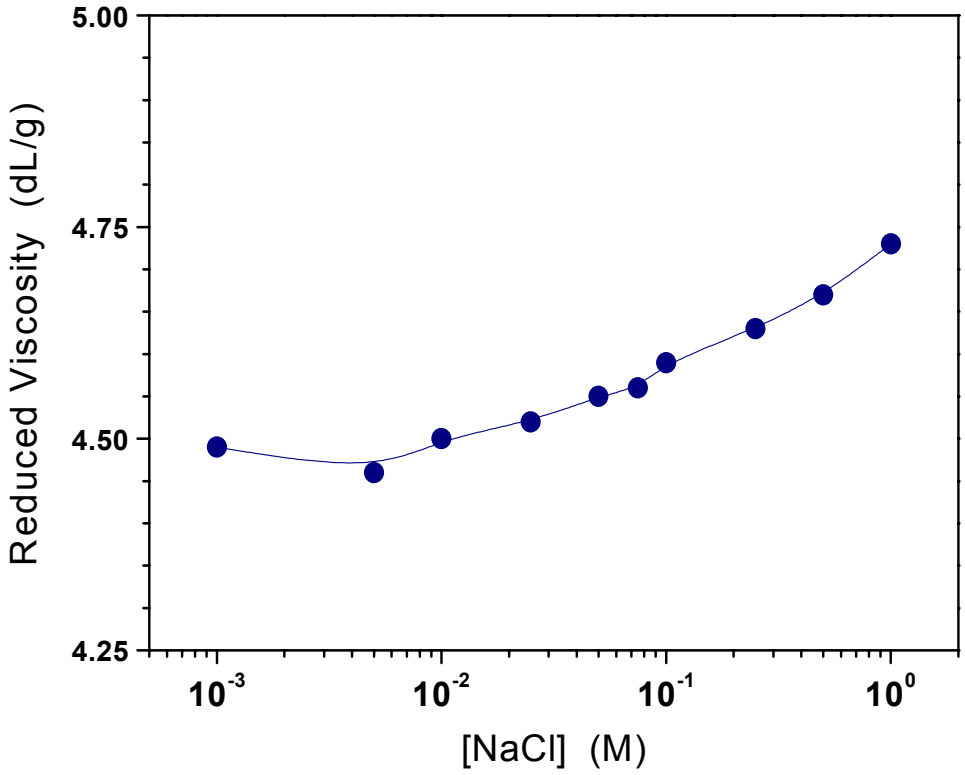

Figure 1.13. Reduced viscosity of PAM homopolymer (*DP* = 1.94 × 10^4) as a function of NaCl concentration at ambient pH (6.5 ± 0.2). Polymer concentration = 0.1 g/dL.

Figure 1.14 shows the reduced viscosity of the unbalanced AMBATAC terpolymers as a function of [NaCl]; the reduced viscosity vs. [NaCl] data for charge-balanced terpolymers of similar charge densities (AMBATAC-5-5 and -7.5-7.5) are also shown for comparison. AMBATAC-3-7 and -7-3 exhibit typical polyelectrolyte behavior, with extremely high solution viscosities at low ionic strengths that decrease dramatically upon increasing [NaCl] (due to screening of charge-charge repulsions along the polymer chains). The viscosity of AMBATAC-7-3 is greater than AMBATAC-3-7 at all ionic strengths; this is most likely due to the difference in *DP* (ca. 3000 repeat units) between the two terpolymers. The data for the unbalanced terpolymers do not show any evidence of charge-charge attractions being screened on electrolyte addition (i.e. no indication of

the "antipolyelectrolyte" effect is observed), thus the excess charge on the unbalanced polyampholytes dominates their solution viscosities. This behavior is consistent with the theories of Higgs and Joanny[44-45] and Dobrynin and Rubinstein.[43] Figure 1.14 also demonstrates that the magnitude of the polyelectrolyte effect observed for the unbalanced systems is significantly greater than the magnitude of the "antipolyelectrolyte" effect exhibited by the charge-balanced systems. The difference is due to the nature of the transitions that occur upon screening of the electrostatic interactions in each system: polyelectrolytes undergo a rod-to-coil contraction,[48] whereas polyampholytes undergo a globule-to-coil expansion.[43,45] Although both systems exist as random coils at high ionic strength, the hydrodynamic volume that is lost in the rod-to-coil transition is much greater than the hydrodynamic volume gained in the globule-to-coil transition.

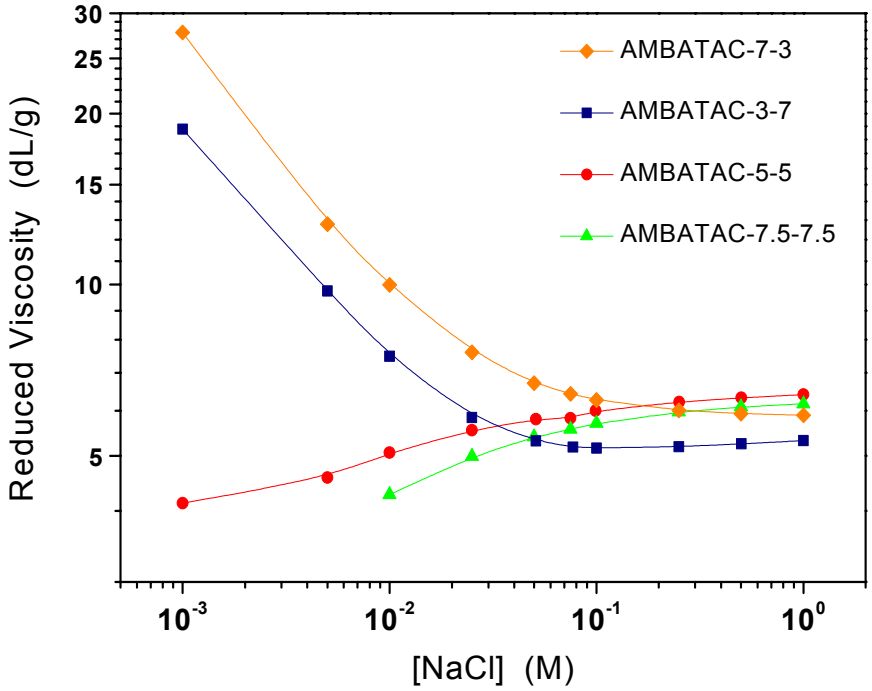

Figure 1.14. Reduced viscosity of unbalanced AMBATAC terpolymers as a function of NaCl concentration at ambient pH (6.5 ± 0.2). Polymer concentration = 0.1 g/dL. AMBATAC-5-5 and AMBATAC-7.5-7.5 (charge-balanced) shown for comparison.

In the absence of electrolytes: Figure 1.15 shows dilute solution (c = 0.1 g/dL) reduced viscosities as a function of pH for the AMBATAC terpolymers in DI water. In the absence of added electrolytes, the terpolymers exhibit the most profound pH response because electrostatic interactions can occur over very long ranges in the salt-free solutions (i.e. charge screening is virtually nonexistent). The charge-balanced terpolymers (Figure 1.15a) all exhibit similar pH-responsive behavior, although the magnitude of the observed behavior is highly dependent on terpolymer charge density. At low solution pH (2–3.5), the charge-balanced terpolymers exist as cationic

polyelectrolytes due to protonation of the AMB carboxylate groups. Below pH 3.5, a distinct polyelectrolyte effect is observed: the extended polyelectrolyte coils undergo conformational contraction due to the increasing ionic strength of the medium as HCl is added to lower the solution pH. As solution pH increases from 3.5 to 7, the AMB units are neutralized, triggering polyampholyte behavior and collapse of the terpolymer coils due to electrostatic attraction. The minima in the pH traces for each terpolymer correspond to the isoelectric points (IEPs) of the solutions. (It should be noted that the observed solution IEPs represent the average IEP for all terpolymers in solution and that the IEP of individual terpolymers in a given sample is likely to occur over a small range of pH due to a) the polydispersity of the samples, and b) slight compositional fluctuations that may occur from polymer to polymer.) Above pH 7.5, the AMB carboxylate groups are completely ionized, and the charge-balanced terpolymers exist as collapsed polyampholyte globules.

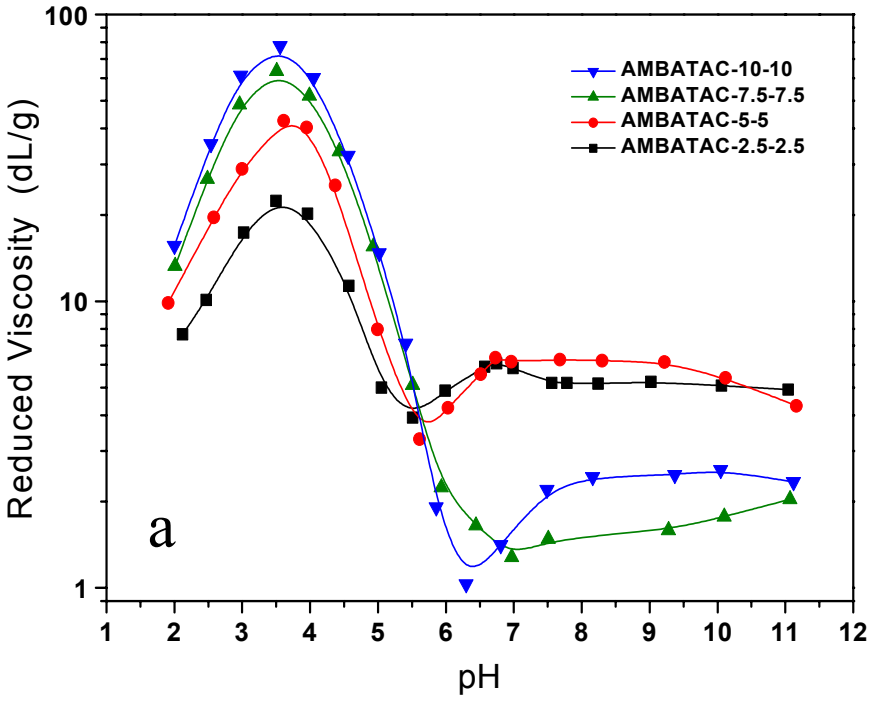

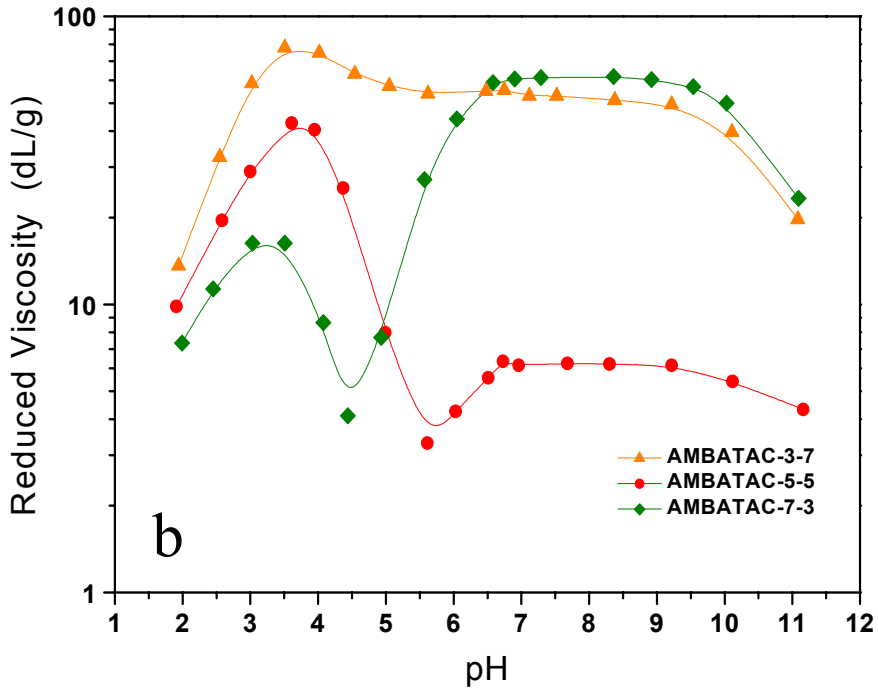

Figure 1.15. Reduced viscosity of the AMBATAC terpolymers in DI water as a function of solution pH: a) charge-balanced terpolymers, b) unbalanced terpolymers with AMBATAC-5-5 (charge-balanced) shown for comparison. Polymer concentration = 0.1 g/dL.

Dobrynin and Rubinstein[43] state that for polyampholytes with charge asymmetries $\sigma N > 1$, the charge excess stretches the collapsed polyampholyte globule into an elongated shape. When fully ionized, AMBATAC-2.5-2.5, -5-5, and -10-10 possess charge asymmetries $\sigma N > 1$ (Figure 1.10), and exhibit significant increases in viscosity above their solution IEPs. This is evidence that the collapsed coils are being stretched as excess AMB units become ionized. Also, a slight polyelectrolyte effect is detectable for AMBATAC-5-5 at high pH values, due to screening of excess AMB negative charges as NaOH is added to the solution to increase pH. In the low pH regime, the charge asymmetries increase to very high asymptotic values ($\sigma N >> 1$) with decreasing pH (Figure 1.10), corresponding to the observed polyelectrolyte behavior.

At low pH, AMBATAC-7.5-7.5 exhibits the same polyelectroyte behavior as the other charge-balanced terpolymers, yet the terpolymer has a charge asymmetry $\sigma N = 0.53$ above its IEP and remains collapsed upon complete ionization of the AMB units. Indeed, a slight "antipolyelectrolyte" effect is observed at higher pH values for AMBATAC-7.5-7.5, due to screening of charge-charge attractions by excess NaOH added to raise solution pH. Figure 1.16a shows the charge asymmetry and reduced viscosity as functions of pH for AMBATAC-7.5-7.5. The charge asymmetry and reduced viscosity decrease in the same manner with increasing pH, suggesting that charge asymmetry is a useful theoretical tool for predicting pH-responsive polyampholyte solution properties. That the curves do not exactly overlap is most likely due to the polydispersity of the AMBATAC-

7.5-7.5 sample (i.e. the theory assumes a monodisperse polyampholyte); nonetheless, there is clear qualitative agreement between the theoretical predictions and experimental observations.

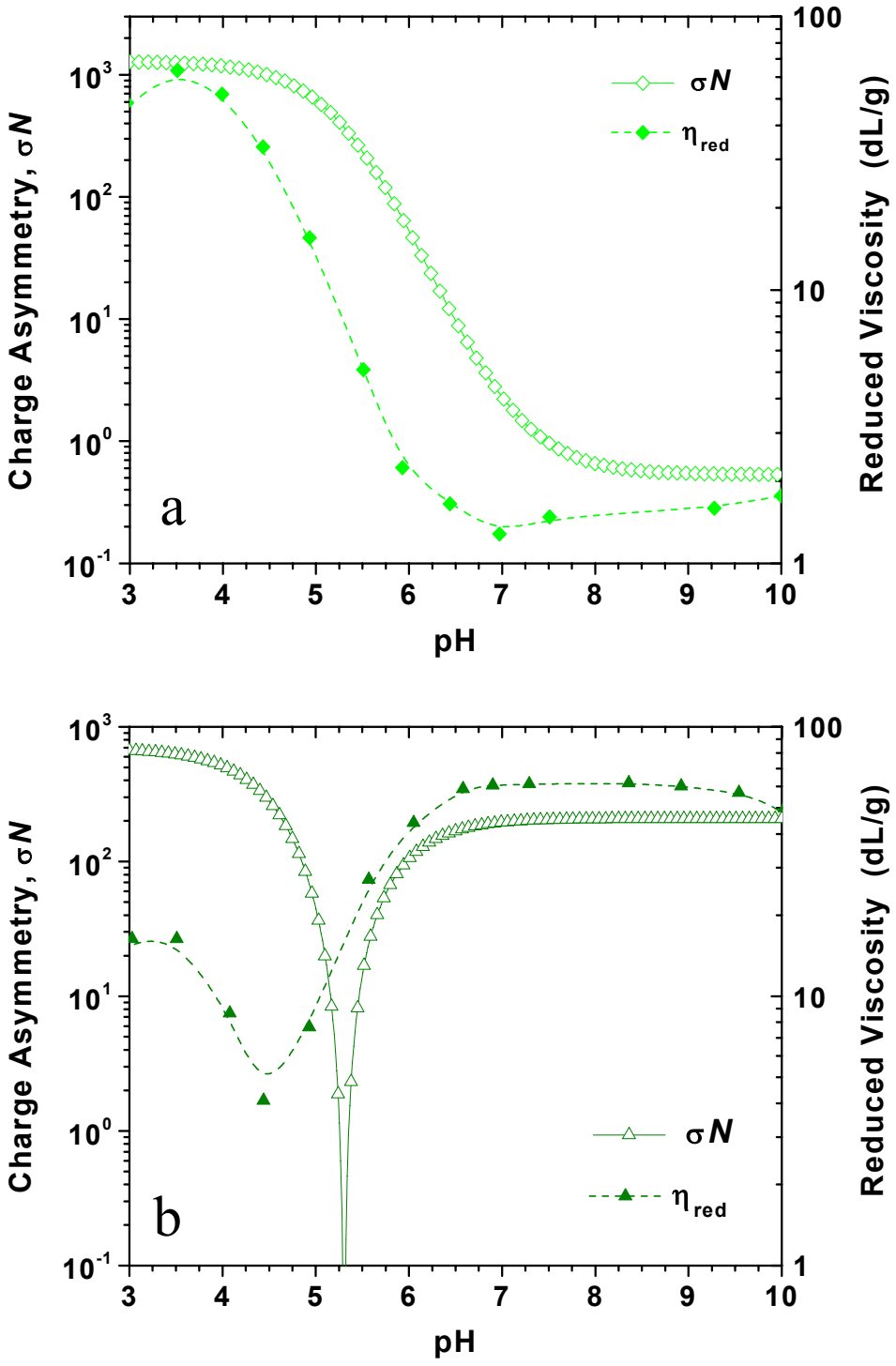

Figure 1.16. Charge asymmetry and reduced viscosity as a function of pH for a) AMBATAC-7.5-7.5, and b) AMBATAC-7-3 in DI water. Polymer concentration = 0.1 g/dL.

The unbalanced terpolymers (Figure 1.15b) exhibit markedly different pH-dependent behavior compared to a charge-balanced terpolymer of similar charge density (AMBATAC-5-5). Due to their large charge asymmetries (Table 1.8, Figure 1.10), the unbalanced terpolymers are expected to exhibit significant polyelectrolyte behavior. AMBATAC-3-7 displays polyelectrolyte behavior over the entire range of solution pH and does not exhibit an IEP (due to the large excess of non-pH-responsive APTA groups); however, a small decrease in solution viscosity is observed from pH 3.5 to 7. The decrease is due to electrostatic attractions that occur upon ionization of the AMB units, causing local collapses along the otherwise extended polyelectrolyte chain. This behavior is consistent with the "necklace" model of Kantor and Kardar,[49-51] as well as the predictions of Dobrynin and Rubinstein's polyampholyte theory.[43]

AMBATAC-7-3 exhibits a more complex reduced viscosity profile as a function of pH. At low solution pH (2–3.5), AMBATAC-7-3 behaves as a weakly-charged cationic polyelectrolyte. As the solution pH is increased, an IEP is observed pH ≈ 4.5; at this pH, the number of ionized AMB repeat units and APTA repeat units are equal. With increasing pH, the number of ionized AMB repeat units begins to greatly exceed the number of APTA units, thus rendering AMBATAC-7-3 an anionic polyelectrolyte at high pH. At high pH, AMBATAC-7-3 also adopts the "necklace" conformation due to unscreened attractions between AMB and APTA units. Figure 1.16b shows the charge asymmetry and reduced viscosity as functions of pH for AMBATAC-7-3. Again, the theoretical charge asymmetry correlates well with the experimental data, although the observed polyampholyte region occurs over a wide range of pH than that predicted by the theoretical relationship, presumably due to the polydispersity of AMBATAC-7-3 sample.

At low ionic strength: Figure 1.17 shows the dilute solution (c = 0.1 g/dL) reduced viscosities as a function of pH for the AMBATAC terpolymers in 0.01 M NaCl. Compared to the solution viscosities in DI water (Figure 1.15), the reduced viscosities at pH values < 6.0 are significantly lower in 0.01 M NaCl, due to screening of the charge-charge repulsions between the cationic APTA groups; however, the electrostatic attractions are still operative at pH values ≥ 5.5, as indicated by decreases in solution viscosity. In the polyampholyte regime (above pH 6.0), the solution viscosities decrease with increasing charge density because the effects of charge asymmetry are no longer operative. The stretching of the charge-balanced polyampholytes with charge asymmetries $\sigma N > 1$ observed in DI water is eliminated by the addition of 0.01 M NaCl (i.e. no viscosity increases or polyelectrolyte effects are observed above the solution IEPs). This is due to screening of the uncompensated charges by the added electrolyte. For the unbalanced terpolymers (Figure 1.17b), the addition of 0.01 M NaCl causes dramatic decreases in solution viscosity across the entire pH range due to screening of the repulsive electrostatic forces. However, the unbalanced terpolymers still exhibit pH-responsive viscosity profiles similar to those observed in Figure 1.15b, with AMBATAC-3-7 displaying a polyampholyte contraction at pH 3–6 and AMBATAC-7-3 exhibiting a solution IEP at pH 4.5 and polyelectrolyte expansion above the IEP.

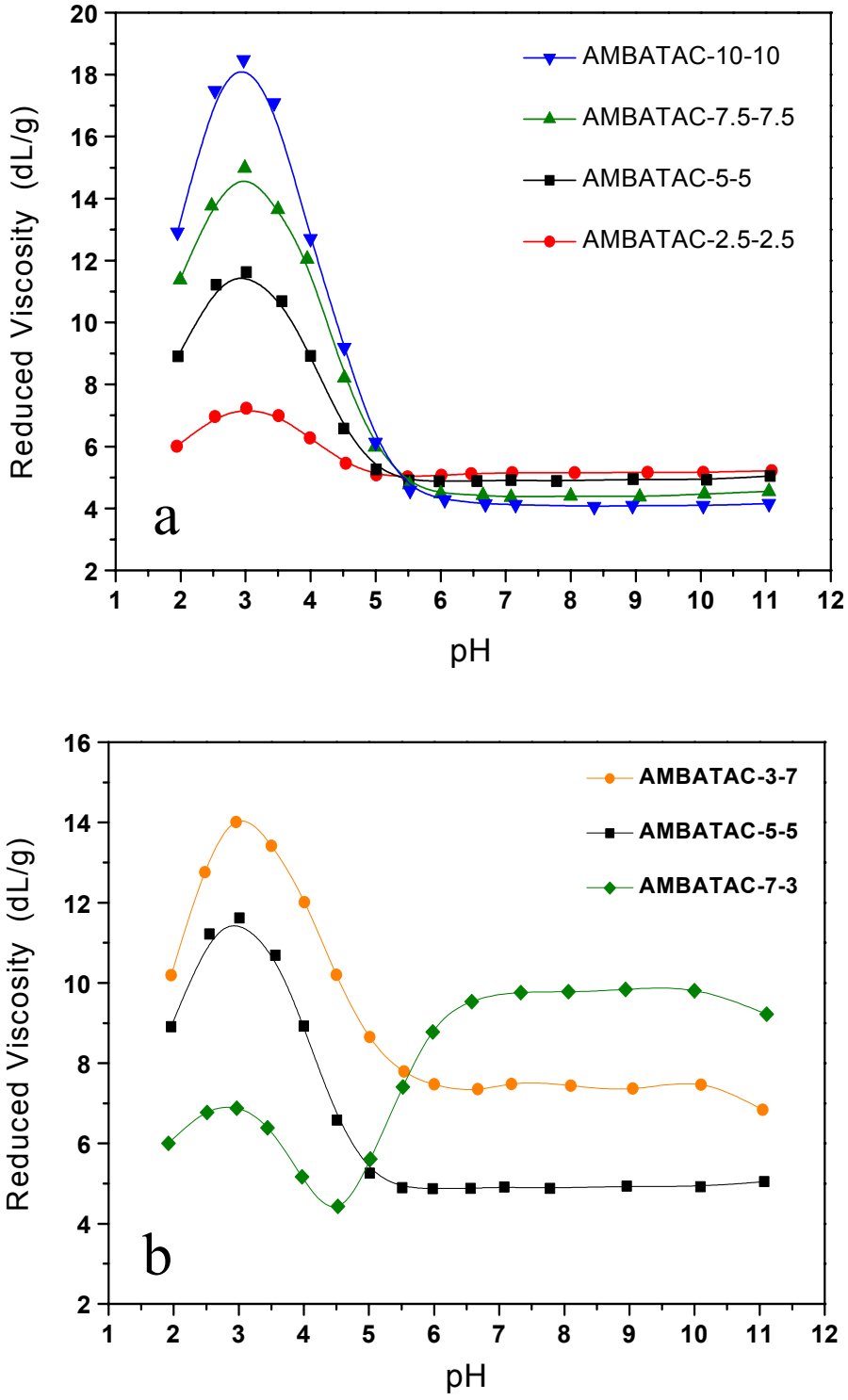

Figure 1.17. Reduced viscosity of the AMBATAC terpolymers in 0.01 M NaCl as a function of solution pH: a) charge-balanced terpolymers, b) unbalanced terpolymers with AMBATAC-5-5 (charge-balanced) shown for comparison. Polymer concentration = 0.1 g/dL.

At high ionic strength: The pH-responsive reduced viscosity profiles of the AMBATAC terpolymers in 0.5 M NaCl are shown in Figure 1.18. In high ionic strength solutions, electrostatic interactions are virtually nonoperative due to extensive charge screening by the added electrolyte, yet the magnitude of the pH-response still increases with increasing ionic comonomer content. In the low pH range (2–4), the charge-balanced terpolymers (Figure 1.18a) exist as cationic polyelectrolytes that are contracted due to screening of electrostatic repulsions and intramolecular hydrogen-bonding associations between protonated AMB carboxylate moieties. Hydrophobic effects due to the uncharged hydrocarbon portions of the ionic comonomers may also contribute to this collapse. At these pH values, the solution viscosities of the terpolymers increase with increasing ionic comonomer content. This is presumably due to the increased chain-stiffness that occurs as higher levels of bulky AMB and APTA pendant groups are incorporated into the terpolymers. The order of solution viscosities below pH 4 in Figure 1.10a suggests that the positive excluded volume contribution due to chain-stiffness is greater than the negative excluded volume contribution due to intramolecular hydrogen-bonding between protonated AMB moieties. As solution pH increases beyond pH 4, coil expansion occurs upon ionization of the AMB functional groups, leading to solution viscosity increases. At solution pH values > 7.0, the charge-balanced systems exhibit constant solution viscosities that increase with increasing charge density in the order AMBATAC-2.5-2.5 < -5-5 ≈ -7.5-7.5 < -10-10. This observation suggests greater chain-stiffness and increased polymer-solvent interaction occur with increasing charge density in the polyampholyte pH regime. In Figure 1.18b, similar behavior is observed for the unbalanced terpolymers, with the magnitude of the pH-induced viscosity change increasing with increasing AMB content in the terpolymer. It is also observed that the charge-balanced terpolymer of similar charge density (AMBATAC-5-5) exhibits higher solution viscosities in the polyampholyte pH regime (pH ≥ 7.0) than the unbalanced systems, presumably due to greater polymer-solvent interaction.

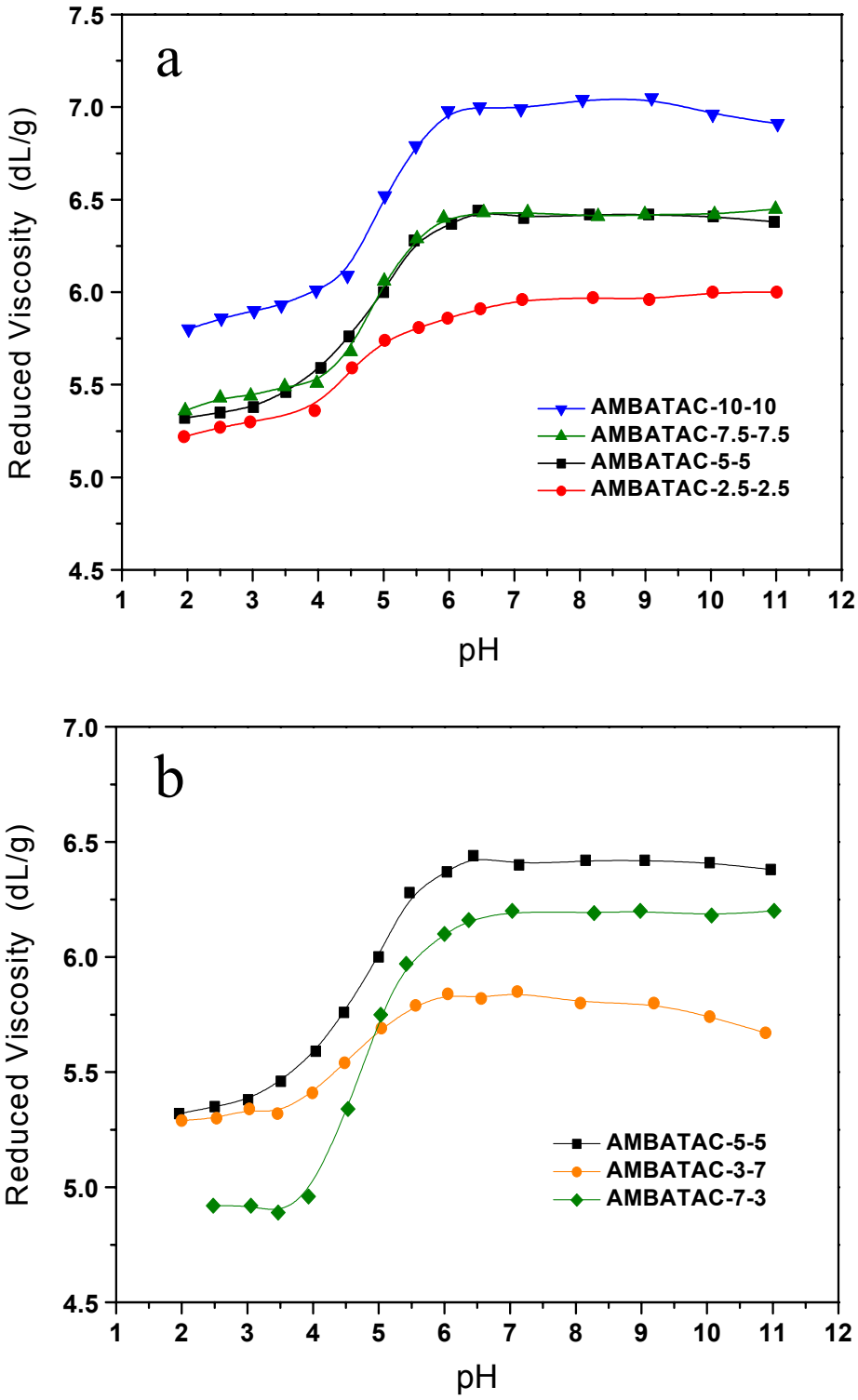

Figure 1.18. Reduced viscosity of the AMBATAC terpolymers in 0.5 M NaCl as a function of solution pH: a) charge-balanced terpolymers, b) unbalanced terpolymers with AMBATAC-5-5 (charge-balanced) shown for comparison. Polymer concentration = 0.1 g/dL.

Combined pH- and salt-responsive behavior

To fully elucidate the pH- and salt-responsive behavior of the AMBATAC terpolymers in dilute solution, the reduced viscosity of AMBATAC terpolymer solutions (c = 0.1 g/dL) was measured as a function of pH at several values of [NaCl] (Figures 1.19 and 1.20). The three-dimensional (3-D) plots shown in Figures 1.19 and 1.20 serve as phase diagrams that map the viscosity response to changes in solution pH and salt concentration. The viscosity response is indicative of the solution behavior (i.e. polyampholyte, polyelectrolyte, or combined) exhibited by the terpolymers at a given solution pH and [NaCl].

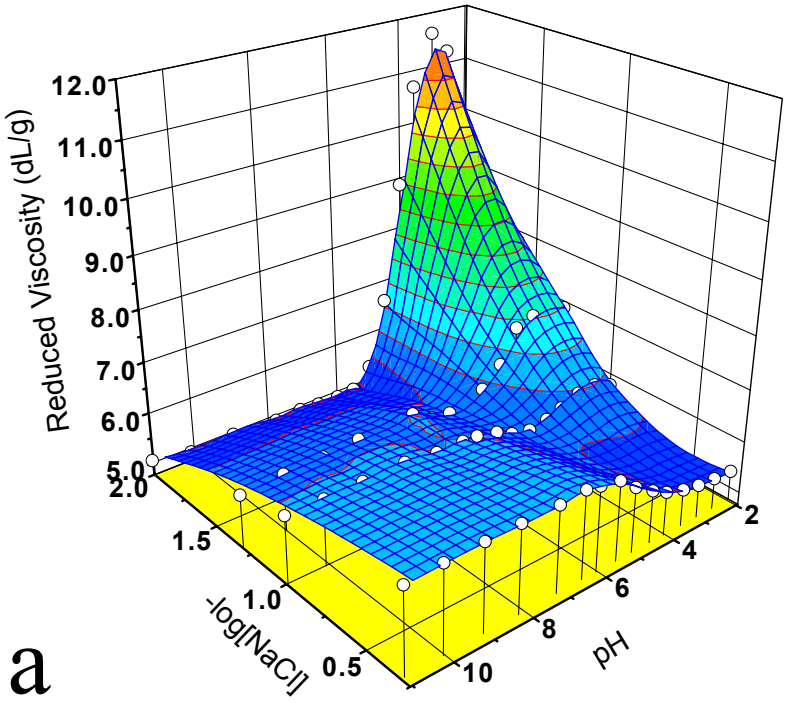

a

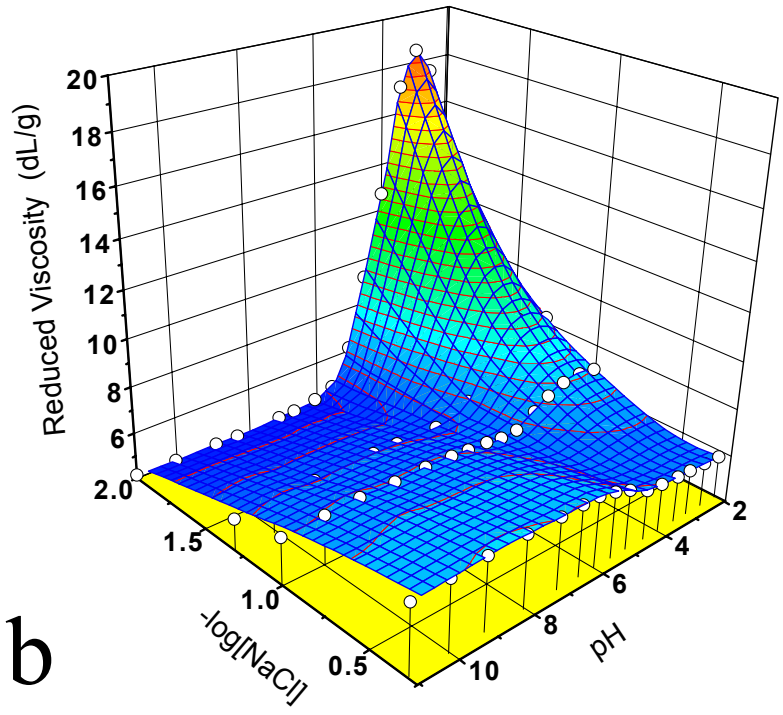

Figure 1.19. Three-dimensional plots of reduced viscosity as functions of [NaCl] and solution pH for charge-balanced terpolymers a) AMBATAC-5-5, and b) AMBATAC-10-10. Polymer concentration = 0.1 g/dL. Open circles indicate actual data points.

In Figure 1.19, four distinct regions are observed in the plots for the charge-balanced terpolymers AMBATAC-5-5 and -10-10: a) At low [NaCl] and low pH, a polyelectrolyte peak is observed, corresponding to coil expansion due to unscreened electrostatic repulsions; b) at low [NaCl] and high pH, a polyampholyte valley is observed, indicating coil collapse due to unscreened electrostatic attractions; c) at high [NaCl] and low pH, a polyelectrolyte valley is observed as the electrostatic repulsions are screened at higher ionic strengths, leading to coil contraction; and d) at high [NaCl] and high pH, a polyampholyte plateau is observed, as the increased ionic strength screens electrostatic attractions, allowing coil expansion. Although the contours of the 3-D plots for AMBATAC-5-5 and -10-10 are very similar, it should be noted that the magnitude of the solution viscosity response is significantly greater in AMBATAC-10-10 due to increased charge density.

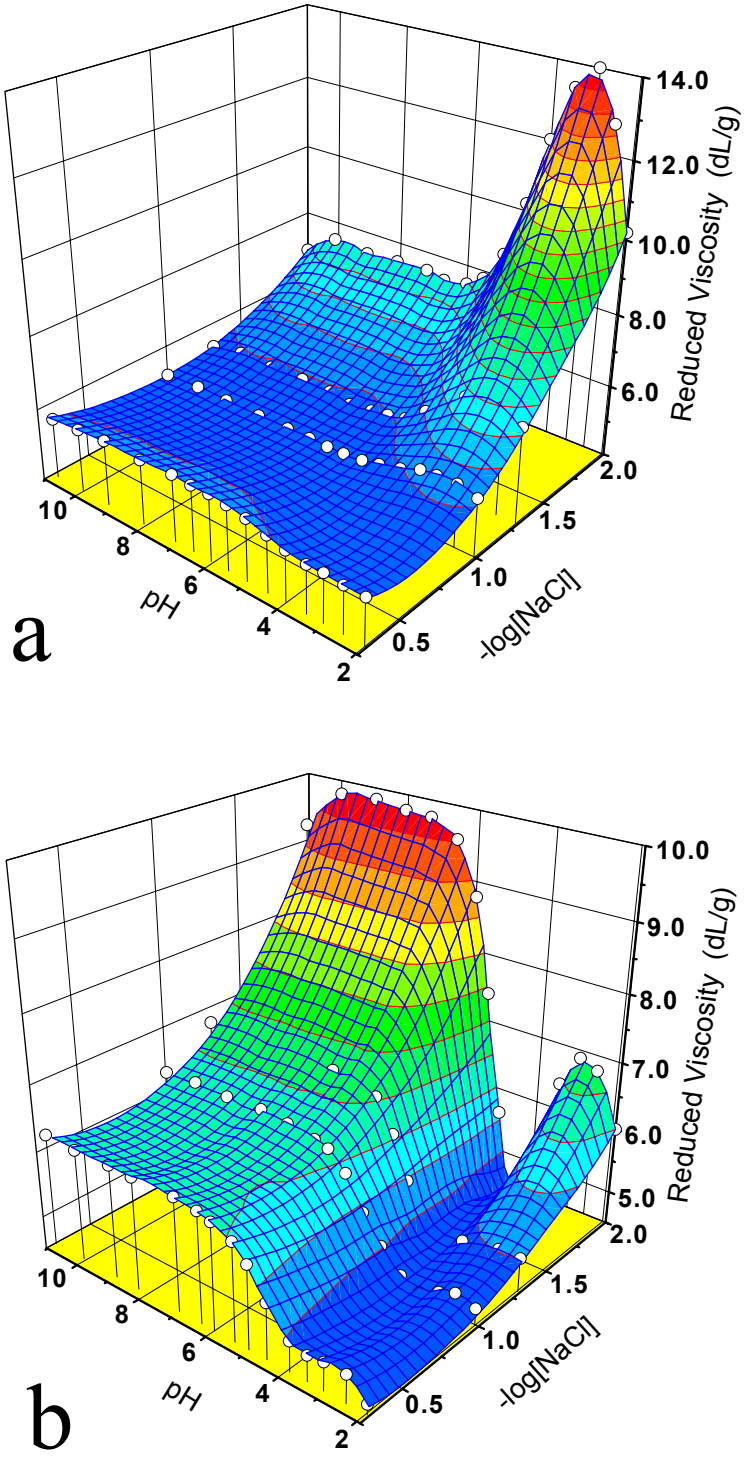

Figure 1.20. Three-dimensional plots of reduced viscosity as functions of [NaCl] and solution pH for unbalanced terpolymers a) AMBATAC-3-7, and b) AMBATAC-7-3. Polymer concentration = 0.1 g/dL. Open circles indicate actual data points.

Figure 1.20 shows similar 3-D plots for the unbalanced terpolymers AMBATAC-3-7 and -7-3. (Note that the axes for pH and -log[NaCl] have been reversed in Figure 1.20 to facilitate an unobstructed view of the entire viscosity response.) Examination of Figure 1.20 reveals that the unbalanced terpolymers behave predominantly as polyelectrolytes over a wide range of solution pH and [NaCl]. However, polyampholyte behavior is still evident in the plots at low [NaCl]. In the low ionic strength regime, a viscosity decrease is observed for AMBATAC-3-7 with increasing pH, indicating coil collapse as AMB units become ionized. At low [NaCl], AMBATAC-7-3 displays a valley at pH ≈ 4.5, corresponding to the solution IEP, and a smaller local polyelectrolyte peak at pH ≈ 3. The polyelectrolyte behavior observed at low pH for AMBATAC-7-3 rapidly diminishes with increasing [NaCl], as is also observed for AMBATAC-3-7. The contours of the plots in Figures 1.19 and 1.20 provide an excellent visualization of the effects of charge density and charge balance on the pH- and salt-responsive solution behavior of the AMBATAC terpolymers and are ideal predictive tools for further studies of dilute solution properties.

Semidilute solution rheology

Figure 1.21 shows the apparent viscosities of semidilute (c = 2.0 g/dL) AMBATAC terpolymer solutions in DI water as a function of shear rate. All of the solutions exhibited pseudoplastic viscosity profiles: Newtonian plateaus are observed at lower shear rates followed by a transition into power law shear-thinning zones at higher shear rates (> 10 s^{-1}). For the charge-balanced terpolymers, the order of zero-shear apparent viscosity increases with increasing charge density in the order AMBATAC-2.5-2.5 < -5-5 ≈ -7.5-7.5 < -10-10. The increase in solution viscosity is attributed to greater intermolecular electrostatic associations that occur with increasing charge density. For the terpolymers of similar charge density and varying charge balance, the viscosities of AMBATAC-5-5 and -7-3 are approximately equal, yet the viscosity of AMBATAC-3-7 is significantly lower, presumably due to the lower MW of AMBATAC-3-7.

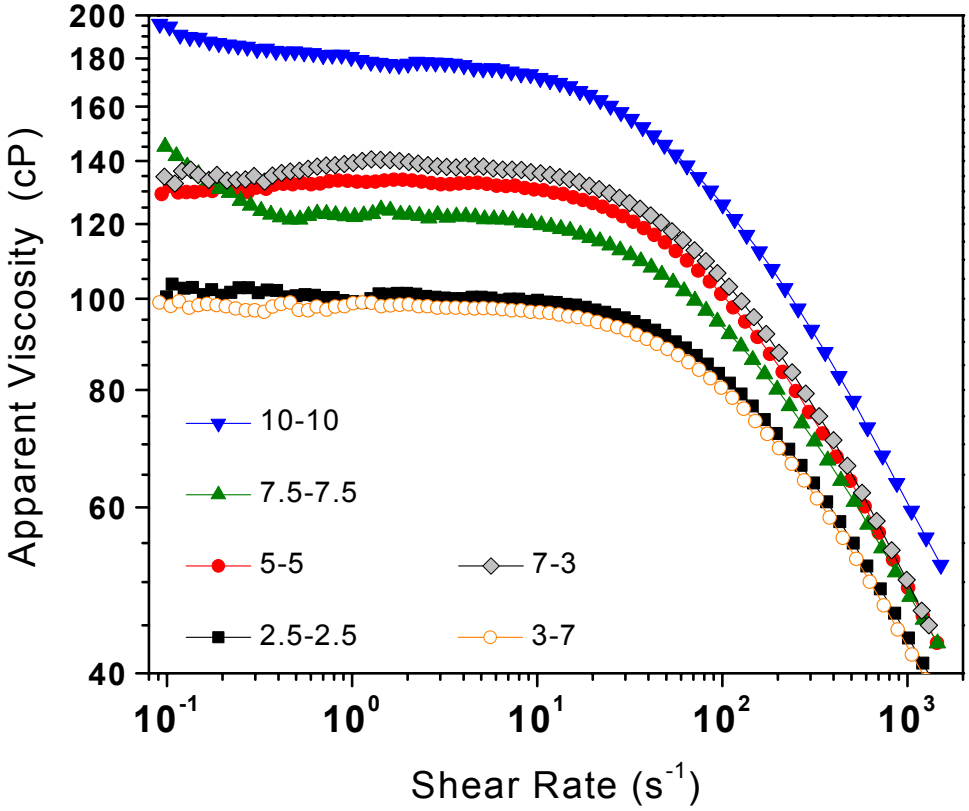

Figure 1.21. Steady-state shear sweep data for the AMBATAC terpolymers in DI water. Polymer concentration = 2.0 g/dL. Solution pH = ambient (6.5 ± 0.2), except for AMBATAC-3-7, ambient pH = 8.2.

To assess the effects of electrostatic interactions on the rheology of charge-balanced AMBATAC solutions, the concentration-dependent viscosity was examined in the absence of added electrolytes and at high ionic strength. Figure 1.22 shows the specific viscosity as a function of concentration for AMBATAC-10-10 in DI water and 0.5 M NaCl. The linear regions of the dilute and semidilute regimes were fit to the power law relationship given by Equation 7, where η_{sp} is the specific viscosity, c is the polymer concentration, A is the preexponential factor, and b is the scaling exponent. The critical overlap concentration (c^*) is given by the intersection of the two lines on a log-log plot of η_{sp} vs. c (Figure 1.20).

$$\eta_{sp} = A \cdot c^{b} \tag{7}$$

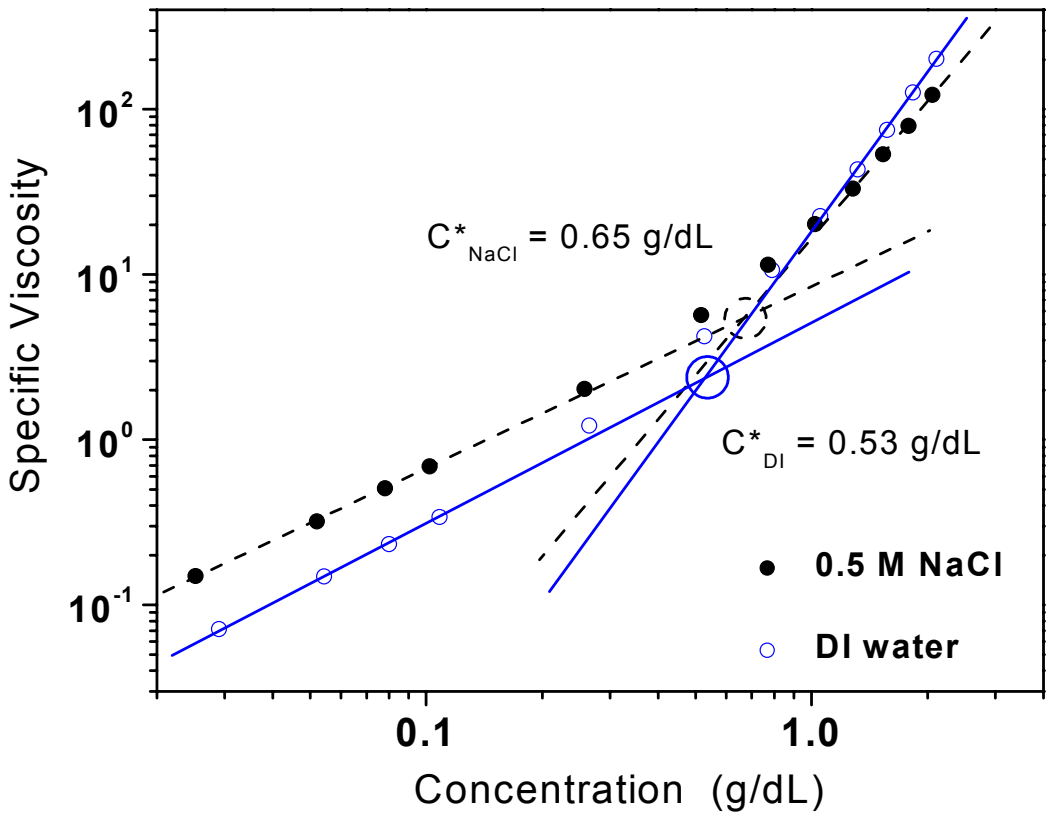

Figure 1.22. Zero-shear specific viscosity as a function of concentration for AMBATAC-10-10 in (○) DI water and (●) 0.5 M NaCl. Solution pH = ambient (6.5 ± 0.2).

At concentrations below c^*, AMBATAC-10-10 exhibits significantly higher specific viscosities in 0.5 M NaCl compared to DI water; this is due to the screening of intramolecular electrostatic attractions which leads to increased coil hydrodynamic volume. However, the dilute regime scaling exponent, b_{dil}, is only slightly higher in DI water than in 0.5 M NaCl (Table 1.9). Coil overlap occurs at a lower concentration in DI water for AMBATAC-10-10 due to the onset of intermolecular electrostatic associations that promote interactions between individual polymer chains; such charge-charge associations are screened in 0.5 M NaCl, causing coil overlap to occur at a higher concentration (Table 1.9). In the semidilute regime ($c > c^*$), the solution viscosity increases more rapidly with increasing polymer concentration in DI water than in 0.5 M NaCl, as indicated by the semidilute regime scaling exponent b_{semi} in Table 1.9. Although AMBATAC-10-10 coils have lower hydrodynamic volumes in DI water, the intermolecular electrostatic attractions that occur above c^* cooperatively increase coil-coil interaction, causing the observed increase in the scaling parameter b_{semi}. Examination of the b and c^* values for AMBATAC-5-5 in DI water and 0.5 M NaCl reveals that the effects of added electrolyte are significantly less for AMBATAC-5-5, indicating greatly decreased levels of intermolecular electrostatic interactions in the lower charge density system.

Table 1.9. Concentration-dependent solution rheology data for AMBATAC-5-5 and -10-10.

Solvent	A_{dil}	b_{dil}	c^* (g/dL)	A_{semi}	b_{semi}
AMBATAC-5-5					
DI water	9.15	1.13	0.67	19.13	2.94
0.5 M NaCl	8.49	1.11	0.70	16.26	2.94
AMBATAC-10-10					
DI water	4.67	1.18	0.53	17.43	3.27
0.5 M NaCl	8.14	1.09	0.65	16.70	2.73

Conclusions

A series of low charge density model polyampholyte terpolymers composed of AM, NaAMB, and APTAC (AMBATAC) have been synthesized via conventional free radical polymerization in aqueous media. The reaction conditions were selected to yield terpolymers with random charge distributions, homogeneous compositions, and well-defined MW and MWDs. Compositional analysis by ^{13}C NMR revealed good agreement between monomer feed compositions and final terpolymer compositions. Elemental analysis for Na^+ and Cl^- indicated extensive self neutralization of the AMBATAC terpolymers following purification via exhaustive dialysis and confirmed terpolymer compositions determined via ^{13}C NMR. The AMBATAC terpolymers were characterized extensively via SEC-MALLS analysis in 0.1 M NaCl pH 7 phosphate buffer at 25 °C. SEC-MALLS analysis showed that the use of NaOOCH as a chain transfer agent eliminated the effects of monomer feed composition on *DP*, allowed control of terpolymer MW, and suppressed excessively broad MWDs. Intrinsic viscosities determined via SEC-MALLS with the Flory-Fox equation were found to agree with intrinsic viscosities determined via dilute solution viscometry. Analysis of the R_g-M and MHS relationships for the AMBATAC terpolymers provided information about the dependence of macromolecular conformation and polymer-solvent interaction on terpolymer composition. Potentiometric titration studies showed that the apparent pK_a values of the charge-balanced AMBATAC terpolymers increased with increasing levels of NaAMB content in the terpolymer and decreased as the ratio of AMB:APTA units decreased.

The aqueous solution properties of the AMBATAC terpolymers, a well-defined series of low charge density PAM-based polyampholytes, have been examined to elucidate the structure-property relationships that govern AMBATAC terpolymer solution behavior. By using a series of model terpolymers with well-defined MWs and MWDs, distinct effects of terpolymer composition (e.g. level of ionic comonomer content and ratio of anionic-to-cationic monomer) on solution behavior are observed.

AMBATAC terpolymers with low charge densities and/or large charge asymmetries exhibited excellent solubility in DI water, and higher charge density terpolymers were readily dispersible in DI water; however, phase separation was observed over time for the higher charge density systems. Extensive examination of the pH- and salt-responsive dilute solution viscosity profiles for the AMBATAC series revealed that polyampholyte or polyelectrolyte behavior can be elicited by changing solution pH; the magnitude of the viscosity response to external stimuli (e.g. solution pH and electrolyte concentration) was found to be highly dependent on terpolymer charge density and charge asymmetry. At low ionic strength, dilute solution viscosity is governed predominantly by electrostatic interactions; however, in high ionic strength solutions, electrostatic interactions are eliminated due to charge screening, and other factors, such as intramolecular hydrogen-bonding, terpolymer chain stiffness, and backbone hydrophobicity, become operative. The observed solution properties are highly consistent with the properties predicted by current theories for polyampholyte solution behavior. At terpolymer concentrations above c^*, solution viscosities were observed to increase with increasing terpolymer charge density, indicating intermolecular electrostatic associations significantly enhance solution viscosity. Upon addition of NaCl, semidilute solution viscosities tend to decrease due to disruption of the intermolecular electrostatic associations.

Nomenclature

	Description
R_g	Polymer radius of gyration
K_{Rg}	Preexponential, Equation (1)
M	Polymer molecular weight
ρ	Polymer shape factor
$[\eta]$	Intrinsic viscosity
ϕ_o	Flory viscosity constant
$[\eta]_{SEC}$	Intrinsic viscosity determined *via* SEC
K_{MHS}	Preexponential, Equation (4)
σ	Charge asymmetry
N	Number of total repeat units
N_-	Number of anionic repeat units
N_+	Number of cationic repeat units
η_{sp}	Specific viscosity
A	Preexponential, Equation (7)
c	Polymer concentration
b	Scaling point

CHAPTER 2

TASK 5: POLYMER MOBILITY CHARACTERIZATION

Dilute Polymer Solution Extensional Viscosity Measurement

Background

In EOR a dilute polymer solution is forced through a porous medium. A complex flow field is induced in which the fluid experiences local velocity fluctuations. Ideally, the fluid drag forces developed at low fluid extension rates will be sufficient to elongate or extend the polymer coils in dilute aqueous solution, and resistance to coil extension will be sufficient to greatly increase the fluid apparent viscosity.

Experimental results obtained prior to the work described in this report indicated enhancement of desired solution properties with increasing polymer coil size. Previous reports[52] dealt with measuring and modeling polymer coil size in dilute solution. More recently, attention has been redirected toward measuring dilute solution extensional viscosity in simulated flow through porous media and quantifying and modeling polymer coil extensional viscosity. The previously proposed correlation between polymer coil intrinsic viscosity and solution extensional behavior will be examined in this report.

Experimental

Initial Considerations. Measuring the extensional viscosity of a non-Newtonian fluid is a complex task. Polymer solution extensional viscosity, η_e, depends on fluid temperature, polymer concentration, extensional strain rate, and the magnitude of extensional strain.[53] To obtain the entire rheologic behavior of a given polymer solution at a fixed temperature, a three-dimensional surface must be generated describing extensional viscosity as a simultaneous function of strain rate and degree of strain.[54] Experimentally, the rate and degree of fluid extension are difficult to control independently.[55]

For the purpose of studying polymer solutions for EOR, exact measurement of solution extensional viscosities is unachievable. Therefore, measurement of the fluid viscosity enhancement caused by dissolved polymer in simulated flow through a porous medium was performed. Though not a direct measure of fluid extensional viscosity, this applied experimentation was considered to provide an indication of polymer solution performance in EOR.

Porous media such as those found in underground oil reservoirs can be simulated by packed beds. A packed bed induces a complex flow field containing both shear and extensional components.[56] Under fluid flow conditions, pressure drop measurements

across the bed can be used to complete an energy balance on the system. The difference in fluid pressure loss between a polymer solution and the pure solvent can be attributed to the energy expended by the polymer coils while being forced through the packing geometry.

A useful packed bed should be geometrically regular to facilitate mapping of the flow field and quantification of viscous losses. Also, the packing should be chosen so that the flow path can be reasonably reconstructed, thus yielding reproducible experimental results. The chosen packing material for the rheometer used in this study was a stack of woven filament nylon screens. The screen stack was intended to mimic a regular array of cylinders. The nylon screens were selected because of their commercial availability, low cost, and geometric consistency. The screen stack provided a regular reproducible flow path that induced a fluid flow field similar to what might exist in underground rock formations. Hence, the custom screen extensional rheometer (SER) was used to test the viscosity enhancing abilities of polymers in dilute solutions flowing through a simulated porous medium. Details of the rheometer design and operation have been reported previously.[57]

Screen Extensional Rheometer Data Analysis

Extensional Flow Through Screens

The nylon screens used in the SER were constructed of a square mesh, overlapping weave of nylon filaments. A scanning electron micrograph of a nylon screen sample is shown in Figure 2.1. The distance between parallel filaments was approximately equal to the filament diameter, d_f = 0.020 mm. The 20 micron mesh was the smallest available size that retained cylindrical filaments (smaller mesh sizes are produced by compression of the 20-micron screens, thus flattening the nylon filaments). The fractional free projected area of the mesh, f, was 0.16. Because of the overlapping construction, the screen thickness was three times the filament diameter. The screen porosity, ϕ, was calculated as the ratio of open volume to total spatial volume, ϕ = 0.515. As purchased, the woven material was precut into circular discs having a diameter, D_s, of ½ inch.

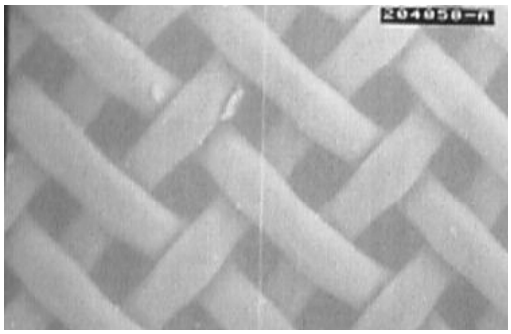

Figure 2.1. Scanning electron micrograph of a sample nylon screen used for packing the screen extensional rheometer.

The nylon screen discs were placed in series in the SER. As a dilute polymer solution flows through the series of screens, the fluid must cyclically accelerate and decelerate as the cross-sectional free volume varies. Given the screen geometry described above, the average fluid extension rate, $\dot{\varepsilon}$, can be calculated as a function of the volumetric fluid flow rate, Q, as Eq. (1).

$$\dot{\varepsilon} = \frac{16\,Q}{3\,\pi\,D_s^{\,2}\,d_f}\,\frac{1-f}{f} \tag{1}$$

Eq. (1) demonstrates that the fluid strain rate can be varied by adjusting the fluid flow rate. At low fluid extension rates, the polymer coils are not deformed by the flow field and remain roughly spherical. When a critical fluid extension rate, $\dot{\varepsilon}_{yield}$, is reached, fluid drag forces become sufficient to induce cyclic extension and compression in the polymer coils as they are carried through the screens. The volumetric fluid flow rate that corresponds to the critical yield strain rate is Q_{yield}. It is assumed that no slippage exists between the polymer coils and the solvent after the yield point, i.e., polymer and solvent move at the same velocity. The number of screens placed in series determines the number of polymer coil strain cycles. The degree of extensional strain, however, is fixed by the packing geometry.

Power Usage by Polymer Coils

A power balance on the SER was performed to determine the energy required to extend and compress an individual polymer coil. SER experimental data is obtained in the form of pressure drop, ΔP, across the screen series versus fluid volumetric flow rate, Q. The total power required by the fluid to traverse the packed bed can be calculated from the flow rate and pressure drop. The difference in power usage between the pure solvent and the polymer solution is considered to be the power used by the individual polymer coils. Knowing the polymer concentration and fluid flow rate, the number of polymer coils passing through the screens per unit time can be determined. Dividing by the number of screens in series, the energy usage per polymer coil per strain cycle can be calculated.

Equation for SER Data Analysis

Eq. (2) is the working equation resulting from the power balance. In Eq. (2), ΔP_s is the polymer solution pressure drop across the screens and ΔP_o is the solvent pressure drop. A characteristic parameter was defined, η_c, which is the polymer coil viscosity. The coil viscosity was determined from the energy expended per polymer coil per strain cycle, and thus represents the coil resistance to extensional strain deformation.

$$\left(\Delta P_s - \Delta P_o\right) = \frac{\eta_c}{\beta}\,Q \tag{2}$$

The parameter β in Eq. (2) is a collection of known constant terms that appear in the power balance derivation. β is given by Eq. (3), where n is the number of screens placed in series.

$$\beta = \frac{\pi D_s^{\,2} d_f f^2}{48 n \phi c_p [\eta] (1-f)^2} \qquad (3)$$

Example SER Data Workup

The left side of Eq. (2) was termed the normalized solution pressure, or NSP. A plot of NSP versus Q should yield a line with a slope equal to η_c / β. As it was defined, η_c is a characteristic property of the polymer coil and should be independent of flow conditions. However, at fluid extension rates below the critical rate required for coil extension, $\dot{\varepsilon}_{yield}$, the polymer coils expend no energy, and the NSP value is zero. Thus, Eq. (2) is only valid under conditions of polymer coil extension, i.e., $\dot{\varepsilon} > \dot{\varepsilon}_{yield}$ or, equivalently, $Q > Q_{yield}$. When $Q < Q_{yield}$, experimental NSP data values are zero. At Q_{yield}, NSP data values become positive and increase linearly with Q. Thus, Q_{yield} can be determined graphically from experimental SER data, and the slope of the data above Q_{yield} can be used to calculate η_c.

Figure 2.2 is a plot of NSP versus Q for a typical SER data set. This example depicts data for a $2x10^6$ g/mol poly(ethylene oxide) or PEO sample in deionized water taken at 10°C. The point where the NSP values depart from the abscissa is Q_{yield}. In Figure 2.2, the value of Q_{yield} can be reasonably determined by visual inspection of the data plot: $Q_{yield} \approx 16$ mL/min. The data above Q_{yield} forms a line, and the slope of the line is proportional to the coil viscosity, η_c. Using known values of the parameters included in the constant β, the value of η_c was calculated from the line slope: $\eta_c = 1.7$ poise.

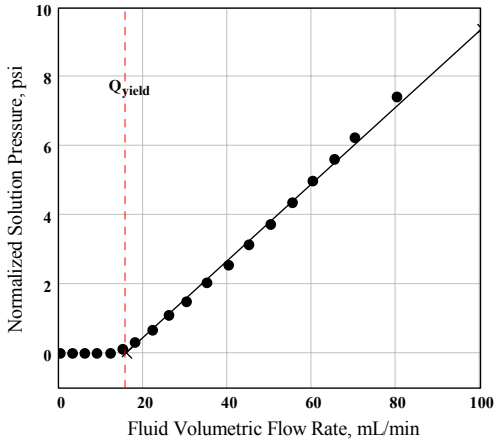

Figure 2.2. Example screen extensional rheometer data plotted as normalized solution pressure versus fluid flow rate. The dashed line marks the yield flow rate for polymer coil deformation. The solid line illustrates the linear trend of the data above the yield point.

Experimental Dilute Polymer Solution Data Collected Using the SER

Data Overview

SER data was collected for several different polymers over a variety of experimental conditions. Experimental variables included polymer molecular weight, solution temperature, and solution ionic strength. The solvent apparent viscosity varied consequently with solution temperature and added NaCl concentration.

Figure 2.3 depicts an example case where the single experimental variable was polymer molecular weight. The SER data represent non-hydrolyzed poly(acrylamide) in a 0.514 M NaCl solution at 25°C. The larger macromolecules began to deform and enhance the solution flow resistance at a lower fluid flow rate than the smaller ones. The lower Q_{yield} is expected for larger polymer coils because of the greater drag force difference they encounter across the coil in an extensional fluid flow field. At flow rates beyond Q_{yield} the higher molecular weight polymer removed more energy from the system resulting in a steeper slope and a greater calculated coil viscosity value, η_c.

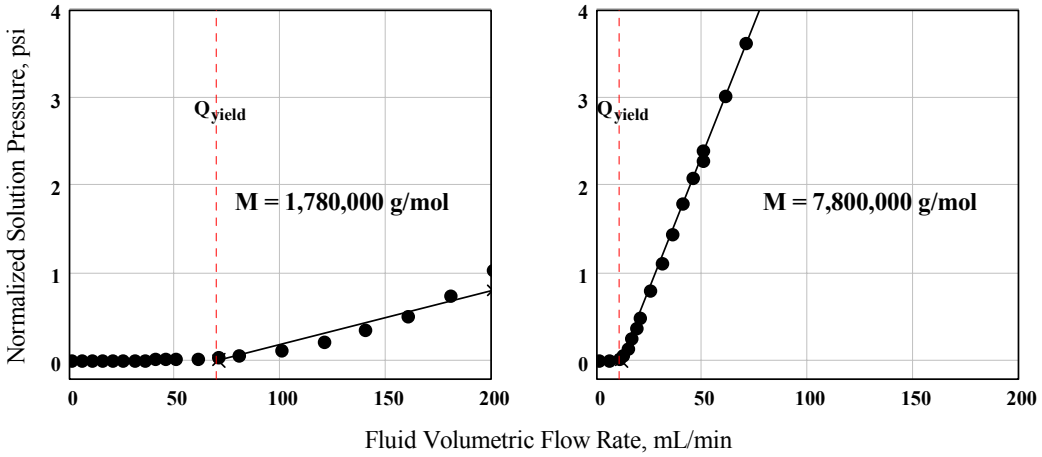

Figure 2.3. SER data for two poly(acrylamide) samples differing only in molecular weight. The higher molecular weight polymer exhibits a lower yield flow rate and a higher coil viscosity. In each plot the dashed line marks the yield flow rate for polymer coil strain, and the solid line illustrates the linear trend of the data above the yield point.

The SER data in Figure 2.4 represent a case where only the fluid temperature was changed. The studied polymer was a commercially available hydrolyzed poly(acrylamide), Alcoflood 1285. The average polymer molecular weight and degree of hydrolysis were reported by the vendor to be 20 x 10^6 and 25%, respectively. Data were collected for a polymer solution containing 0.514 M NaCl.

The observed polymer solution extensional flow behavior at the two experimental temperatures was not entirely expected. The hypothesis prior to experimentation was that η_c would increase and Q_{yield} would decrease as the polymer hydrodynamic size (intrinsic viscosity) increased. Previously reported data[58] showed that the solution intrinsic viscosity of this polymer increased by approximately 25% as temperature was elevated from 25°C to 50°C. Though Q_{yield} did not change appreciably, the experimental coil viscosity, η_c, was lower at the higher temperature where the intrinsic viscosity was greater. Possible explanations for the unanticipated result are discussed in a later section of this report.

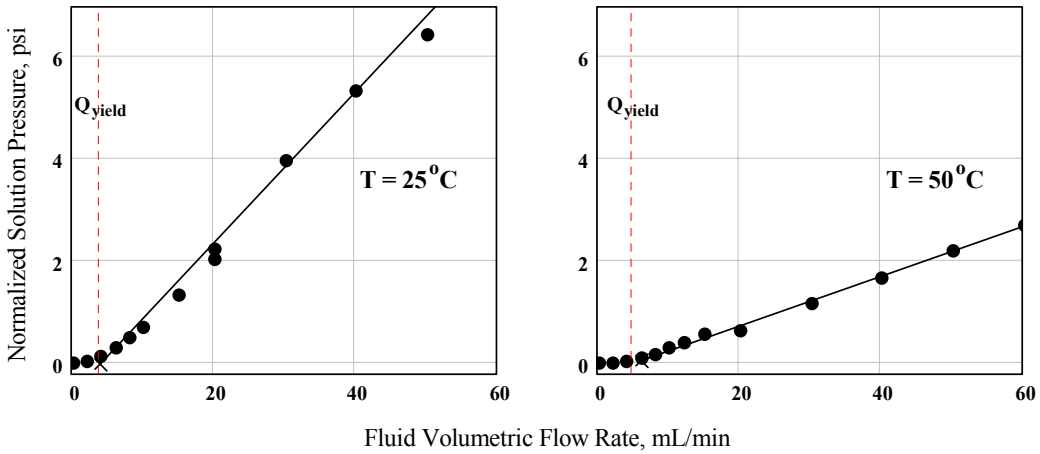

Figure 2.4. SER data for a 25% hydrolyzed poly(acrylamide) sample at two fluid temperatures. In each plot the dashed line marks the yield flow rate for polymer coil strain, and the solid line illustrates the linear trend of the data above the yield point.

Figure 2.5 contains SER data collected at 25°C for a 25% hydrolyzed poly(acrylamide) synthesized in-house. The single experimental variable was the solution ionic strength, which was adjusted by adding NaCl. Measured intrinsic viscosity values of this polyelectrolyte indicated a strong decrease in coil size with increasing solution ionic strength. The observed yield flow rate in Figure 2.5 was greater at the higher ionic strength, though the difference does not sufficiently reflect the intrinsic viscosity increase. The coil viscosity, proportional to the slope of the plotted data, was much greater for the smaller coil configuration. Thus, the prediction that coil viscosity would increase with increasing intrinsic viscosity failed for this pair of experimental data sets.

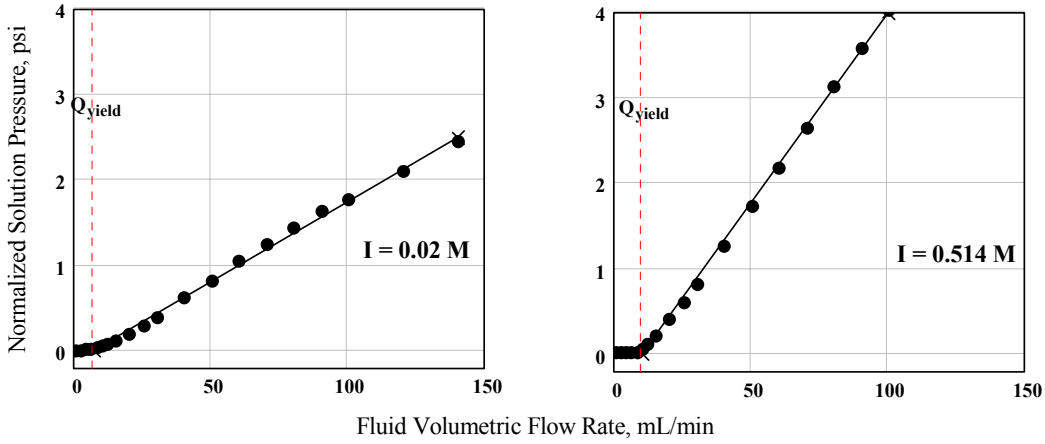

Figure 2.5. SER data for a 25% hydrolyzed poly(acrylamide) sample at two solution ionic strengths. In each plot the dashed line marks the yield flow rate for polymer coil strain, and the solid line illustrates the linear trend of the data above the yield point.

Not all data sets collected using the SER were as well defined as the one depicted in Figure 2.2. Some showed curvature rather than a sharp upturn at the yield flow rate, making an exact value for Q_{yield} difficult to visually determine. Such curvature is likely caused by sample polydispersity. Other data sets, especially those taken for larger macromolecules, exhibited a curved downward deviation from linearity at high flow rates. This effect was attributed to polymer coil slippage at high extension rates, thus decreasing the degree of polymer coil extension and, consequently, the energy expended by the dissolved polymer. Data scatter was often observably greater at elevated temperatures; a rational effect considering the decreased signal level (lower fluid viscosity at higher temperature generates less system pressure) and increased noise level (gaseous bubble formation in the rheometer is unavoidable) expected at elevated temperatures.

Overall, the screen extensional rheometer was judged to be a suitable instrument for measuring the fluid apparent viscosity enhancing capabilities of dissolved polymers in an extensional flow field. Several SER experiments were repeated, some several times, and satisfactory reproducibility was obtained. The SER dilute polymer solution data offer a practical estimate of the resistance to fluid flow that a solution might generate in underground porous media.

Experimental Data

When preparing a dilute polymer solution for extensional viscosity measurements, the intrinsic viscosity at the experimental conditions must be known to determined the target polymer concentration, $c_p = 0.1 / [\eta]$. Therefore, the polymers used in SER data collection were ones for which solution intrinsic viscosities had been previously determined.

Polymers included in the SER study were three poly(ethylene oxide) or PEO samples, two molecular weight fractions of non-hydrolyzed poly(acrylamide) or PAM, and two commercial hydrolyzed poly(acrylamide) samples, Alcoflood 1235 and 1285. The latter two polymers will be referred to as Af-1285 and Af-1235, respectively. Additionally, a 25% hydrolyzed poly(acrylamide) was synthesized in-house and is denoted as HPAM.

Other materials studied were copolymers of acrylamide with each of three ionizable monomers. Monomer structures and copolymer compositions were reported previously. The samples are referred to by the comonomer acronyms followed by a number representing the mole percent comonomer in the copolymer, the balance being acrylamide. The copolymer names follow: AMBA-10, AMBA-5, AMPS-10, APTAC-10, APTAC-5.

Two other polymers studied were copolymers containing approximately 90% acrylamide and 10% AMBA. The samples were taken from two different batches synthesized by solution free radical polymerization without a chain transfer agent. Reaction time was varied to yield two different polymer molecular weights. The samples will be referred to as AM-AMB1 and AM-AMB2.

Table 2.1 is a compilation of experimental parameters and results. Data reported in Table 2.1 where the experimental conditions did not vary were experimental repetitions, e.g., the AM-AMB1 data.

Many of the polyelectrolyte copolymers failed to yield below the maximum volumetric flow rate capability of the syringe pump. Since no increase in pressure drop could be detected at the fluid flow rate limit, the yield points and coil viscosities could not be determined for these polymers. The reasons for the lack of coil extension are not clear. Polymer molecular weights were intentionally kept near 10^6 g/mol because larger polymers could not be accurately characterized using size exclusion chromatography. Higher molecular weight samples of similar copolymer compositions should have lower yield flow rates.

Table 2.1
SER Experimental Conditions and Results

Polymer	$M \times 10^{-6}$, g/mol	I, mol/L	T, K	$[\eta]$, dL/g	η_c, Poise	Q_{yield}, mL/min	d_h, Å	$\mu_o \times 10^2$, cP	$V_c \times 10^{-9}$, Å^3
PEO	0.9	0	297	5.8	0.25	50	1180	0.911	0.867
PEO	0.9	0	329	4.2	0.05	100	1060	0.496	0.620
PEO	2.0	0	283	12.4	1.7	16	1990	1.31	4.12
PEO	2.0	0	312	9.4	0.90	23	1810	0.665	3.13
PEO	2.0	0	348	5.5	0.24	55	1520	0.378	1.83
PEO	8.0	0	297	32	3.7	4	4330	0.911	42.5
PEO	8.0	0	329	23	1.3	10	3880	0.496	30.6
Af-1235	5.0	0.514	298	19	0.9	12	3110	0.943	15.8
Af-1235	5.0	0.514	323	20	0.45	9	3170	0.580	16.6
Af-1285	20.0	0.514	298	39	2.2	5	6280	0.943	130
Af-1285	20.0	0.514	298	39	2.3	4	6280	0.943	130
Af-1285	20.0	0.514	323	48	0.81	6	6730	0.580	159
PAM	1.78	0.514	298	5.8	0.096	70	1490	0.943	1.71
PAM	7.8	0.514	298	18	0.86	11	3550	0.943	23.3
AM-AMB1	4.0	1.0	298	11.6	0.28	40	2450	0.997	7.7
AM-AMB1	4.0	1.0	298	11.6	0.33	20	2450	0.997	7.7
AM-AMB1	4.0	1.0	298	11.6	0.29	40	2450	0.997	7.7
AM-AMB2	10	0.514	298	23	0.88	7	4180	0.943	38.2
AM-AMB2	10	0.514	323	21	0.55	15	4050	0.580	34.8
HPAM	7.8	0.01	298	145	0.23	6	7110	0.890	188
HPAM	7.8	0.02	298	104	0.30	7	6360	0.891	135
HPAM	7.8	0.04	298	68	0.37	8.5	5520	0.893	88.1
HPAM	7.8	0.514	298	29	0.69	10	4160	0.943	37.7
AMPS-10	1.1	0.01	298	24	N/A	N/A	2030	0.890	4.39

Table 2.1 continued

Polymer	M x 10^{-6}, g/mol	I, mol/L	T, K	[η], dL/g	η_c, Poise	Q_{yield}, mL/min	d_h, Å	μ_o x 10^2, cP	V_c x 10^{-9}, $Å^3$
AMBA-5	1.05	0.01	298	9.7	N/A	N/A	1480	0.890	1.68
AMBA-5	1.05	0.02	298	8.3	N/A	N/A	1400	0.891	1.44
AMBA-5	1.05	0.04	298	6.7	N/A	N/A	1310	0.893	1.16
AMBA-5	1.05	0.514	298	5.2	N/A	N/A	1200	0.943	0.90
AMBA-10	1.09	0.01	298	25	N/A	N/A	2050	0.890	4.52
AMBA-10	1.09	0.02	298	15	N/A	N/A	1730	0.891	2.72
AMBA-10	1.09	0.044	298	11.8	N/A	N/A	1600	0.893	2.14
AMBA-10	1.09	0.13	298	22	N/A	N/A	1970	0.899	3.98
AMBA-10	1.09	0.32	298	7.2	N/A	N/A	1350	0.926	1.29
AMBA-10	1.09	0.514	298	12	N/A	N/A	1610	0.943	2.17
APTAC-5	0.89	0.01	298	6.9	N/A	N/A	1250	0.890	1.02
APTAC-5	0.89	0.02	298	5.4	N/A	N/A	1150	0.891	0.80
APTAC-5	0.89	0.04	298	4.4	N/A	N/A	1080	0.893	0.65
APTAC-5	0.89	0.514	298	3.7	N/A	N/A	1020	0.943	0.55
APTAC-10	0.89	0.01	298	9.4	N/A	N/A	1380	0.890	1.39
APTAC-10	0.89	0.02	298	7.4	N/A	N/A	1280	0.891	1.09
APTAC-10	0.89	0.04	298	5.2	N/A	N/A	1140	0.893	0.77
APTAC-10	0.89	0.514	298	3.3	N/A	N/A	976	0.943	0.49

Theoretical Polymer Coil Yield Extension Rate

Polymer Coil Hydrodynamic Diameter

A flexible, linear polymer molecule in a good solvent assumes a dynamic random coil conformation. The coil is roughly spherical and undergoes continuous thermal fluctuations. The hydrodynamic volume of a solvated polymer coil can be calculated from the solution intrinsic viscosity, $V_c = M [\eta] / N_A$. The equation for the volume of a sphere can be used to calculate the coil hydrodynamic diameter, d_h, from the coil volume, V_c. Eq. (4) expresses the coil diameter in terms of coil volume or intrinsic viscosity.

$$d_h = \left(\frac{6}{\pi} V_c\right)^{1/3} = \left(\frac{6}{\pi} \frac{[\eta] M}{N_A}\right)^{1/3} \quad (4)$$

Polymer Coil Extension Rate

When a dilute polymer solution undergoes fluid flow, the solvated polymer coils experience drag forces. Because of the axial velocity gradient in an extensional fluid flow field, the downstream side of a polymer coil is subjected to greater drag forces than is the upstream side. The resulting drag force gradient is the driving force for coil extension, and, in part, determines the rate of coil extension, R_E.[59]

The drag force gradient across a solvated polymer coil in an extensional flow field increases as the fluid extensional strain rate, $\dot{\varepsilon}$, the solvent apparent viscosity, μ_o, and the polymer coil size increase. Therefore, the rate of coil extension, R_E, is expected to be proportional to the product of the fluid strain rate, the solvent viscosity, and the hydrodynamic diameter of the polymer coil. This relationship is expressed as Eq. (5) where k_1 is a proportionality constant.

$$R_E = k_1 \, d_h \, \dot{\varepsilon} \, \mu_o \quad (5)$$

Polymer Coil Recovery Rate

Macromolecular thermal motions lead to coil deformation recovery, which counteracts coil extension. A polymer coil persistently relaxes toward its equilibrium random coil conformation. The rate of coil extensional strain recovery, R_C, depends on the solution temperature as well as certain macromolecular characteristics. Durst[56] and Hassager[60] predicted that, in dilute solutions, the polymer coil recovery rate from a strain deformation would be inversely proportional to the product of the polymer coil characteristic recovery time, λ_c, and the fluid strain rate, $\dot{\varepsilon}$. Thus, the rate of coil recovery from an extensional strain is given by Eq. (6), where k_2 is a proportionality constant and x is an exponent.

$$R_C = \frac{k_2}{(\lambda_c \, \dot{\varepsilon})^x} \quad (6)$$

A measure of the polymer coil characteristic recovery time is the Zimm response time, λ_Z, which can be estimated using Eq. (7), where R is the gas law constant.

$$\lambda_c = \lambda_Z \approx \frac{25 \, M \, [\eta] \, \mu_o}{6 \, \pi^2 \, R \, T} \quad (7)$$

By substituting Boltzmann's constant, $k_B = R / N_A$, and Eq. (4) into Eq. (7), the polymer coil characteristic recovery time can be expressed in terms of the coil hydrodynamic diameter as Eq. (8).

$$\lambda_c = \frac{25 \, \mu_o \, d_h^3}{36 \, \pi \, k_B \, T} \quad (8)$$

Polymer Coil Yield Extension Rate

If the coil extension rate is less than the strain recovery rate, i.e., $R_E < R_C$, the coil will not extend substantially because any coil extension induced by the fluid flow field is instantaneously recovered by random macromolecular fluctuations. To achieve significant polymer coil extension, fluid extension rates must be sufficiently high that $R_E > R_C$. The fluid extensional strain rate at which a polymer coil yields and becomes extended by the flow field can be estimated by assuming that coil extension starts when the rate of coil extension, R_E, is equal to the rate of coil recovery from an extensional strain, R_C. Thus, the polymer coil yield extension rate can be determined by equating Eqs. (5) and (6) and rearranging to form Eq. (9).

$$\dot{\varepsilon}_{yield} = k_3 \, \mu_o^{-1} \, d_h^{-\left(\frac{1+3x}{1+x}\right)} \tag{9}$$

In Eq. (9), k_3 is the following group of constants: $k_3 = \left(\frac{k_2}{k_1}\right)^{\frac{1}{1+x}} \left(\frac{36 \pi k_B T}{25}\right)^{\frac{x}{1+x}}$

Note that temperature, which did vary in a small number of the experimental data sets, was included as a constant in the k_3 term. However, on an absolute scale the temperature range does not differ from room temperature by more than a few percent. Therefore, fluid temperature was approximated to be constant. The influence of experimental fluid temperature is reflected in a significant variation of the solvent viscosity, μ_o.

Eq. (1) can be used to express the fluid yield strain rate in terms of the measured polymer coil yield flow rate, Eq. (10).

$$\dot{\varepsilon}_{yield} = \frac{16 \, Q_{yield}}{3 \pi \, D_s^{\,2} \, d_f} \frac{1-f}{f} \tag{10}$$

Eqs. (9) and (10) were equated and rearranged to form Eq. (11), where $b = -\frac{1+3x}{1+x}$, and $\kappa = \frac{3 \pi \, k_3 \, D_s^{\,2} \, d_f}{16} \frac{f}{1-f}$.

$$\mu_o \, Q_{yield} = \kappa \, d_h^{\,b} \tag{11}$$

Because the parameters defining κ were constant in all of the SER polymer solution experiments, Eq. (11) predicts that for any polymer solution Q_{yield} is only a function of the polymer coil hydrodynamic diameter and the solvent viscosity. Furthermore Eq. (11) suggests that a log-log plot of the product (μ_o Q_{yield}) versus d_h should yield a linear relationship in which the straight line intercept, a, and slope, b, are related to x and κ, i.e., $\kappa = 10^a$ and $x = -(1 + b)/(3 + b)$. The work of Hassager[60] suggests

that the value of x should be near unity; therefore, the b value should approximately equal -2.0.

Discussion of Results

Comparison of Theory to Experimental Results

Figure 2.6 is a logarithmic space plot of all experimental SER data where polymer coil extension was detected. Data was plotted according to Eq. (11), and the line in the figure represents the fit function of the equation to the data. Though there is significant scatter, the twenty-three data points tend to form a common line with a correlation coefficient of 0.883. Polymer solution yield flow rate tended to decrease with increasing polymer coil hydrodynamic diameter. Also, a higher solvent viscosity resulted in a lower yield point. Both of the effects are reasonable in view of the drag forces experienced by a polymer coil in an extensional flow field. It is possible that other factors not investigated could partially determine polymer coil yield point.

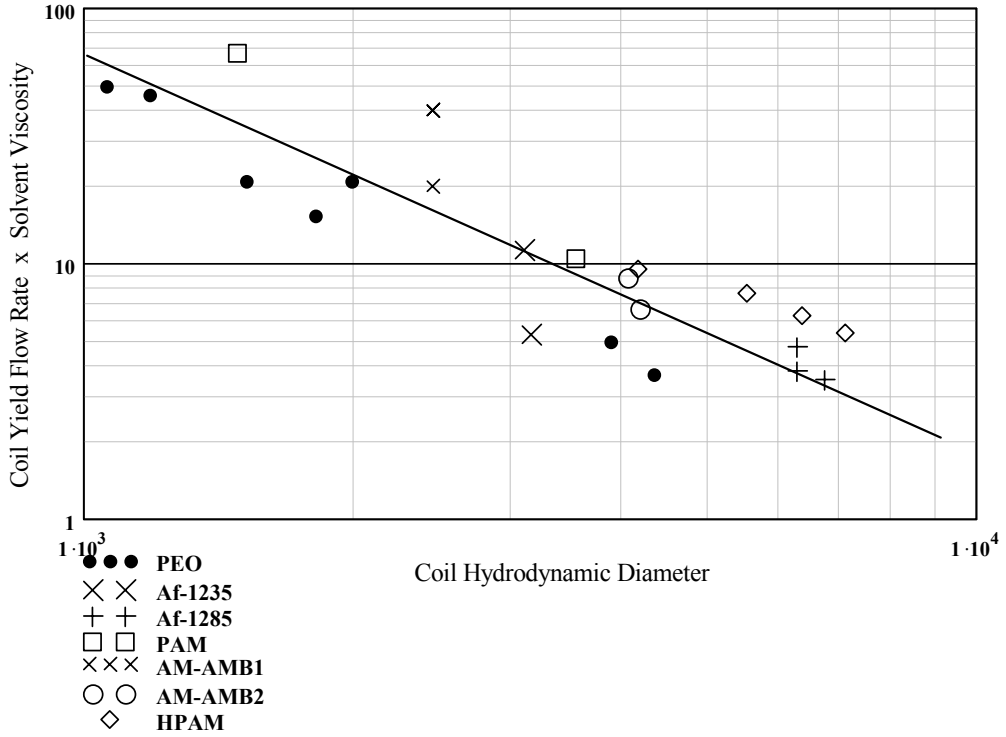

Figure 2.6. Log-log plot of screen extensional rheometer data according to Eq. (11). Plot symbols are: PEO - filled circles, PAM - boxes, HPAM - diamonds, Af-1235 - large x's, Af-1285 - pluses, AM-AMB1 - small x's, AM-AMB2 - open circles. The solid line represents the fit function.

Regression of Eq. (11) to the experimental data resulted in the following parameter values: b = -1.57 and $\kappa = (3.32 \times 10^6$ mL cP $Å^{1.57}$ $min^{-1})$. The value for b is

about 20% less than that expected from the work of Hassager.[60] Thus, it appears that a correlation exists as Hassager's work suggests, but the relationship determined in this work is not exactly as found by Hassager.

The coil viscosity was anticipated to be proportional to the polymer solution intrinsic viscosity. Assuming a power law relationship, $\eta_c = k_4 [\eta]^p$, where k_4 is a proportionality constant and p is an exponent, a logarithmic plot of coil viscosity versus intrinsic viscosity should yield a common line with a slope equal to p and an intercept equal to the logarithm of k_4.

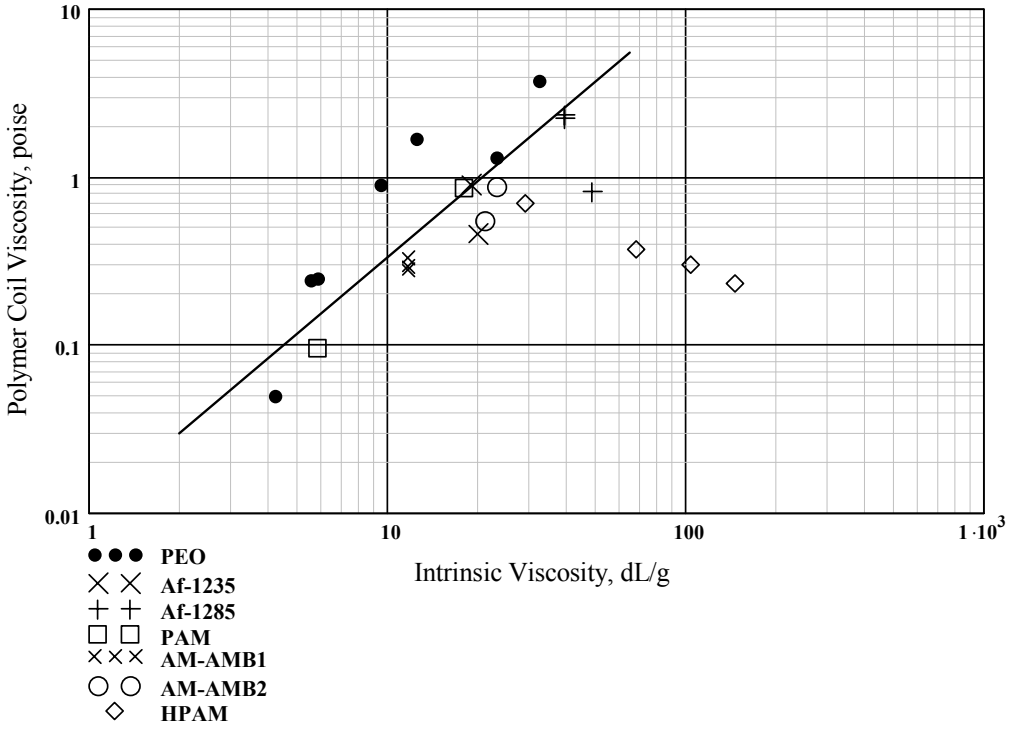

Figure 2.7. Log-log plot of screen extensional rheometer data according to Eq. (11). Plot symbols are: PEO - filled circles, PAM - boxes, HPAM - diamonds, Af-1235 - large x's, Af-1285 - pluses, AM-AMB1 - small x's, AM-AMB2 - open circles. The solid line represents the fit function to the data, excluding the HPAM data.

Figure 2.7 is a log-log plot of η_c versus $[\eta]$. Anomalous behavior of the HPAM polymer is immediately apparent. The HPAM data, which represents solution extensional viscosity measurements for a single polymer sample at four solution ionic strengths, exhibits decreasing coil viscosity with increasing intrinsic viscosity. Thus, the HPAM data points were omitted in fitting the power law function to the data. The values of k_4 and p determined from regression of the power law expression to the experimental data, excluding the HPAM data, were (0.02 poise $g^{1.25}$ $dL^{-1.25}$) and 1.25, respectively. The correlation coefficient between log η_c and log $[\eta]$ using the nineteen data points was 0.816.

While some correlation of coil viscosity with intrinsic viscosity seemed to exist, the relationship was not as significant as expected. Recall that the coil viscosity reflects the increase in energy per polymer coil required for polymer solution fluid flow across the packed bed of screens as compared to the pure solvent. Various mechanisms of energy conversion by the polymer coils are conceivable. Correlations were investigated for several different parameters and combinations of parameters, which were thought to possibly affect the coil viscosity.

A possible source of energy loss is the disruption or pumping of solvent as the polymer coil undergoes cyclic deformations. Since the vast majority of matter inside a polymer coil volume is solvent, some solvent property is likely to influence the measured polymer coil viscosity. The quality of polymer-solvent interactions could be of importance. Also, the solvent apparent viscosity was considered. The influence of the solvent viscosity was tested in a similar method to that used in Eq. (11), but inclusion of the parameter slightly weakened the correlation. Polymer solution intrinsic viscosity appeared to be the most important factor determining dilute polymer solution resistance to flow through the screen extensional rheometer.

The reason for the negative slope of the HPAM data is not understood. The four data points form a line with very little scatter. Because of its polyelectrolyte character, changing the solution ionic strength altered the intrinsic viscosity of HPAM. As the solution ionic strength was decreased, the intrinsic viscosity increased and the measured coil viscosity consistently decreased. The trend continued throughout the three measurements made at low ionic strength, where the solvent apparent viscosity was virtually constant; therefore the behavior cannot be explained by a variation of solvent viscosity with NaCl concentration.

The HPAM data point collected at the highest solution ionic strength, 0.514 mol/L, appears to agree with the general data trend. Data is included in Figure 2.7 for polyelectrolytes other than HPAM, but these data were all taken at high ionic strength (i.e., $I \geq 0.514$ mol/L). Therefore, the three data points that disagree most describe a polyelectrolyte at low ionic strength. The unusual coil viscosity behavior of the HPAM polymer could be due to electrostatic effects on coil flexibility. Electrostatic repulsions expand the polymer coils at lower ionic strengths, and these intramolecular interactions could hinder polymer coil strain deformation. If so, the effect is desirable for EOR because the coil viscosity would be greater at the higher ionic strengths found underground.

Conclusions

The polymers solution properties reported here were studied for their potential applicability to polymer flooding in EOR processes. With current enhanced oil recovery methods, the harsh underground environment is detrimental to polymer solution

performance. An improved polymer solution would take advantage of reservoir conditions.

Polymer enhancement of the water flood viscosity relies on the polymer coil resistance to extensional deformation. A correlation was demonstrated in this report between polymer coil hydrodynamic diameter and the fluid extension rate at which polymer coil extension begins. Ideally, the macromolecules should have a collapsed coil configuration during injection into the reservoir to reduce both pumping costs and shear degradation at the well-head, where fluid extension rates are highest. Also, because fluid extension rates decrease away from the injection well-head, polymer coils should expand after injection to reduced their yield extension rate and increase their solution extensional viscosity within the reservoir.

The solution environment in underground reservoirs is characterized by high temperature, basic pH, and the presence of monovalent and divalent ions. Thus, the desired complex polymer solution behavior may be achieved with synthetic polymers that can change their macromolecular conformation upon encountering certain environmental stimuli such as variations in solution temperature, pH, and electrolyte concentration. Proper molecular design and synthesis facilitated by theoretical prediction of the relationships among polymer chemical structure and solvent flow properties should lead to improved sweep efficiency during polymer flooding.

Nomenclature

Symbol	Description
η_e	fluid extensional viscosity
c_p	solution polymer concentration
$[\eta]$	polymer solution intrinsic viscosity
d_f	nylon screen filament diameter
f	fractional free projected area of nylon screen
ϕ	nylon screen porosity
D_s	nylon screen disk diameter
$\dot{\varepsilon}$	fluid extension rate
Q	fluid volumetric flow rate

$\dot{\varepsilon}_{yield}$	critical fluid strain rate for polymer coil extension
Q_{yield}	critical volumetric fluid flow rate for polymer coil extension
ΔP_s	polymer solution pressure drop across packed bed
ΔP_o	solvent pressure drop across packed bed
η_c	polymer coil viscosity
β	collection of constants
n	number of screens packed into screen extensional rheometer
d_h	polymer coil hydrodynamic diameter
V_c	polymer coil hydrodynamic volume in solution
M	average polymer molecular weight
N_A	Avogadro's number
R_E	polymer coil extension rate
μ_o	solvent apparent viscosity
k_1	proportionality constant in polymer coil extension rate equation
R_C	polymer coil strain recovery rate
λ_c	polymer coil characteristic recovery time
k_2	proportionality constant in polymer coil strain recovery rate equation
x	variable exponent in polymer coil strain recovery rate equation
λ_Z	polymer coil Zimm response time
R	gas law constant
T	absolute temperature
k_B	Boltzmann's constant

$\dot{\varepsilon}_{yield}$	polymer coil yield extension rate
k_3	grouping of constants in Eq. V-9
κ	grouping of constants in Eq. V-11
b	exponential term in Eq. V-11
k_4	proportionality constant
p	exponent in power law relationship

CHAPTER 3

TASK 5: POLYMER MOBILITY CHARACTERIZATION

Dispersion Corrections for Size Exclusion Chromatography

Background

Chromatography is extensively used in our research to characterize the molecular weights of the water-soluble polymers synthesized for potential use as mobility control agents in oil reservoir flooding operations. Accurate determination of polymer molecular weights requires that dispersion corrections be made when analyzing chromatography results. These dispersion corrections are not trivial. This report details the procedures and calculations performed to obtain dispersion corrected polymer molecular weights using chromatography analysis.

Introduction

Size Exclusion Chromatography

As shown in Figure 3.1, chromatography is a flow system having three basic components; (1) solvent or mobile phase, (2) micro porous packing or a stationary phase, and (3) polymer molecules in solution. A polymer sample in solution is injected into the system mobile phase and pumped through a column filled with a micro porous packing material. Because the packing material is micro porous, polymer molecules will diffuse between the mobile phase located in the interstitial volume between packing particles and the more stagnant mobile phase found within the packing micro pores. If there are no secondary interactions between the polymer and packing surface such as adsorption or repulsion, the penetration of polymer molecules into the packing micro pore volume is dependent only upon the hydrodynamic size of the macromolecule in solution relative to the size of the packing pores. If secondary interactions are absent, we refer to this type chromatography as size exclusion chromatography (SEC).

In SEC[61] the total volume of fluid within a packed column, V_t, can be divided into two parts: (1) the interstitial volume, V_o, made up of large macro channels between packing particles and (2) the smaller channels or pores within the micro pore volume, V_p.

$$V_t = V_o + V_p \qquad (1)$$

The macro channels are usually much larger than the size of the polymer molecules. Thus, all polymer molecules, regardless of their size, will penetrate the interstitial volume. However, if a polymer molecule is too large to enter a micro pore, its penetration into this volume is excluded. Therefore, polymer molecular weight or

hydrodynamic size separation occurs as the polymers flow through the packed column because micro pores are present that exclude the larger polymer molecules.

The smaller a polymer molecule, the more micro pore volume it will penetrate. Smaller molecules elute later from the SEC system at a greater volume than larger molecules. A very large molecule will penetrate only the interstitial volume, V_o. A very small molecule will penetrate all the permeation volume, V_t. Molecules of intermediate size will penetrate all of the interstitial volume but only a fraction of micro pore volume. The fraction of the micro pore volume penetrated by a molecule is called the distribution coefficient, K. Thus, the volume penetrated by a molecule V_e, the elution volume, is defined by

$$V_e = V_o + K\,V_p \qquad (2)$$

To use equation (2) to determine the molecular weight distribution of polymer molecules in solution, a calibration of the SEC system must be performed. An SEC calibration relates a polymer property, usually hydrodynamic size or molecular weight, to the elution volume. The calibration is based on a SEC separation model.

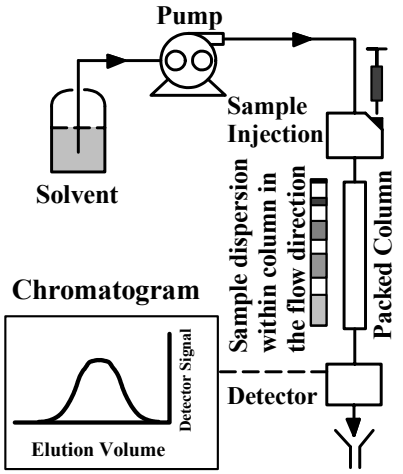

Figure 3.1 : Liquid Chromatography System

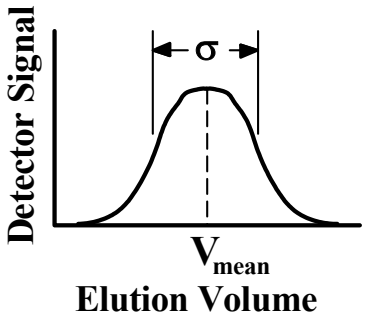

Figure 3.2 : Chromatogram of a monodispersed sample

Experimental

Benoit Size Exclusion Model

The Benoit model[62] uses the logarithm of M [0] versus elution volume for SEC calibration. The product of molecular weight, M, and intrinsic viscosity, [0], is proportional to the hydrodynamic volume occupied by a polymer molecule in solution. The calibration relationship is given by Equation (3). Unfortunately the Benoit calibration is inadequate in describing SEC behavior at elution volumes near V_o and V_t.

$$V_e = A + B \log\left(M[\eta]\right) \qquad (3)$$ where A and B are calibration constants.

Calibration can be done by measuring the elution volume of several polymer standards having known M [0] (hydrodynamic volume). When using standards of the same type polymer then Equation (3) can be expressed as

$M = D_1 \exp(-D_2 \ Ve)$ (4) where D_1 and D_2 are calibration constants.

To get accurate molecular weights the calibration relationships must be corrected for polymer separation not due to size exclusion. This macromolecular separation not due to macromolecular size exclusion is called dispersion.

Dispersion in Size Exclusion Chromatography

If a fluid sample containing single size molecules is injected onto an SEC column, the sample forms a volume plug within the column. As the sample plug migrates downstream, its width increases. The sample plug volume becomes more dispersed in the direction of flow. This dispersion is detrimental to molecular weight analysis by SEC. Dispersion is caused by (1) variability in the mobile phase velocity from point to point across the packed column, (2) non-equilibrium in transfer of solute (polymer molecules) between the mobile phase fluid and packing stationary phase fluid, and (3) molecular diffusion of the solute in the direction of flow.

Dispersion can be explained by a plate theory[63] or model. In this theory the SEC column is divided into N number of adjoining separate zones, with each volume zone having a length such that complete equilibrium of the solute exists between the mobile and stationary phases. Each zone is called a "theoretical plate" and the zone length is called the "height equivalent to a theoretical plate," H.

As solute travels from one plate to the next, only a fraction of solute is carried to the next plate. This repetitive partition process leads to a solute Gaussian distribution among many neighboring plates. From plate theory, the height of a theoretical plate, H, can be determined from the shape of the elution chromatogram of a low molecular weight, mono-dispersed sample. See Figure 3.2.

$$H = \frac{L}{N} = \left(\frac{\sigma^2}{V_{mean}^2}\right) L \qquad (5)$$ In equation (5) H equals the height

of a single plate, L is the length of the packed column, N is the total number of theoretical plates within the packed column, V_{mean} is the mean sample elution volume, and F is half of chromatogram width between the chromatogram's two inflection points. Smaller values of H signify more efficient SEC separation systems. Insufficient packing, larger packing particle size, and higher mobile phase velocities cause H to increase. Usually the best obtainable value for H varies with the type packing material type and geometry.

Type Packing	Expected Plate Height, H, cm
Silica gels	0.15
Porous glass	0.08
Cross-linked polystyrene gels	0.05

Tung's Dispersion Model

Dispersion or band broadening corrections must be performed before SEC chromatograms can be quantitatively analyzed to determine polymer molecular distribution. Dispersion corrections are unique to each SEC system and operating condition. Dispersion corrections for one SEC system cannot be applied to a different SEC system or to the same system operating at different conditions.

The correction for SEC dispersion can be obtained by solving Tung's integral equation[64] for the dispersion corrected chromatogram, w(y):

$$f(v) = \int_{-\infty}^{+\infty} [w(y)] \left(\frac{H}{\pi}\right) \exp\{-H(v-y)^2\}\, dy \qquad (6) \qquad \text{where}$$

v and y are elution volumes, f(v) is the observed uncorrected chromatogram, w(y) is the dispersion corrected chromatogram, and H is the spreading factor. Each SEC system has a unique spreading factor associated with the SEC system and its operating conditions. After Tung's equation is solved using polymer standards having known distributions, dispersion corrected chromatogram and correct molecular weight distributions can be made for polymer samples having unknown molecular weight distributions.

Solution of Tung's equation is difficult and no symbolic solution exists. Thus, a solution to determine the corrected chromatogram requires a computer program involving a numerical algorithm that simulates Tung's equation and uses several chromatograms of polymer standards having known molecular weight distributions.

Results

Application of the TBS Dispersion Method in Aqueous SEC

A recent method to correct SEC dispersion has been advanced by Hamielec[65] at McMaster University. This TBS method is based on having **t**wo **b**road molecular weight polymer **s**tandards, A and B, with known number average molecular weights, Mn_{true}, and known weight average molecular weights, Mw_{true}. The TBS method does not have to

have a spreading function that is a Gaussian distribution as in other dispersion correction methods. Also the TBS method allows simultaneous determination of both the Benoit SEC molecular weight calibration curve and the dispersion spreading parameters. In the TBS method, four equations are solved for four parameters. Two of the parameters are the SEC calibration constants, D_1 and D_2. The second set of parameters determined is the dispersion spreading values for the two polymer standards, X_A and X_B.

$$Mn_{trueA} \exp\left(\frac{-D_2^{\,2} X_A}{2}\right) = D_1 \left[\int_0^{\infty} F_A(v) \exp(D_2\, v)\, dv\right]^{-1} \qquad (7)$$

$$Mn_{trueB} \exp\left(\frac{-D_2^{\,2} X_B}{2}\right) = D_1 \left[\int_0^{\infty} F_B(v) \exp(D_2\, v)\, dv\right]^{-1} \qquad (8)$$

$$Mw_{trueA} \exp\left(\frac{D_2^{\,2} X_A}{2}\right) = D_1 \left[\int_0^{\infty} F_A(v) \exp(-D_2\, v)\, dv\right] \qquad (9)$$

$$Mw_{trueB} \exp\left(\frac{D_2^{\,2} X_B}{2}\right) = D_1 \left[\int_0^{\infty} F_B(v) \exp(-D_2\, v)\, dv\right] \qquad (10)$$

The right sides of Equations (7) and (8) are the apparent number average molecular weights of the polymer standards A and B. The right sides of Equations (9) and (10) are the apparent weight average molecular weights of the polymer standards A and B.

Solution of the TBS Integral Equations

After the four integrals in the four equations are transformed into summations, a computer algorithm can be constructed to solve for the four parameters. A MathCad worksheet[66] is provided in Appendix A which shows in detail the operations required to obtain the four parameters when using poly(ethylene oxide) standards in aqueous SEC chromatography. Referring to the MathCad worksheet, the following operations are performed in sequence.

1) Nine poly(ethylene oxide) standards were analyzed on the SEC system. Elution results are described with molecular weights and SEC mean elution volumes. Using this information, the two uncorrected Benoit calibration constants for the SEC system are determined and an Apparent SEC Calibration plot is made. The calibration function plotted is not corrected for dispersion.

2) The functions “Reduce”, “Norm”, “FilterRows” and “place” are defined. Details describing these functions are described in the worksheet. In general, these functions enable manipulation of the vast amount of data (detector signal and elution volume) describing a chromatogram.

3) The path and data file name for poly(ethylene oxide) standard A are specified. The raw chromatogram data for standard A is input into the worksheet and plotted. Note that both a refractive index (RI) signal and ultraviolet (UV) signal are shown in the plot. The dispersion analysis will only use the RI signals.

4) The raw standard A chromatogram is reduced to provide only the data at the elution times of standard A. The baseline is removed and the modified standard A refractive index detector chromatogram is plotted.

5) The path and data file name for poly(ethylene oxide) standard B are specified. The raw chromatogram data is input and plotted.

6) The raw standard B chromatogram is reduced to provide only the RI data at the elution times of standard B. The baseline is removed and the modified standard B refractive index detector chromatogram is plotted.

7) The uncorrected apparent number average and weight average molecular weights are determined for both standard A and standard B using summation equations. Note that the uncorrected calibration constants are used.

8) The four TBS equations in summation format are combined to solve for the corrected calibration constant D2 (referred to as DC_2 in the worksheet).

9) The corrected calibration constant D2 is then used with the TBS equations to find the corrected calibration constant D1 (referred to as DC_1 in the worksheet).

10) The Benoit dispersion corrected D1 and D2 constants are now used to plot the corrected calibration function. The uncorrected calibration function is also plotted that shows how the dispersion correction has changed the SEC calibration.

11) The corrected apparent number average and weight average molecular weights are determined for both standard A and standard B using summations in place of integrations. The dispersion corrected calibration constants are used.

12) The two dispersion spreading values, X_A and X_B, are now determined. Thereafter the spreading value is made a linear function of the elution volume.

13) Using the dispersion spreading values, the number and weight average molecular weight corrections are determined. The molecular weight corrections are then used to calculate the final number average and weight average molecular weights for both polymer standards.

14) Using the corrected Benoit SEC calibration constants, D1 and D2, the molecular weight distributions for both standards are plotted. The uncorrected molecular weight distributions for both standards are also plotted for comparison.

Conclusion

Although SEC dispersion corrections are complex, computer analysis has simplified the task and the corrections described in this report are now routinely performed in our laboratory. Accurate SEC molecular weight distribution information has enabled a more complete understanding of the reaction mechanism occurring in polymer synthesis. This knowledge is assisting in developing superior synthetic polymers for use in enhanced oil recovery.

Nomenclature

Symbol	Description
A	Calibration constant, Equation (3)
B	Calibration constant, Equation (3)
D_1	Calibration constant, Equation (4)
D_2	Calibration constant, Equation (4)
F(v)	Number normalized distribution of macromolecules as a function of elution volume
f(v)	Uncorrected molecular weight distribution
H	Plate height
K	Distribution coefficient
L	Packed column length
M	Molecular weight
M_{ntrue}	Number average molecular weight
M_{wtrue}	Weight average molecular weight
N	Number of plates
v	Elution volume associated with the uncorrected molecular weight distribution
V_e	Elution volume
V_{mean}	Mean elution volume
V_o	Interstitial volume
V_p	Micro pore volume
V_t	Total volume
X	Dispersion spreading value
y	Elution volume associated with the corrected molecular weight distribution
$[\eta]$	Polymer intrinsic viscosity
σ	Standard deviation of mono dispersed sample chromatogram

Appendix A : SEC Calibration with Dispersion Corrections Using TBS Method

RDH 9/10/04

Input poly(ethylene oxide) standards chromatography information

$$mole := 1$$

$$PEOMW := \begin{pmatrix} 3450 \\ 11840 \\ 20300 \\ 43520 \\ 74900 \\ 124700 \\ 272500 \\ 460000 \\ 761300 \end{pmatrix} \cdot \frac{gm}{mole} \qquad MeanElutionVolume := \begin{pmatrix} 13.592 \\ 12.308 \\ 11.714 \\ 10.997 \\ 10.465 \\ 10.188 \\ 9.32 \\ 8.786 \\ 8.361 \end{pmatrix} \cdot mL$$

$$FlowRate := 0.5 \cdot \frac{mL}{min}$$

Calibration Function

M = molecular weight
Ve = elution volume

$$M = D1 \cdot \exp(-D2 \cdot V_e)$$

$$\ln(M) = \ln(D1) - D2 \cdot V_e$$

$$D1 := \exp\left(intercept\left(\frac{MeanElutionVolume}{mL}, \ln\left(\frac{PEOMW}{\frac{gm}{mole}}\right)\right)\right) \qquad D2 := -slope\left(\frac{MeanElutionVolume}{mL}, \ln\left(\frac{PEOMW}{\frac{gm}{mole}}\right)\right)$$

$D1 = 4.399 \times 10^9$ $D2 = 1.041$ <= Apparent or uncorrected calibration constants

$j := 0 .. 35$ $V_{e_j} := \frac{j + 15}{3}$ $M_j := D1 \cdot \exp(-D2 \cdot V_{e_j})$ < Calibration function

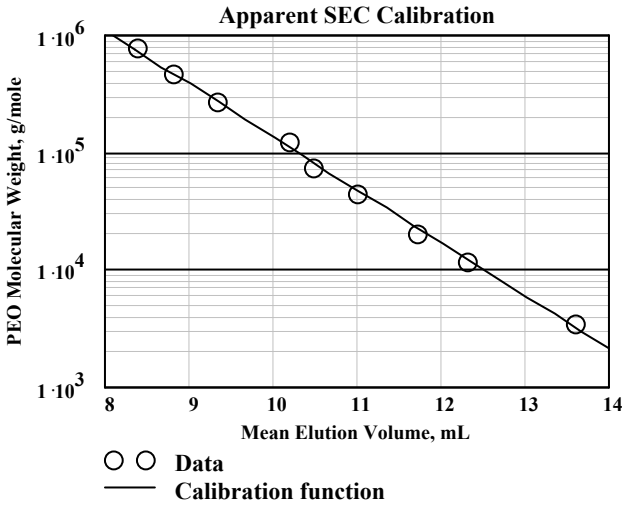

The calibration function fits the SEC data over the range shown.

For the function Reduce(MM, factor,place) factor is the number of rows or columns remaining in the matrix MM after the elements are removed from the matrix. The MM matrix can be reduced with respect to either rows or columns by setting place equal to "rows" or "cols".

Data matrix reduction function

$$\begin{aligned}
&\textbf{Reduce}(MM, factor, place) := \\
&\quad MM \leftarrow MM^{T} \ \textbf{if} \ place = \text{"rows"} \\
&\quad factor \leftarrow 3 \ \textbf{if} \ factor < 3 \\
&\quad factor \leftarrow factor - 1 \\
&\quad imax \leftarrow cols(MM) - 1 \\
&\quad factor \leftarrow imax \ \textbf{if} \ imax < factor \\
&\quad \textbf{for} \ i \in 0..factor \\
&\quad\quad I \leftarrow i \cdot \frac{imax}{factor} - \text{mod}\left(i \cdot \frac{imax}{factor}, 1\right) \\
&\quad\quad filter^{\langle i \rangle} \leftarrow MM^{\langle I \rangle} \\
&\quad filter \leftarrow filter^{T} \ \textbf{if} \ place = \text{"rows"} \\
&\quad filter
\end{aligned}$$

Function Norm (A,V) is used to make a chromatogram area equal to 1. The chromatogram is the detector signals in array A and the corresponding elution volumes in array V.

$$\begin{aligned}
&\textbf{Norm}(A, V) := \\
&\quad NumberElements \leftarrow last(A) \\
&\quad Area_0 \leftarrow 0 \\
&\quad \textbf{for} \ i \in 1..NumberElements \\
&\quad\quad Area_i \leftarrow (V_i - V_{i-1}) \cdot \left(\frac{A_i + A_{i-1}}{2}\right) \\
&\quad CumArea_0 \leftarrow 0 \\
&\quad \textbf{for} \ j \in 1..NumberElements \\
&\quad\quad CumArea_j \leftarrow Area_j + CumArea_{j-1} \\
&\quad A \leftarrow \frac{A}{CumArea_{last(CumArea)}} \\
&\quad Area \leftarrow \frac{Area}{CumArea_{last(CumArea)}} \\
&\quad CumArea \leftarrow \frac{CumArea}{CumArea_{last(CumArea)}} \\
&\quad Aout \leftarrow A \\
&\quad Aout
\end{aligned}$$

FilterRows removes any row from the matrix M that has a value V in column number C of the matrix.

```
FilterRows(M, C, V) :=
    End ← cols(M) − 1
    for i ∈ (0.. rows(M) − 1)
        ZZ ← submatrix(M, i, i, 0, End)  if  M_{i, C} ≠ V
        k ← i  if  M_{i, C} ≠ V
        break  if  M_{i, C} ≠ V
    for i ∈ k + 1.. rows(M) − 1
        for j ∈ (0.. End)
            Z ← submatrix(M, i, i, 0, End)  if  M_{i, C} ≠ V
        ZZ ← stack(ZZ, Z)  if  M_{i, C} ≠ V
    ZZ
```

Function to find a given place in a matrix

```
place(matrix, position) :=
    for i ∈ 0.. rows(matrix) − 1
        for j ∈ 0.. cols(matrix) − 1
            Point_0 ← i  if  matrix_{i, j} = position
            Point_1 ← j  if  matrix_{i, j} = position
    Point
```

Select two PEO standards to use to establish dispersion correction

See Omorodion, S. N. E., and A. E. Hamielec, *J. Applied Poly. Sci*., *39*, 875-92 (1990**Set path and name of data file**

```
path := "C:\Documents and Settings\rdhester\My Documents\SEC\"        datafile := "peo 11840"        Name := concat(path, datafile)

Name = "C:\Documents and Settings\rdhester\My Documents\SEC\peo 11840"
```

Standard A

```
X1 := READPRN(Name)        S1 := if(rows(X1) > 1600, Reduce(X1, 1600, "rows"), X1)

MW_NtrueA := 10980        MW_WtrueA := 11310
```

<= Number average and weight average polymer molecular weights reported by vendor.

$\text{rows}(S1) = 1600$ $\quad S1^{\langle 0 \rangle} := \frac{S1^{\langle 0 \rangle}}{60} \bullet \frac{\text{FlowRate}}{\frac{mL}{min}}$ $\quad S1^{\langle 0 \rangle} := \text{round}\left(S1^{\langle 0 \rangle}, 3\right)$ $\quad \Delta 1V := 0.480$ <= Difference in volume between detectors

$MAXS11 := \max\left(S1^{\langle 1 \rangle} - \min\left(S1^{\langle 1 \rangle}\right)\right)$ $\quad S1^{\langle 1 \rangle} := \frac{S1^{\langle 1 \rangle} - \min\left(S1^{\langle 1 \rangle}\right)}{MAXS11}$

$MAXS12 := \max\left(S1^{\langle 2 \rangle} - \min\left(S1^{\langle 2 \rangle}\right)\right)$ $\quad S1^{\langle 2 \rangle} := \frac{S1^{\langle 2 \rangle} - \min\left(S1^{\langle 2 \rangle}\right)}{MAXS12}$

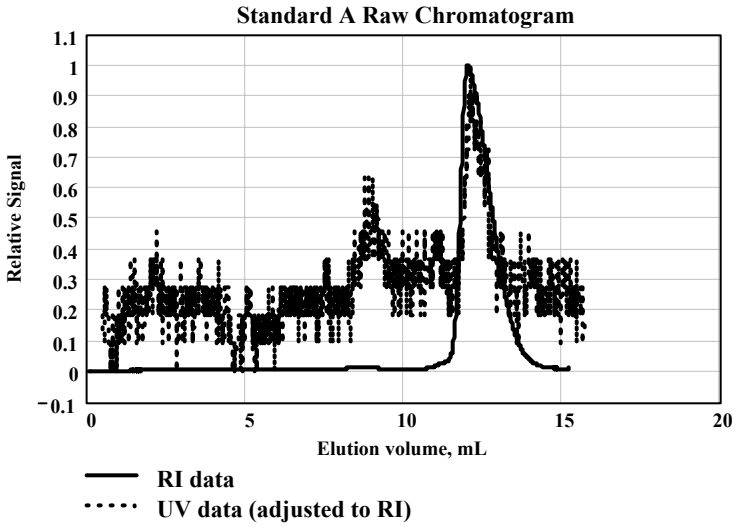

$S1 =$

	Elution Volume	RI Signal	UV Signal
	0	1	2
0	0.0000	0.0009	0.1818
1	0.0090	0.0009	0.1818
2	0.0190	0.0011	0.1818
3	0.0270	0.0009	0.0909
4	0.0380	0.0016	0.1818
5	0.0460	0.0014	0.2727
6	0.0570	0.0016	0.1818
7	0.0650	0.0016	0.1818
8	0.0760	0.0016	0.1818

Define elution volume limits for RI chromatogram

$StartA := \text{place}\left(S1^{\langle 0 \rangle}, 10.826\right)_0$ $\quad StartA = 1141$ $\quad EndA := \text{place}\left(S1^{\langle 0 \rangle}, 14.535\right)_0$ $\quad EndA = 1532$

$\left(S1^{\langle 0 \rangle}\right)_{StartA} = 10.826$ $\quad \left(S1^{\langle 1 \rangle}\right)_{StartA} = 0.013$ $\quad \left(S1^{\langle 0 \rangle}\right)_{EndA} = 14.535$ $\quad \left(S1^{\langle 1 \rangle}\right)_{EndA} = 0.012$

These operations are used to isolate the data for the chromatogram peak.

$j := 0 .. EndA - StartA$ $RIA_j := \left(S1^{\langle 1 \rangle}\right)_{j+StartA}$ $MAXA := max(RIA)$ $RIA := \frac{RIA}{MAXA}$ $EVA_j := \left(S1^{\langle 0 \rangle}\right)_{j+StartA}$

Define Baseline

$$ABaseSlope := \frac{RIA_0 - RIA_{EndA-StartA}}{EVA_0 - EVA_{EndA-StartA}} \qquad ABaseSlope = -6.11 \times 10^{-5}$$

$$ABaseIntercept := RIA_0 - ABaseSlope \bullet EVA_0 \qquad ABaseIntercept = 1.34 \times 10^{-2}$$

Remove baseline from chromatogram

$ACorrection_j := (ABaseIntercept + ABaseSlope \bullet EVA_j)$

$RIA_j := RIA_j - ACorrection_j$ $RIA := Norm(RIA, EVA)$

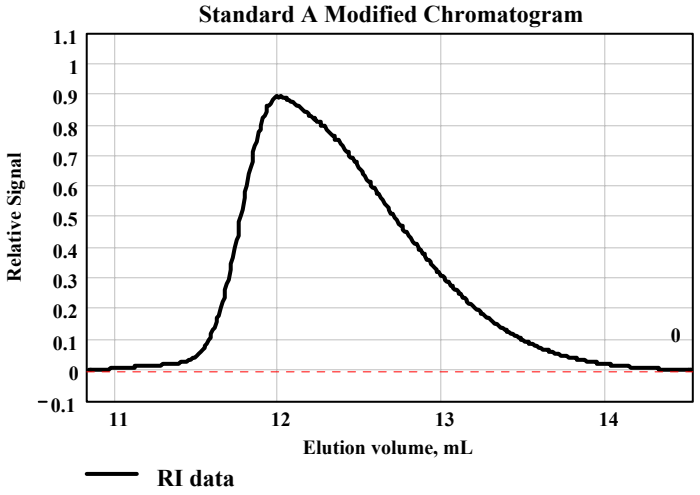

Max & Min in Standard A RI Signal

$max(RIA) = 0.892$ $min(RIA) = 0$

$rows(RIA) = 392$

$$place(RIA, min(RIA)) = \begin{pmatrix} 391 \\ 0 \end{pmatrix}$$

Number of data points (rows) defining the chromatogram

Standard B

datafile := "peo 460000" Name := concat(path, datafile) $X2 := READPRN(Name)$

$S2 := if(rows(X2) > 1600, Reduce(X2, 1600, "rows"), X2)$ $rows(S2) = 1600$ $S2^{\langle 0 \rangle} := \frac{S2^{\langle 0 \rangle}}{1.0 \bullet 60} \bullet \frac{FlowRate}{\frac{mL}{min}}$

$MW_{NtrueB} := 442300$ $MW_{WtrueB} := 469250$ <= Number average and weight average polymer molecular weights reported by vendor.

$S2^{\langle 0 \rangle} := round\left(S2^{\langle 0 \rangle}, 3\right)$ $\Delta 2V := 0.48$

$$MAXS21 := \max\left(S2^{\langle 1\rangle} - \min\left(S2^{\langle 1\rangle}\right)\right) \qquad S2^{\langle 1\rangle} := \frac{S2^{\langle 1\rangle} - \min\left(S2^{\langle 1\rangle}\right)}{MAXS21}$$

$$MAXS22 := \max\left(S2^{\langle 2\rangle} - \min\left(S2^{\langle 2\rangle}\right)\right) \qquad S2^{\langle 2\rangle} := \frac{S2^{\langle 2\rangle} - \min\left(S2^{\langle 2\rangle}\right)}{MAXS22}$$

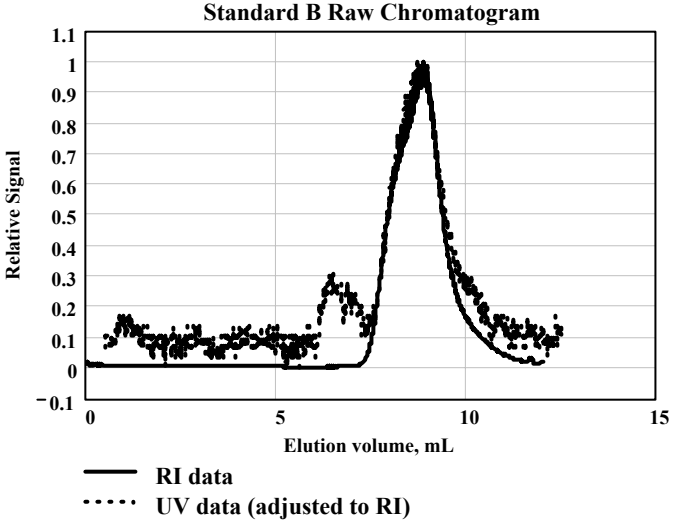

$S2 =$

	Elution Volume	RI Signal	UV Signal
	0	1	2
0	0.0000	0.0167	0.1034
1	0.0070	0.0167	0.1034
2	0.0140	0.0173	0.1034
3	0.0220	0.0173	0.1034
4	0.0290	0.0173	0.0690
5	0.0360	0.0180	0.1034
6	0.0450	0.0173	0.1034
7	0.0520	0.0180	0.1034
8	0.0580	0.0167	0.1034

Define elution volume limits for RI chromatogram

$$StartB := place\left(S2^{\langle 0\rangle}, 7.284\right)_0 \qquad StartB = 970 \qquad \left(S2^{\langle 0\rangle}\right)_{StartB} = 7.284 \qquad \left(S2^{\langle 1\rangle}\right)_{StartB} = 0.019$$

$$EndB := place\left(S2^{\langle 0\rangle}, 11.506\right)_0 \qquad EndB = 1532 \qquad \left(S2^{\langle 0\rangle}\right)_{EndB} = 11.506 \qquad \left(S2^{\langle 1\rangle}\right)_{EndB} = 0.022$$

These operations are used to isolate the data for the chromatogram peak.

$$j := 0..EndB - StartB \qquad RIB_j := \left(S2^{\langle 1\rangle}\right)_{j+StartB} \qquad MAXB := \max(RIB) \qquad RIB := \frac{RIB}{MAXB} \qquad EVB_j := \left(S2^{\langle 0\rangle}\right)_{j+StartB}$$

Define Baseline

$$BBaseSlope := \frac{RIB_0 - RIB_{EndB-StartB}}{EVB_0 - EVB_{EndB-StartB}} \qquad BBaseSlope = 5.87 \times 10^{-4} \qquad BBaseIntercept := RIB_0 - BBaseSlope \cdot EVB_0$$

Remove baseline from chromatogram

$$BCorrection_j := \left(BBaseIntercept + BBaseSlope \cdot EVB_j\right) \qquad RIB_j := RIB_j - BCorrection_j$$

$$RIB := Norm(RIB, EVB)$$

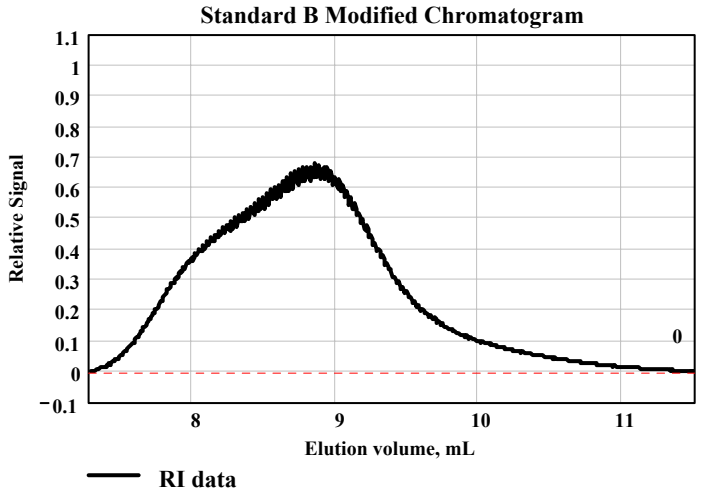

Max & Min in Standard B
RI Signal

$\max(RIB) = 0.678$

$\min(RIB) = 0$

$place(RIB, \min(RIB)) = \begin{pmatrix} 562 \\ 0 \end{pmatrix}$

$rows(RIB) = 563$

Number of data points (rows)
defining the chromatogram

Calculate Apparent Molecular Weights Using Uncorrected SEC Calibration Constants

$$MWAU := \frac{D1}{2} \cdot \frac{\sum_{j=0}^{rows(EVA)-2} \left[\left(\frac{RIA_j}{\exp(-D2 \cdot EVA_j)} + \frac{RIA_{j+1}}{\exp(-D2 \cdot EVA_{j+1})} \right) \cdot \left(-\exp(-D2 \cdot EVA_{j+1}) + \exp(-D2 \cdot EVA_j) \right) \cdot \left(\exp(-D2 \cdot EVA_{j+1}) + \exp(-D2 \cdot EVA_j) \right)^2 \right]}{\sum_{j=0}^{rows(EVA)-2} \left[\left(\frac{RIA_j}{\exp(-D2 \cdot EVA_j)} + \frac{RIA_{j+1}}{\exp(-D2 \cdot EVA_{j+1})} \right) \cdot \left(-\exp(-D2 \cdot EVA_{j+1}) + \exp(-D2 \cdot EVA_j) \right) \cdot \left(\exp(-D2 \cdot EVA_{j+1}) + \exp(-D2 \cdot EVA_j) \right) \right]}$$

$$MWBU := \frac{D1}{2} \cdot \frac{\sum_{j=0}^{rows(EVB)-2} \left[\left(\frac{RIB_j}{\exp(-D2 \cdot EVB_j)} + \frac{RIB_{j+1}}{\exp(-D2 \cdot EVB_{j+1})} \right) \cdot \left(-\exp(-D2 \cdot EVB_{j+1}) + \exp(-D2 \cdot EVB_j) \right) \cdot \left(\exp(-D2 \cdot EVB_{j+1}) + \exp(-D2 \cdot EVB_j) \right)^2 \right]}{\sum_{j=0}^{rows(EVB)-2} \left[\left(\frac{RIB_j}{\exp(-D2 \cdot EVB_j)} + \frac{RIB_{j+1}}{\exp(-D2 \cdot EVB_{j+1})} \right) \cdot \left(-\exp(-D2 \cdot EVB_{j+1}) + \exp(-D2 \cdot EVB_j) \right) \cdot \left(\exp(-D2 \cdot EVB_{j+1}) + \exp(-D2 \cdot EVB_j) \right) \right]}$$

$$MNBU := \frac{\frac{D1}{2} \cdot \sum_{j=0}^{rows(EVB)-2} \left[\left(\frac{RIB_j}{\exp(-D2 \cdot EVB_j)} + \frac{RIB_{j+1}}{\exp(-D2 \cdot EVB_{j+1})} \right) \cdot \left(-\exp(-D2 \cdot EVB_{j+1}) + \exp(-D2 \cdot EVB_j) \right) \cdot \left(\exp(-D2 \cdot EVB_{j+1}) + \exp(-D2 \cdot EVB_j) \right) \right]}{\sum_{j=0}^{rows(EVB)-2} \left[\left(\frac{RIB_j}{\exp(-D2 \cdot EVB_j)} + \frac{RIB_{j+1}}{\exp(-D2 \cdot EVB_{j+1})} \right) \cdot \left(-\exp(-D2 \cdot EVB_{j+1}) + \exp(-D2 \cdot EVB_j) \right) \right]}$$

$$MNAU := \frac{\frac{D1}{2} \cdot \sum_{j=0}^{rows(EVA)-2} \left[\left(\frac{RIA_j}{\exp(-D2 \cdot EVA_j)} + \frac{RIA_{j+1}}{\exp(-D2 \cdot EVA_{j+1})} \right) \cdot \left(-\exp(-D2 \cdot EVA_{j+1}) + \exp(-D2 \cdot EVA_j) \right) \cdot \left(\exp(-D2 \cdot EVA_{j+1}) + \exp(-D2 \cdot EVA_j) \right) \right]}{\sum_{j=0}^{rows(EVA)-2} \left[\left(\frac{RIA_j}{\exp(-D2 \cdot EVA_j)} + \frac{RIA_{j+1}}{\exp(-D2 \cdot EVA_{j+1})} \right) \cdot \left(-\exp(-D2 \cdot EVA_{j+1}) + \exp(-D2 \cdot EVA_j) \right) \right]}$$

$MNAU = 1.254 \times 10^4$ $MWAU = 1.523 \times 10^4$ <= Apparent molecular weights for standard A using uncorrected calibration constants

$MNBU = 5.692 \times 10^5$ $MWBU = 7.918 \times 10^5$ <= Apparent molecular weights for standard B using uncorrected calibration constants

Determine new dispersion corrected calibration constants Find corrected value for calibration constant D2

$D2 = 1.041$ $DStart := D2 - 0.15 \cdot D2$ $DEnd := D2 + 0.15 \cdot D2$ $endjj := 4$ $jj := 0 .. endjj$

$$D_{jj} := DStart + \frac{DEnd - DStart}{endjj} \cdot jj \qquad RatioMW := \frac{MW_{NtrueA} \cdot MW_{WtrueA}}{MW_{NtrueB} \cdot MW_{WtrueB}} \qquad RatioMW = 5.983 \times 10^{-4}$$

$$MWAC_{jj} := \frac{\left[\sum_{j=0}^{rows(EVA)-2} \left[\left(\frac{RIA_j}{\exp(-D_{jj} \cdot EVA_j)} + \frac{RIA_{j+1}}{\exp(-D_{jj} \cdot EVA_{j+1})} \right) \cdot \left(-\exp(-D_{jj} \cdot EVA_{j+1}) + \exp(-D_{jj} \cdot EVA_j) \right) \cdot \left(\exp(-D_{jj} \cdot EVA_{j+1}) + \exp(-D_{jj} \cdot EVA_j) \right)^2 \right] \right]}{\left[\sum_{j=0}^{rows(EVA)-2} \left[\left(\frac{RIA_j}{\exp(-D_{jj} \cdot EVA_j)} + \frac{RIA_{j+1}}{\exp(-D_{jj} \cdot EVA_{j+1})} \right) \cdot \left(-\exp(-D_{jj} \cdot EVA_{j+1}) + \exp(-D_{jj} \cdot EVA_j) \right) \cdot \left(\exp(-D_{jj} \cdot EVA_{j+1}) + \exp(-D_{jj} \cdot EVA_j) \right) \right] \right]}$$

$$MWBC_{jj} := \frac{\sum_{j=0}^{rows(EVB)-2}\left[\left(\frac{RIB_j}{\exp(-D_{jj}\cdot EVB_j)}+\frac{RIB_{j+1}}{\exp(-D_{jj}\cdot EVB_{j+1})}\right)\cdot\left(-\exp(-D_{jj}\cdot EVB_{j+1})+\exp(-D_{jj}\cdot EVB_j)\right)\cdot\left(\exp(-D_{jj}\cdot EVB_{j+1})+\exp(-D_{jj}\cdot EVB_j)\right)^2\right]}{\sum_{j=0}^{rows(EVB)-2}\left[\left(\frac{RIB_j}{\exp(-D_{jj}\cdot EVB_j)}+\frac{RIB_{j+1}}{\exp(-D_{jj}\cdot EVB_{j+1})}\right)\cdot\left(-\exp(-D_{jj}\cdot EVB_{j+1})+\exp(-D_{jj}\cdot EVB_j)\right)\cdot\left(\exp(-D_{jj}\cdot EVB_{j+1})+\exp(-D_{jj}\cdot EVB_j)\right)\right]}$$

$$MNBC_{jj} := \frac{\sum_{j=0}^{rows(EVB)-2}\left[\left(\frac{RIB_j}{\exp(-D_{jj}\cdot EVB_j)}+\frac{RIB_{j+1}}{\exp(-D_{jj}\cdot EVB_{j+1})}\right)\cdot\left(-\exp(-D_{jj}\cdot EVB_{j+1})+\exp(-D_{jj}\cdot EVB_j)\right)\cdot\left(\exp(-D_{jj}\cdot EVB_{j+1})+\exp(-D_{jj}\cdot EVB_j)\right)\right]}{\sum_{j=0}^{rows(EVB)-2}\left[\left(\frac{RIB_j}{\exp(-D_{jj}\cdot EVB_j)}+\frac{RIB_{j+1}}{\exp(-D_{jj}\cdot EVB_{j+1})}\right)\cdot\left(-\exp(-D_{jj}\cdot EVB_{j+1})+\exp(-D_{jj}\cdot EVB_j)\right)\right]}$$

$$MNAC_{jj} := \frac{\sum_{j=0}^{rows(EVA)-2}\left[\left(\frac{RIA_j}{\exp(-D_{jj}\cdot EVA_j)}+\frac{RIA_{j+1}}{\exp(-D_{jj}\cdot EVA_{j+1})}\right)\cdot\left(-\exp(-D_{jj}\cdot EVA_{j+1})+\exp(-D_{jj}\cdot EVA_j)\right)\cdot\left(\exp(-D_{jj}\cdot EVA_{j+1})+\exp(-D_{jj}\cdot EVA_j)\right)\right]}{\sum_{j=0}^{rows(EVA)-2}\left[\left(\frac{RIA_j}{\exp(-D_{jj}\cdot EVA_j)}+\frac{RIA_{j+1}}{\exp(-D_{jj}\cdot EVA_{j+1})}\right)\cdot\left(-\exp(-D_{jj}\cdot EVA_{j+1})+\exp(-D_{jj}\cdot EVA_j)\right)\right]}$$

$$Diff_{jj} := RatioMW - \frac{MNAC_{jj}\cdot MWAC_{jj}}{MNBC_{jj}\cdot MWBC_{jj}}$$

$$D = \begin{pmatrix} 0.885 \\ 0.963 \\ 1.041 \\ 1.119 \\ 1.197 \end{pmatrix}$$

$$Diff = \begin{pmatrix} -8.0266\times10^{-4} \\ -1.7280\times10^{-4} \\ 1.7471\times10^{-4} \\ 3.6602\times10^{-4} \\ 4.7113\times10^{-4} \end{pmatrix}$$

Diff should have values that are both positive and negative.

The corrected calibration is the value of D when Diff = 0

$$BR := regress(D, Diff, 2)$$

See plot below

$$BR = \begin{pmatrix} 3 \\ 3 \\ 2 \\ -0.019 \\ 0.033 \\ -0.014 \end{pmatrix}$$

$$p := 0..50 \qquad D_{fit_p} := min(D) + \frac{(max(D) - min(D))\cdot p}{50}$$

$$\mathrm{Diff}_{\mathrm{fit}_p} := \sum_{i=0}^{\mathrm{BR}_2} \left[\mathrm{BR}_{i+3} \cdot \left(\mathrm{D}_{\mathrm{fit}_p} \right)^i \right] \qquad \mathrm{DC}_2 := \mathrm{root}\left[\sum_{i=0}^{\mathrm{BR}_2} \left[\mathrm{BR}_{i+3} \cdot (\mathrm{D2})^i \right], \mathrm{D2}, \min(\mathrm{D}), \max(\mathrm{D}) \right] \qquad \mathrm{DC}_2 = 1.00129$$

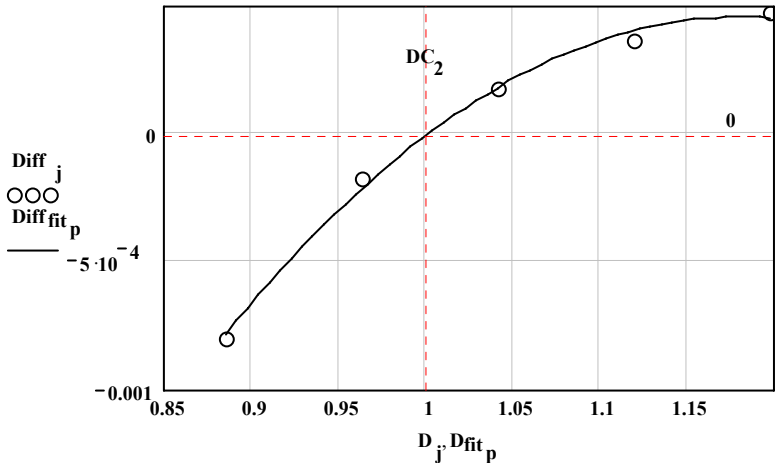

Find corrected value for calibration constant D1

$$\mathrm{DC1AW} := 2 \cdot \mathrm{MW}_{\mathrm{WtrueA}} \cdot \frac{\sum_{j=0}^{\mathrm{rows(EVA)}-2} \left[\left(\frac{\mathrm{RIA}_j}{\exp\left(-\mathrm{DC}_2 \cdot \mathrm{EVA}_j\right)} + \frac{\mathrm{RIA}_{j+1}}{\exp\left(-\mathrm{DC}_2 \cdot \mathrm{EVA}_{j+1}\right)} \right) \cdot \left(-\exp\left(-\mathrm{DC}_2 \cdot \mathrm{EVA}_{j+1}\right) + \exp\left(-\mathrm{DC}_2 \cdot \mathrm{EVA}_j\right) \right) \cdot \left(\exp\left(-\mathrm{DC}_2 \cdot \mathrm{EVA}_{j+1}\right) + \exp\left(-\mathrm{DC}_2 \cdot \mathrm{EVA}_j\right) \right) \right]}{\sum_{j=0}^{\mathrm{rows(EVA)}-2} \left[\left(\frac{\mathrm{RIA}_j}{\exp\left(-\mathrm{DC}_2 \cdot \mathrm{EVA}_j\right)} + \frac{\mathrm{RIA}_{j+1}}{\exp\left(-\mathrm{DC}_2 \cdot \mathrm{EVA}_{j+1}\right)} \right) \cdot \left(-\exp\left(-\mathrm{DC}_2 \cdot \mathrm{EVA}_{j+1}\right) + \exp\left(-\mathrm{DC}_2 \cdot \mathrm{EVA}_j\right) \right) \cdot \left(\exp\left(-\mathrm{DC}_2 \cdot \mathrm{EVA}_{j+1}\right) + \exp\left(-\mathrm{DC}_2 \cdot \mathrm{EVA}_j\right) \right)^2 \right]}$$

$$DC1BW := 2 \cdot MW_{WtrueB} \cdot \frac{\sum_{j=0}^{rows(EVB)-2} \left[\left(\frac{RIB_j}{\exp(-DC_2 \cdot EVB_j)} + \frac{RIB_{j+1}}{\exp(-DC_2 \cdot EVB_{j+1})} \right) \cdot \left(-\exp(-DC_2 \cdot EVB_{j+1}) + \exp(-DC_2 \cdot EVB_j) \right) \cdot \left(\exp(-DC_2 \cdot EVB_{j+1}) + \exp(-DC_2 \cdot EVB_j) \right) \right]}{\sum_{j=0}^{rows(EVB)-2} \left[\left(\frac{RIB_j}{\exp(-DC_2 \cdot EVB_j)} + \frac{RIB_{j+1}}{\exp(-DC_2 \cdot EVB_{j+1})} \right) \cdot \left(-\exp(-DC_2 \cdot EVB_{j+1}) + \exp(-DC_2 \cdot EVB_j) \right) \cdot \left(\exp(-DC_2 \cdot EVB_{j+1}) + \exp(-DC_2 \cdot EVB_j) \right)^2 \right]}$$

$$DC1BN := 2 \cdot MW_{NtrueB} \cdot \frac{\sum_{j=0}^{rows(EVB)-2} \left[\left(\frac{RIB_j}{\exp(-DC_2 \cdot EVB_j)} + \frac{RIB_{j+1}}{\exp(-DC_2 \cdot EVB_{j+1})} \right) \cdot \left(-\exp(-DC_2 \cdot EVB_{j+1}) + \exp(-DC_2 \cdot EVB_j) \right) \right]}{\sum_{j=0}^{rows(EVB)-2} \left[\left(\frac{RIB_j}{\exp(-DC_2 \cdot EVB_j)} + \frac{RIB_{j+1}}{\exp(-DC_2 \cdot EVB_{j+1})} \right) \cdot \left(-\exp(-DC_2 \cdot EVB_{j+1}) + \exp(-DC_2 \cdot EVB_j) \right) \cdot \left(\exp(-DC_2 \cdot EVB_{j+1}) + \exp(-DC_2 \cdot EVB_j) \right) \right]}$$

$$DC1AN := 2 \cdot MW_{NtrueA} \cdot \frac{\sum_{j=0}^{rows(EVA)-2} \left[\left(\frac{RIA_j}{\exp(-DC_2 \cdot EVA_j)} + \frac{RIA_{j+1}}{\exp(-DC_2 \cdot EVA_{j+1})} \right) \cdot \left(-\exp(-DC_2 \cdot EVA_{j+1}) + \exp(-DC_2 \cdot EVA_j) \right) \right]}{\sum_{j=0}^{rows(EVA)-2} \left[\left(\frac{RIA_j}{\exp(-DC_2 \cdot EVA_j)} + \frac{RIA_{j+1}}{\exp(-DC_2 \cdot EVA_{j+1})} \right) \cdot \left(-\exp(-DC_2 \cdot EVA_{j+1}) + \exp(-DC_2 \cdot EVA_j) \right) \cdot \left(\exp(-DC_2 \cdot EVA_{j+1}) + \exp(-DC_2 \cdot EVA_j) \right) \right]}$$

$DC1AW = 2.039 \times 10^9$ $DC1BW = 1.904 \times 10^9$ $DC1AN = 2.375 \times 10^9$ $DC1BN = 2.444 \times 10^9$

$DC_1 := (DC1AW + DC1BW + DC1AN + DC1BN) \cdot 0.25$ $DC_1 = 2.191 \times 10^9$ <= Average value

	Uncorrected Calibration Constants		Corrected Calibration Constants	
Summary=>	$D1 = 4.399 \times 10^9$	$D2 = 1.04107$	$DC_1 = 2.1905 \times 10^9$	$DC_2 = 1.00129$

$j := 0..35$ $V_{e_j} := \frac{j + 15}{3}$ $MC_j := DC_1 \cdot \exp(-DC_2 \cdot V_{e_j})$

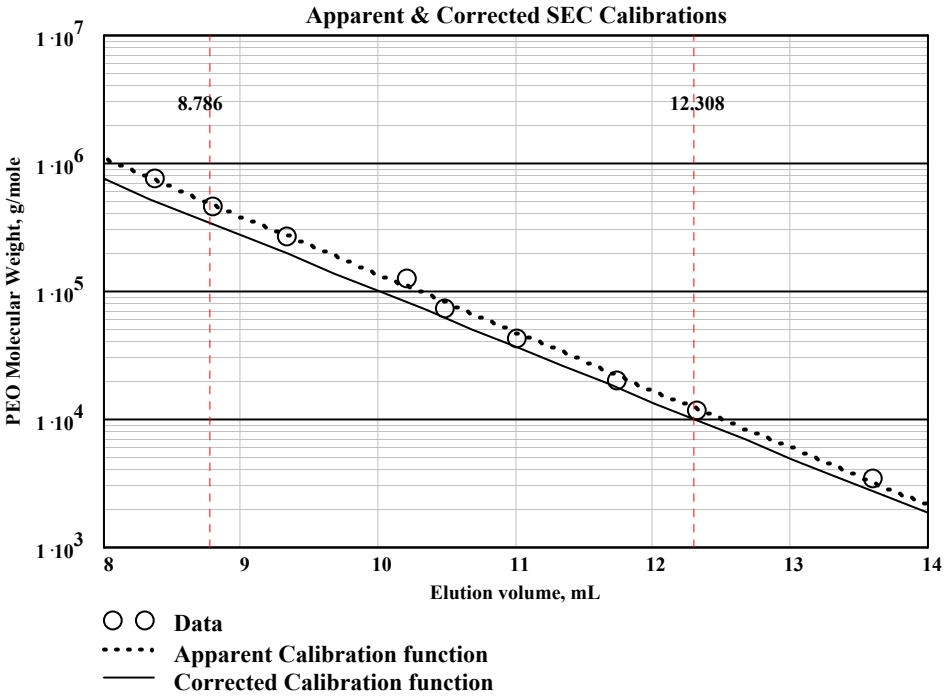

Corrected SEC calibration function

where MC = molecular weight, g/mole
Ve = elution volume, mL
DC1 and DC2 are corrected calibration constants

Calibration is based on RI detector and PEO standards

Calculate Apparent Molecular Weights Using Corrected SEC Calibration Constants

$$MWA := \frac{DC_1}{2} \bullet \frac{\sum_{j=0}^{rows(EVA)-2} \left[\left(\frac{RIA_j}{\exp(-DC_2 \bullet EVA_j)} + \frac{RIA_{j+1}}{\exp(-DC_2 \bullet EVA_{j+1})} \right) \bullet \left(-\exp(-DC_2 \bullet EVA_{j+1}) + \exp(-DC_2 \bullet EVA_j) \right) \bullet \left(\exp(-DC_2 \bullet EVA_{j+1}) + \exp(-DC_2 \bullet EVA_j) \right)^2 \right]}{\sum_{j=0}^{rows(EVA)-2} \left[\left(\frac{RIA_j}{\exp(-DC_2 \bullet EVA_j)} + \frac{RIA_{j+1}}{\exp(-DC_2 \bullet EVA_{j+1})} \right) \bullet \left(-\exp(-DC_2 \bullet EVA_{j+1}) + \exp(-DC_2 \bullet EVA_j) \right) \bullet \left(\exp(-DC_2 \bullet EVA_{j+1}) + \exp(-DC_2 \bullet EVA_j) \right) \right]}$$

$$MWB := \frac{DC_1}{2} \cdot \frac{\sum_{j=0}^{rows(EVB)-2} \left[\left(\frac{RIB_j}{\exp(-DC_2 \cdot EVB_j)} + \frac{RIB_{j+1}}{\exp(-DC_2 \cdot EVB_{j+1})} \right) \cdot \left(-\exp(-DC_2 \cdot EVB_{j+1}) + \exp(-DC_2 \cdot EVB_j) \right) \cdot \left(\exp(-DC_2 \cdot EVB_{j+1}) + \exp(-DC_2 \cdot EVB_j) \right)^2 \right]}{\sum_{j=0}^{rows(EVB)-2} \left[\left(\frac{RIB_j}{\exp(-DC_2 \cdot EVB_j)} + \frac{RIB_{j+1}}{\exp(-DC_2 \cdot EVB_{j+1})} \right) \cdot \left(-\exp(-DC_2 \cdot EVB_{j+1}) + \exp(-DC_2 \cdot EVB_j) \right) \cdot \left(\exp(-DC_2 \cdot EVB_{j+1}) + \exp(-DC_2 \cdot EVB_j) \right) \right]}$$

$$MNB := \frac{\frac{DC_1}{2} \cdot \sum_{j=0}^{rows(EVB)-2} \left[\left(\frac{RIB_j}{\exp(-DC_2 \cdot EVB_j)} + \frac{RIB_{j+1}}{\exp(-DC_2 \cdot EVB_{j+1})} \right) \cdot \left(-\exp(-DC_2 \cdot EVB_{j+1}) + \exp(-DC_2 \cdot EVB_j) \right) \cdot \left(\exp(-DC_2 \cdot EVB_{j+1}) + \exp(-DC_2 \cdot EVB_j) \right) \right]}{\sum_{j=0}^{rows(EVB)-2} \left[\left(\frac{RIB_j}{\exp(-DC_2 \cdot EVB_j)} + \frac{RIB_{j+1}}{\exp(-DC_2 \cdot EVB_{j+1})} \right) \cdot \left(-\exp(-DC_2 \cdot EVB_{j+1}) + \exp(-DC_2 \cdot EVB_j) \right) \right]}$$

$$MNA := \frac{\frac{DC_1}{2} \cdot \sum_{j=0}^{rows(EVA)-2} \left[\left(\frac{RIA_j}{\exp(-DC_2 \cdot EVA_j)} + \frac{RIA_{j+1}}{\exp(-DC_2 \cdot EVA_{j+1})} \right) \cdot \left(-\exp(-DC_2 \cdot EVA_{j+1}) + \exp(-DC_2 \cdot EVA_j) \right) \cdot \left(\exp(-DC_2 \cdot EVA_{j+1}) + \exp(-DC_2 \cdot EVA_j) \right) \right]}{\sum_{j=0}^{rows(EVA)-2} \left[\left(\frac{RIA_j}{\exp(-DC_2 \cdot EVA_j)} + \frac{RIA_{j+1}}{\exp(-DC_2 \cdot EVA_{j+1})} \right) \cdot \left(-\exp(-DC_2 \cdot EVA_{j+1}) + \exp(-DC_2 \cdot EVA_j) \right) \right]}$$

$MNA = 1.013 \times 10^4$ $MWA = 1.215 \times 10^4$ <= Apparent molecular weights for standard A using corrected calibration constants

$MNB = 3.964 \times 10^5$ $MWB = 5.4 \times 10^5$ <= Apparent molecular weights for standard B using corrected calibration constants

Find Dispersion Spreading Values

$$X_{AN} := \frac{2}{-(DC_2)^2} \cdot \left(\ln(MNA) - \ln(MW_{NtrueA}) \right) \qquad X_{AN} = 0.161$$

$$X_{AW} := \frac{2}{(DC_2)^2} \cdot \left(\ln(MWA) - \ln(MW_{WtrueA}) \right) \qquad X_{AW} = 0.143$$

$X_A := (X_{AN} + X_{AW}) \cdot 0.5$ $X_A = 0.152$ Average X value for sample A

$$X_{BN} := \frac{2}{-(DC_2)^2} \bullet \left(\ln(MNB) - \ln\left(MW_{NtrueB}\right)\right) \qquad X_{BN} = 0.219$$

$$X_{BW} := \frac{2}{(DC_2)^2} \bullet \left(\ln(MWB) - \ln\left(MW_{WtrueB}\right)\right) \qquad X_{BW} = 0.28$$

$$X_B := \left(X_{BN} + X_{BW}\right) \bullet 0.5 \qquad X_B = 0.249$$

Average X value for sample B

Let broading parameter, X, be a linear function of the elution volume.

$VeA := 12.308$ $VeB := 8.786$ mean elution volumes of standards

$$xx := \begin{pmatrix} VeA \\ VeB \end{pmatrix} \qquad yy := \begin{pmatrix} X_A \\ X_B \end{pmatrix}$$

$a := intercept(xx, yy)$ $a = 0.492$

$b := slope(xx, yy)$ $b = -0.028$

$X(Ve) := a + b \bullet Ve$ $X(VeA) = 0.152$ $X(VeB) = 0.249$

Average Molecular weight corrections

Assume the corrections below are valid for all PEO samples, regardless of molecular weight, when the column is operating at a flow rate of 0.5 mL/min.

$$MWCorrection_{AWeight} := \left[\exp\left[\frac{-(DC_2)^2 \bullet X(VeA)}{2}\right]\right] \qquad MWCorrection_{BWeight} := \exp\left[\frac{-(DC_2)^2 \bullet X(VeB)}{2}\right]$$

$$MWCorrection_{ANumber} := \exp\left[\frac{(DC_2)^2 \bullet X(VeA)}{2}\right] \qquad MWCorrection_{BNumber} := \exp\left[\frac{(DC_2)^2 \bullet X(VeB)}{2}\right]$$

$MWCorrection_{ANumber} = 1.079$ $MWCorrection_{AWeight} = 0.927$

$MWCorrection_{BNumber} = 1.133$ $MWCorrection_{BWeight} = 0.882$

<= Corrections to apparent number and weight average apparent molecular weights

Corrected Molecular Weights

Apparent Mol. Weights

$MNA = 1.013 \times 10^4$

$MWA = 1.215 \times 10^4$

Application of Correction

$MW_{NAC} := MNA \bullet MWCorrection_{ANumber}$

$MW_{WAC} := MWA \bullet MWCorrection_{AWeight}$

Apparent Mol. Weights

$MNB = 3.964 \times 10^5$

$MWB = 5.4 \times 10^5$

Application of Correction

$MW_{NBC} := MNB \bullet MWCorrection_{BNumber}$

$MW_{WBC} := MWB \bullet MWCorrection_{BWeight}$

Calculated True Mol. Weights

$MW_{NAC} = 1.093 \times 10^4$

$MW_{WAC} = 1.126 \times 10^4$

$MW_{NBC} = 4.491 \times 10^5$

$MW_{WBC} = 4.765 \times 10^5$

Vendor Reported True Mol. Weights

$MW_{NtrueA} = 1.098 \times 10^4$ <= Standard A MW_N

$MW_{WtrueA} = 1.131 \times 10^4$ <= Standard A MW_W

$MW_{NtrueB} = 4.423 \times 10^5$ <= Standard B MW_N

$MW_{WtrueB} = 4.692 \times 10^5$ <= Standard B MW_W

Molecular Weight Distributions

$f(V_e) := D1 \bullet \exp(-D2 \bullet V_e)$

Uncorrected calibration function to determine molecular weight at a given elution volume, Ve.

$F(V_e) := DC_1 \bullet \exp(-DC_2 \bullet V_e)$

Corrected calibration function to determine molecular weight at a given elution volume, Ve.

PEO Sample A

$M_{PEOAC} := F(EVA)$

$M_{PEOAU} := f(EVA)$

$NumPEOAC := \overrightarrow{\left(\frac{RIA}{M_{PEOAC}}\right)}$

$NumPEOAU := \overrightarrow{\left(\frac{RIA}{M_{PEOAU}}\right)}$

PEO Sample B

$M_{PEOBC} := F(EVB)$ $M_{PEOBU} := f(EVB)$ $NumPEOBC := \overrightarrow{\left(\frac{RIB}{M_{PEOBC}}\right)}$ $NumPEOBU := \overrightarrow{\left(\frac{RIB}{M_{PEOBU}}\right)}$

Note that the dispersion correction results in a more narrow molecular weight distribution for both standards.

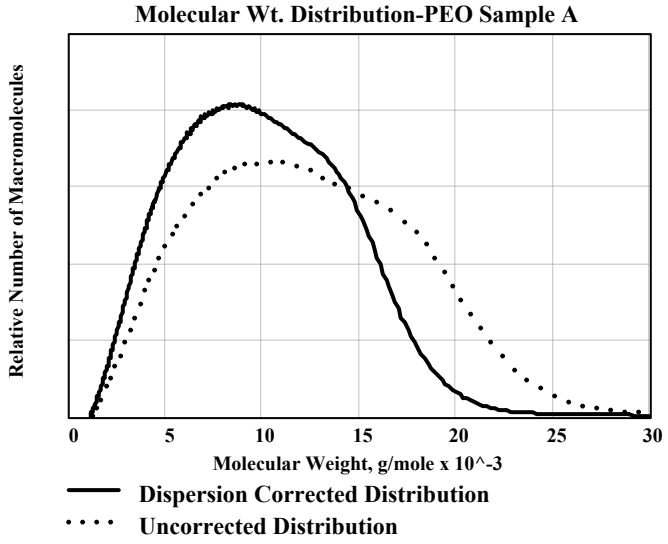

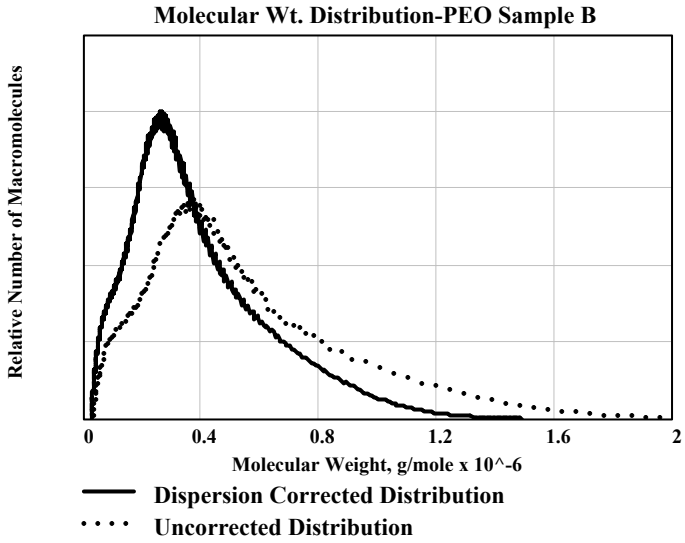

References

1 Lowe, A. B. and McCormick, C. L. *Chem. Rev.* **2002**, *102*(11), 4177-4189.

[2] Morawetz, H. *Macromolecules in Solution, 2nd Ed*. Robert E. Krieger Publishing Co.: Malabar, FL, 1983, p. 315.

[3] Bekturov, E. A.; Kudaibergenov, S. E.; Rafikov, S. R. *Macromol. Chem. Phys*. **1990**, *C30*, 233.

[4]. Hart, R.; Timmerman, D. J. *Polymer Sci.* **1958**, *28*, 638.

[5]. Schulz, D. N.; Peiffer, D. G.; Agarwal, P.K.; Larabee, J.; Kaladas, J. J.; Soni, L.; Handwerker, B.; Garner, R. T.; *Polymer* **1986**, *27*, 1734.

[6]. Schulz, D. N.; Kitano, K.; Danik, J.A.; Kaladas, J. J. *Polym. Mat. Sci. Eng.* **1987**, *147*, 149.

[7]. Huglin, M.B.; Radwan, M.A. *Polymer International* **1991**, *26*, 97.

[8]. Konack, C.; Rathi, R. C.; Kopeckova, P.; Kopecek, J. *Polymer* **1993**, *34*, 4767.

[9]. Konack, C.; Rathi, R. C.; Kopeckova, P.; Kopecek, J. *Macromolecules* **1994**, *27*, 1992.

[10]. Monroy Soto, V. M.; Galin, J. C. *Polymer* **1984**, *25*, 121.

[1]1. Monroy Soto, V. M.; Galin, J. C. *Polymer* **1984**, *25*, 254.

[1]2. Wielema, T. A., Engberts, Jan B. F. N. *European. Polymer Journal* **1987**, *23*, 947.

[1]3. Kathmann, E. E.; Davis, D. D.; McCormick, C. L. *Macromolecules* **1994**, *27*, 3156.

[1]4. Lee, W-F.; Tsai, C-C *Polymer* **1995**, *36*, 357.

[1]5. Salamone, J. C.; Volksen, W.; Israel, S.C.; Olson, A. P.; Raia, D. C. *Polymer* **1977**, *18*, 1058.

[1]6. Salamone, J. C.; Volksen, W.; Olson, A. P.; Israel, S.C. *Polymer* **1978**, *19*, 1157.

[1]7. Wielema, T. A.; Engberts, J. B. F. N. *European Polymer Journal*, **1990**, *26*, 639.

[1]8. Lowe, A.B., Billingham, N.C., and Armes, S.P. *Macromolecules*, **1999**, *32*, 2141.

[1]9. Lowe, A.B., Billingham, N.C., and Armes, S.P. *Macromolecules* **1998**, *31*, 5991.

20. McCormick, C. L.; Blackmon, K. P. *J. Polym. Sci., Part A: Polym. Chem.* **1986**, *24*, 2635-2645.

21. McCormick, C. L.; Blackmon, K. P.; Elliott, D. L. *J. Polym. Sci., Part A: Polym. Chem.* **1986**, *24*, 2619-2634.

22. McCormick, C. L.; Blackmon, K. P. *U.S. Patent 4,584,358*, 1986.

23. McCormick, C. L.; Elliott, D. L. *Macromolecules* **1986**, *19*, 542-547.

24. McCormick, C. L.; Salazar, L. C. *J. Appl. Polym. Sci.* **1993**, *48*, 1115-1120.

25. McCormick, C. L.; Salazar, L. C. *J. Polym. Sci., Part A: Polym. Chem.* **1993**, *31*, 1099-1104.

26. McCormick, C. L.; Johnson, C. B. *Polymer* **1990**, *31*, 1100-1107.

27. McCormick, C. L.; Salazar, L. C. *Polymer* **1992**, *33*, 4384-4387.

28. McCormick, C. L.; Johnson, C. B. *J. Macromol. Sci., Chem.* **1990**, *A27*, 539-547.

29. Salamone, J. C.; Ahmed, I.; Rodriguez, E. L.; Quach, L.; Watterson, A. C. *J. Macromol. Sci., Chem.* **1988**, *25*, 811-837.

30. McCormick, C. L.; Salazar, L. C. *J. Macromol. Sci., Chem.* **1992**, *A29*, 193-205.

31. Johnson, C. B. *Ph.D. Dissertation*; Univeristy of Southern Mississippi: Hattiesburg, MS, 1987.

32. Salazar, L. C. *Ph.D. Dissertation*; University of Southern Mississippi: Hattiesburg, MS, 1991.

33. McCormick, C. L.; Salazar, L. C. *Macromolecules* **1992**, *25*, 1896-1900.

34. Fevola, M. J.; Hester, R. D.; McCormick, C. L. *J. Polym. Sci., Part A: Polym. Chem.* **2003**, *41*, 560-568.

35. Thomas, W. M.; Wang, D. W. In *Encycl. Polym. Sci. Eng, Second Ed.*, Second ed.; H. F. Mark, N. M. B., C. G. Overberger, G. Menges, J. I. Kroschwitz, Ed.; Wiley Interscience: New York, 1985; Vol. 1, pp 176-177.

36. Gleason, E. H.; Miller, M. L.; Sheats, F. *J. Polym. Sci.* **1959**, *38*, 133.

37. Neyret, S.; Candau, F.; Selb, J. *Acta Polym.* **1996**, *47*, 323-332.

38. McCormick, C. L.; Johnson, C. B. *Macromolecules* **1988**, *21*, 686-693.

39. Schittenhelm, N.; Kulicke, W.-M. *Macromol. Chem. Phys.* **2000**, *201*, 1976-1984.

40. Yamakawa, H. *Modern Theory of Polymer Solutions*; Harper & Row: New York, 1971.

41. Tirrell, M. In *Rheology: Principles, Measurements, and Applications*; Macoscko, C. W., Ed.; VCH Publishers, Inc.: New York, 1994; pp 475-512.

42. Kurata, M.; Tsunashima, Y. In *Polymer Handbook*, Fourth ed.; Brandrup, J.; Immergut, E. H.; Grulke, E. A., Eds.; John Wiley & Sons, Inc.: New York, 1999; pp 265-289.

43. Dobrynin, A. V.; Rubinstein, M. *J. Phys. II* **1995**, *5*, 677-695.

44. Candau, F.; Joanny, J. F. In *Polym. Mater. Encycl.*; Salamone, J. C., Ed.; CRC Press: Boca Raton, FL, 1996; Vol. 7, pp 5462-5476.

45. Higgs, P. G.; Joanny, J. F. *J. Chem. Phys.* **1991**, *94*, 1543-1554.

46. Everaers, R.; Johner, A.; Joanny, J. F. *Macromolecules* **1997**, *30*, 8478-8498.

47. Munk, P.; Aminabhavi, T. M.; Williams, P.; Hoffman, D. E.; Chmelir, M. *Macromolecules* **1980**, *13*, 871-875.

48. Dobrynin, A. V.; Colby, R. H.; Rubinstein, M. *Macromolecules* **1995**, *28*, 1859-1871.

49. Kantor, Y.; Kardar, M. *Europhys. Lett.* **1994**, *27*, 643-648.

50. Kantor, Y.; Kardar, M. *Phys. Rev. E: Stat. Phys., Plasmas, Fluids, Relat. Interdiscip. Top.* **1995**, *51*, 1299-1312.

51. Kantor, Y.; Kardar, M.; Ertas, D. *Physica A* **1998**, *249*, 301-306.

52. McCormick, C. L. and Hester, R. D., DOE Reports, BC01531701, BC01531702, BC01531703, BC01531704, BC01531705

53. Ferguson, J.; Hudson, N. E.; Odriozola, M. A. *Journal of Non-Newtonian Fluid Mechanics* 1997, 68, 241-257.

54. Ferguson, J.; Hudson, N. E.; Forsyth, J. F. *Journal of Non-Newtonian Fluid Mechanics* 1998, 79, 213-223.

55. Tirtaatmadja, V.; Sridhar, T. *Journal of Rheology* **1993**, 37(6), 1061-1102.

56. Durst, F. and R. Hass, *Rheol. Acta.*, **1981**.20, 179.

57. McCormick, C. L. and Hester, R. D., DOE Report, BC01531702

58. McCormick, C. L. and Hester, R. D., DOE Report, BC01531701

59. Odell, J. A. and A. Keller, *J. Poly. Sci., Poly. Phys., B24*, **1986**,1889.

60. Hassager, F., *J. Chem. Phys*., *60,* **1974,** 2111.

61. Hester, R. D. and P. H. Mitchell, *J. Poly. Sci., C, 18*, **1980**, 1727.

62. Benoit, H., F. Grubisic, etal., *J. Chim. Phys., 63*, **1966,** 1507.

63. Yau, W. W., J. J. Kirkland, and D. D. Bly, *Modern Size-Exclusion Liquid Chromatography*, John Wiley & Sons, N. Y. 1979.

64. Tung, L. H., *J. Appl. Polym. Sci., 10*, **1966**, 375.

65. Omorodion, S. N. E. and A. E. Hamielec, *J. Appl. Polym. Sci., 39*, **1990**, 875.

66. MathCad 11 Software, MathSoft, Inc. Cambrige, MA.